“Uptake of gold nanoparticles in microvascular endothelial cells”

D i s s e r t a t i o n

zur Erlangung des Grades

„Doktor der Naturwissenschaften“

am Fachbereich Biologie

der Johannes Gutenberg-Universität in Mainz

Christian Freese

geb. am 02.10.1980

in Wiesbaden-Sonnenberg

Mainz, den 21.07.2011

Dekan:

1. Berichterstatter:

2. Berichterstatter:

Tag der mündlichen Prüfung: 06.10.2011

Es gibt Dinge,

die sind unbekannt,

und es gibt Dinge,

die sind bekannt.

Dazwischen gibt es Türen.

William Blake

Abbreviation

BBB	blood-brain barrier
BCRP	breast cancer resistance protein
CAM	cell adhesion molecule
CD31	cluster of differentiation
cm	centimeter
DNA	deoxyribonucleic acid
ELISA	Enzyme-linked immunosorbent assay
FCS	fetal calf serum
GFAP	glial fibrillary acidic protein
h	hour
HDMEC	human dermal microvascular endothelial cells
IL	Interleukin
LPS	lipopolysaccharide
MCP-1	monocyte chemotactic protein-1
MDR-1	multidrug-resistance
min	minute
ml	milliliter
mM	millimolar
MRP	multidrug-resistance (associated) protein
nm	nanometer
PBEC	porcine brain endothelial cells
PBS	phosphate buffered saline
PCR	polymerase chain reaction
PFA	Paraformaldehyde
P-gp	P-glycoprotein
RNA	ribonucleic acid
s	second
SMA	alpha smooth muscle actin
TEER	transendothelial electrical resistance
TNFα	tumor necrosis factor α
vWF	von Willebrand factor

ZO-1	zonula occludens
µg	microgram
µl	microliter
µM	micromolar

Abstract

The physicochemical properties of nanoparticles make them suitable for biomedical applications. Due to their ‘straight-forward’ synthesis, their known biocompatibility, their strong optical properties, their ability for targeted drug delivery and their uptake potential into cells gold nanoparticles are highly interesting for biomedical applications. In particular, the therapy of brain diseases (neurodegenerative diseases, ischemic stroke) is a challenge for contemporary medicine and gold nanoparticles are currently being studied in the hope of improving drug delivery to the brain.

In this thesis three major conclusions from the generated data are emphasized.

1. After improvement of the isolation protocol and culture conditions, the formation of a monolayer of porcine brain endothelial cells on transwell filters lead to a reproducible and tight *in vitro* monoculture which exhibited *in vivo* blood brain barrier (BBB) characteristics. The transport of nanoparticles across the barrier was studied using this model.
2. Although gold nanoparticles are known to be relatively bioinert, contaminants of the nanoparticle synthesis (i.e. CTAB or sodium citrate) increased the cytotoxicity of gold nanoparticles, as shown by various publications. The results presented in this thesis demonstrate that contaminants of the nanoparticle synthesis such as sodium citrate increased the cytotoxicity of the gold nanoparticles in endothelial cells but in a more dramatic manner in epithelial cells. Considering the increased uptake of these particles by epithelial cells compared to endothelial cells it was demonstrated that the observed decrease of cell viability appeared to be related to the amount of internalized gold nanoparticles in combination with the presence of the contaminant.
3. Systematically synthesized gold nanoparticles of different sizes with a variety of surface modifications (different chemical groups and net charges) were investigated for their uptake behaviour and functional impairment of endothelial cells, one of the major cell types making up the BBB. The targeting of these different nanoparticles to endothelial cells from different parts of the body was investigated in a comparative study of human microvascular dermal and cerebral endothelial cells. In these experiments it was demonstrated that different properties of the nanoparticles resulted in a variety of uptake patterns into cells. Positively charged gold nanoparticles were internalized in high amounts, while PEGylated nanoparticles were not taken up by both cell types. Differences in the uptake behavior were also demonstrated for neutrally charged particles of different sizes, coated with hydroxypropylamine or glucosamine. Endothelial cells of the brain specifically internalized 35nm neutrally charged hydroxypropylamine-coated gold nanoparticles in larger amounts compared to dermal microvascular endothelial cells, indicating a "targeting" for brain endothelial cells. Co-localization studies with flotillin-1 and flotillin-2 showed that the gold nanoparticles were internalized by endocytotic pathways. Furthermore, these nanoparticles exhibited transcytosis across the endothelial cell barrier in an *in vitro* BBB model generated with primary porcine brain endothelial cells (1.). In conclusion, gold nanoparticles with different sizes and surface characteristics showed different uptake patterns in dermal and cerebral endothelial cells. In addition, gold nanoparticles with a specific size and defined surface modification were able to cross the blood-brain barrier in a porcine *in vitro* model and may thus be useful for controlled delivery of drugs to the brain.

Zusammenfassung

Die physikochemischen Eigenschaften von Nanopartikeln machen diese zu viel versprechenden Werkzeugen der Wissenschaft und Medizin. Die „straight-forward"-Synthese von Goldnanopartikeln, die Biokompatibilität, die guten optischen Eigenschaften, sowie das gute Aufnahmepotential in Zellen machen Goldnanopartikel zu einem interessanten Wissenschaftsobjekt. Besonders die Behandlung von neurogenerativen Erkrankungen und Hirnschlag ist heutzutage eine große Herausforderung für die Medizin. Daher könnte der Einsatz von Goldnanopartikeln durch gezielte Gabe von Medikamenten die Heilungschancen verbessern.

Drei Forschungsergebnisse der vorliegenden Arbeit sollen im Folgenden hervorgehoben werden:

1. Nach der Verfeinerung des Isolationsprotokolls, der Kulturbedingungen von Schweinehirnendothelzellen und der Bildung eines intakten einschichtigen Zellrasens auf einem Transwellfiltersystems, konnte eine dichte *in vitro* Monokultur von Endothelzellen generiert werden, die ähnliche Eigenschaften der *in vivo* Bluthirnschranke aufweist. Der Transport von Goldnanopartikeln über die Bluthirnschranke konnte anhand dieses Modells untersucht werden.
2. Obwohl Goldnanopartikel als relativ biokompatibel angesehen werden können, konnte in mehreren Publikationen gezeigt werden, dass Reste von Syntheseprodukten, wie z.B. CTAB oder Natriumzitrat, die Zytotoxizität erhöht. Die Ergebnisse dieser Arbeit wiederum zeigen, dass Natriumzitrat die Zytotoxizität von Endothelzellen erhöht, jedoch der Einfluss auf Epithelzellen massiver ist. Die erhöhte Menge an Goldnanopartikeln in Epithelzellen gegenüber Endothelzellen konnte mit der geringeren Zellvitalität in Verbindung gebracht werden, die des Weiteren auch von der Menge an Natriumzitrat abhängig ist.
3. Nach der Herstellung von Goldnanopartikeln verschiedener Größen mit einer Vielfalt an verschiedenen Oberflächenmodifikationen (verschiedene chemische Gruppen und Ladungen) wurde die Aufnahmefähigkeit sowie die Beeinflussung von Endothelzellen untersucht. Dabei wurde die gezielte Aufnahme von Partikeln in Endothelzellen verschiedener Herkunft (humane dermale und zerebrale Endothelzellen) mit einander verglichen. Es konnte gezeigt werden, dass die verschiedenen Veränderungen der Partikeloberfläche in einem unterschiedlichen Aufnahmepotential in Endothelzellen resultierten. Positiv geladene Partikel wurden gut aufgenommen, während Goldnanopartikel mit Poly(ethylenglykol) von beiden Endothelzelltypen weniger gut aufgenommen wurden. Unterschiede gab es auch bei neutral geladenen Goldnanopartikeln verschiedener Größen, die mit Hydroxypropylamin oder Glukosamin beschichtet sind. Besonders die 35nm großen Hydroxypropylamin-beschichteten Goldnanopartikel werden verstärkt aufgenommen. Zusätzlich konnte gezeigt werden, dass die Menge dieser Partikel in Hirnendothelzellen höher ist, als die von dermalen Endothelzellen. Somit kann man von einer „gezielten" Aufnahme in Hirnendothelzellen sprechen. Durch Kolokalisationsuntersuchungen mit Flotillin-1 und -2 konnte unterdessen gezeigt werden, dass die Partikel von den Zellen über Endozytose aufgenommen werden. Des Weiteren wurde aufgezeigt, dass die Partikel über die Barriere von Hirnendothelzellen gelangen können. Dies wurde anhand des Schweinemodells der Bluthirnschranke gezeigt (siehe 1.). Zusammenfassend kann festgehalten werden, dass Goldnanopartikel mit verschiedenen Größen, Ladungen und Oberflächencharakteristika unterschiedlich in verschiedene Endothelzelltypen aufgenommen werden. Die Verknüpfung einer bestimmten Größe und Oberfläche von Goldnanopartikeln kann somit für einen gezielten Transport in Hirnendothelzellen und einen Transport über diese genutzt werden.

Content

1 Introduction 1
1.1 Nanotechnology 1
1.2 Nanoparticles 4
1.2.1 Physicochemical properties of nanoparticles 4
1.2.2 Drug delivery 7
1.2.3 Gold nanoparticles 11
1.3 The Blood-brain barrier 15
1.4 Aim of the study 22
2 Materials 24
2.1 Instruments 24
2.2 Microscopes 24
2.3 Consumables 25
2.4 Chemicals 26
2.5 Buffers 27
2.6 Solutions and cell culture media 28
2.7 Enzymes 29
2.8 FITC-Dextrans (FD) 30
2.9 Nanoparticles 30
2.10 Antibodies 31
2.11 Standards 33
2.12 Oligonucleotide 33
2.13 Kit-Systems 34
2.14 Primary cells and cell lines 34
3 Methods 36
3.1 Isolation of primary human endothelial cells 36
3.2 Isolation of primary porcine endothelial cells and pericytes 37
3.3 Cell culture 38
3.3.1 Coating of culture surfaces 38

3.3.2 Cell passage and cell seeding 39
3.3.3 Freezing / defreezing of cells 39
3.3.4 Angiogenesis 40
3.3.5 Determination of transendothelial electrical resistance (TEER) 40
3.3.6 Permeability studies with sodium fluorescein and FITC-Dextrans 41
3.3.7 Generation of mAb-3G5 by 3G5 hybridoma cells in a bioreactor 41
3.4 Treatment with gold nanoparticles and detection methods 42
3.4.1 Incubation with transferrin-Texas Red 42
3.4.2 Incubation with nanoparticles 42
3.4.3 Detection of gold nanoparticles by microscopy and spectroscopy 42
3.4.4 Transmission electron microscopy (TEM) 42
3.4.5 Scanning electron microscopy (SEM) 43
3.4.6 Quantification of gold nanoparticles using inductively coupled plasma atomic emission spectroscopy (ICP-AES) 43
3.5 Cytotoxicity assays 43
3.5.1 Calcein-AM cell viability assay 43
3.5.2 Viability test (MTS-Assay) 44
3.5.3 Proliferation assay (Ki-67) 44
3.5.4 Crystal violet staining 45
3.5.5 Cytotoxicity assay (release of lactate dehydrogenase (LDH)) 45
3.6 Molecular biology 45
3.6.1 Cell characterization by polymerase chain reaction 45
3.6.2 Isolation and quantification of RNA 46
3.6.3 cDNA-synthesis: reverse transcription polymerase chain reaction (RT-PCR) 46
3.6.4 Polymerase chain reaction (PCR) 46
3.6.5 Quantitative real-time PCR 47
3.7 Protein biochemical methods 48
3.7.1 ELISA 48
3.7.2 Staining of cell compartments and cell membrane proteins 49

4 Results 50

4.1 Characterization of human cerebral microvascular endothelial cells (hCMEC) .. 50

4.2 Characterization of primary porcine brain microvascular endothelial cells (PBEC) and pericytes 53

4.3 Establishment of BBB-Models: Monocultures 56

4.3.1 Blood-brain barrier formation by PBEC 56

4.3.2 Improvement and additional characterization of the blood-brain barrier model formed by hCMEC/D3 59

4.4 Adhesion and internalization of nano-structured materials in different human endothelial and epithelial cell types 62

4.4.1 Exposure of different human endothelial and epithelial cells to gold nanoparticles with different amounts of sodium citrate 63

4.4.2 Exposure of human microvascular endothelial cells to gold nanoparticles with different sizes and various surface modifications 69

4.4.3 Exposure of PBECs cultured on transwell filters with different sizes of hydroxypropylamine-coated gold nanoparticles 89

5 Discussion 93

5.1 Establishment of *in vitro* blood-brain barrier models 93

5.2 Effects of the presence of sodium citrate on the surface of gold nanoparticles on cytotoxicity and uptake behavior in different human endothelial cells 98

5.3 Screening of gold nanoparticles with different sizes and various surface modifications synthesized by the same procedure 101

5.4 Detailed investigation of different sized hydroxylpropylamine-coated gold nanoparticles 105

6 Appendix 113

7 References 114

8 List of figures 125

9 List of tables 127

10 Curriculum vitae ..... **Fehler! Textmarke nicht definiert.**

1 Introduction

1.1 Nanotechnology

Nanotechnology is one of the most promising new technologies of the 21st century. With a high public funding of nearly 6 billion dollars worldwide in 2010 this interdisciplinary field of nanotechnology is the technology with the highest financial support (see www.nanopost.com). In nanotechnology materials and systems which have sizes in the nanometer range are used. This definition implies that at least one dimension of the nanomaterials / nanoparticles is less than 100nm in size (NSTC, 2002). These small dimensions lead to two important properties which make nanoobjects behave differently compared to larger objects. On the one hand, in such small dimensions quantum effects become more obvious compared to macroobjects and on the other hand the ratio of surface to volume increases considerably with decreasing size. These properties exert great influence on nanoparticle physics, chemistry and biology. The large ratio of surface to volume is one of the most important properties for the application of nanoparticles as drug-delivery systems (DDS) (Kim et al., 2009a).

Everyone is exposed to nanotechnology daily. Nanoparticles are present in cosmetics and are used by the electronic industry. Zinc oxide and titanium dioxide particles are incorporated into sun creams and are responsible for protecting the skin from ultraviolet radiation. In other commercially available care products such as deodorant, soap, toothpaste, shampoo, hair conditioner, lipstick, face powder, perfume, etc. nanoparticles are also often present (Greßler et al.). In the electronic industry carbon nanotubes are used to produce nanoelectronic devices with conductivity as high as copper, heat resistance as high as diamonds and strength 100 times higher than steel. Moreover, in the car industry, nanoparticles are used to build nanosensors or more effective catalytic converters. In addition, carbon black nanomaterials improve the elasticity and adhesion of tires (Saxl; NanoCare Consortium, 2009).

Nanoparticles are also employed in the textile and food industries. Flavors, vitamins, minerals and even pharmaceutical drugs that are unstable, are often encapsulated in nanomaterials such as liposomes or micelles to prolong their stability in food or drinks. Nestlé, for example, utilizes encapsulation technologies for the delivery of active ingredients in food (Ubbink and Krüger, 2006; Greßler et al., 2010b). The packaging of food is also improved by nanotechnology and provides a better barrier against contamination by using silver, titanium dioxide and silicium dioxide particles

(Greßler et al., 2010b). In the textile industry the use of nanomaterials is mostly concentrated on antibacterial properties by including silver particles into textile fibers especially in sportswear (Greßler et al., 2010c).

The most prominent example in nature that is related to nanotechnology is the so-called 'Lotus-Effect'. The leaves of the lotus plant (*Nelumbo nucifera*) are superhydrophobic, which means that due to its nano-sized structure of wax droplets on the surface of the epidermal cells the contact angle of a water droplet and the surface of the leaf is larger than 150°. Therefore the water forms a spherical droplet with very low attraction forces on the leaf and the water droplet tends to roll off the surface. By the rolling-off dirt molecules are also washed away. The imitation of the 'Lotus-Effect' is difficult because the surface of the leaf is continuously renewing itself. This is not possible in manufactured materials but indeed some 'Easy-to-Clean' surfaces with hydrophobic and oleophobic nano-sized coatings have been developed by today's industry (Greßler et al., 2010a).

In addition to the progress of nanotechnology in the different industrial branches, nano-sized materials play a key role in the future of medicine and biology. Many biomedical applications for engineered nanostructures are being investigated and some are already being applied in contemporary medicine. Nanotechnologically-modified biomaterials for tissue engineering and tissue regeneration, diagnostics, imaging, cancer therapy and gene/drug delivery are only some examples in fields in which nanotechnology has contributed to the generation of new biomedical products.

Different tools that have evolved from nanotechnology such as nano-particles, nano-structures, nano-surface coatings and nano-devices have been developed and are being used in biomaterial research. The coating of biomaterials with nano-sized structures can influence the biomaterial in different ways and can improve biomimetic properties. On the one hand, nanomaterial coatings prevent the adhesion of cells to the biomaterial surface and are helpful in the case of pacemakers (bioinert biomaterials). On the other hand, some coatings improve cell adhesion to help rebuild both soft and hard tissues (bioactive biomaterials).

Imaging agents are also improved by the use of nanomaterials. Iron oxide nanoparticles coupled with magnetic resonance imaging (MRI) can identify inflammation in stroke which is the third leading cause of death after cancer and myocardial infarction (Chauveau et al., 2010). The group of Choi et al. synthesized Co@Pt-gold nanoparticles[1] and investigated in conjunction with MRI the detection of

[1] (cobalt magnetic core with a platinum shell fused to a gold nanoparticle)

amyloid β (Aβ) peptides in their reversible stage (Choi et al., 2008). The assembly process of Aβ-peptides is only reversible in early stages. The detection of the protein assemblies by Co@Pt-gold nanoparticles and MRI enables the treatment of patients to reassemble the Aβ fibrils and prevent Alzheimer disease.

In addition, hyperthermia therapy, a method not yet established for clinical routine, uses nanoparticles to treat tumors. The nanoparticles are directly injected into the tumor and are internalized by the surrounding tumor cells. These nanoparticles generate heat after an external electromagnetic field is applied, and this kills the tumor cells by overheating/hyperthermia (Jordan et al., 2006).

Nanotechnology has also improved diagnostic methodologies. Thus, high-throughput screening has become more and more important for biomedical investigations and has replaced standard assays such as representational difference analysis (RDA), subtractive hybridization and differential display analysis. Microarrays are especially useful for screening expression patterns of thousands of genes (DNA chips) or proteins (protein chips) in just a single assay with a small sample volume. Nanoparticles can also be used directly for diagnostic purposes. Gold nanoparticles, for example, can be used for the detection of DNA fragments or proteins. This technique is an alternative to the labeling with fluorophores and results in a higher sensibility and longer stability. In combination with gold nanoparticles Nam et al. used this method to detect early signs of breast cancer (Nam et al., 2009).

In addition to the above mentioned applications, the improvement of gene and drug delivery by nanotechnology is currently being investigated. Different nanoparticles have been reported to be a good alternative for viral vectors (Luo and Saltzman, 2000; Cai et al., 2005). Polyethylenimine (PEI) conjugated to gold nanoparticles is an efficient gene vector and exhibits a ~ 60-fold higher transfection efficiency compared to PEI (25kDa) in 10% serum-containing medium (Hu et al., 2010). Details of targeted drug delivery are summarized in chapter 1.2.2.

As described above nano-sized particles can be used in many applications. The quantity of different engineered nanoparticles is enormous, so that a direct comparison of all of these different nanoparticles *in vitro* or *in vivo* is impossible. However, through the use of standardized methods, a multifacetted and accurate characterization of the particles can be performed and a comparison of individual nanoparticles obtained. In the following sections the most important properties of nanoparticles are discussed.

1.2 Nanoparticles

1.2.1 Physicochemical properties of nanoparticles

Particles which exhibit a size of between 0.1µm and 2.5µm are defined as fine particles while particles that are larger than 2.5µm are summarized as microparticles. Particles with a size smaller than 100nm are classified as nanoparticles. All of these particles can be found naturally in the environment and are mainly derived from soils and wear processes and since the industrial revolution from the combustion of fossils fuels. Since nanomaterials are used in several industrial manufacturing processes the number of synthetic engineered nanoparticles found in the environment has increased with time, thus increasing the likelihood of humans coming into contact with these compounds.

In general, the term 'nanoparticle' does not describe the shape and the structure of the particles. Nanoparticles can be nanogels (Vinogradov et al., 2005a; Vinogradov et al., 2005b; Vinogradov, 2010), nanostructured particles as well as nanoclusters which exhibit a concrete number of atoms (e.g., Au_{55}-cluster[2]). Nanostructured particles in turn can be nanotubes (long tubes with a diameter in the nanorange), nanospheres (round nanoparticles smaller than 100nm), nanorods (rods smaller than 100nm in at least one dimension), nanocapsules, or even nanocrystals. The shape of the particles is of great importance on account of the fact that this parameter influences the mode of ad- and absorption to all kinds of substances and can therefore influence the reaction of living cells and organisms after exposure.

Nanoparticles can be synthesized by numerous physical or chemical processes and can consist of nearly any bulk material. The composition of the nanoparticles is the second characteristic that may influence the reaction to cells.

Although the size of nanoparticles is defined as smaller than 100nm there are also differences in the behavior of different sized nanoparticles. After synthesis of nanoparticles the suspension contains nanoparticles with various sizes. For scientific studies the nanoparticle suspension should exhibit a narrow size distribution due to the fact that various particle sizes can interact with cells in different ways. In theory, a suspension with one size of particles rarely exists. The size distribution (which is seldom the Gaussian distribution) is calculated by determining the mean size of the particles in suspension and the calculation of the standard deviation (geometric standard deviation ($\ln \sigma_g$)). For $\sigma_g < 1.1$ the suspension is called monodisperse (in theory only $\sigma_g = 1$ is monodisperse), whereas

[2] Au_{55}-cluster: gold cluster which exhibit 55 gold atoms

for all $\sigma_g > 1.1$ a suspension is defined as polydisperse. It is important to remember that the stated sizes of nanoparticles are always mean diameters. In the literature the polydispersity index (PDI) is usually determined and is calculated by taking the weight average molecular weight divided by the number average molecular weight (see appendix). Therefore, the PDI is a unit for the mass distribution and traditionally used in polymer chemistry. A polydispersity index of 1 defines a monodisperse nanoparticle suspension. The sizes of nanoparticles are commonly determined by dynamic light scattering (DLS), UV/vis spectroscopy and transmission electron microscopy (TEM).

By DLS it is also possible to detect agglomerations/aggregates of nanoparticles in suspension. While the formation of nanoparticle aggregates is irreversible, the interactions of nanoparticles in agglomerations are less strong. Nevertheless, the formation of agglomerates (and especially aggregates) should be prevented due to the fact that nanoparticle agglomerations influence cells in a different way than single particles do. By stabilizing the surface of nanoparticles after synthesis the formation of agglomeration and aggregates can be prevented by using steric repulsion, electrostatic repulsion or a combination of both; the electrosteric repulsion. Different types of stabilizing agents can be used and steric stabilization can be achieved by using organic stabilizers such as surfactants, for example CTAB (Kim et al., 2009b), or polymers (PVP[3], PVA[4], PEG[5]) (Luo et al., 2010). By the addition of chloride (Cl^-) or citrate ions (sodium citrate) an electrostatic stabilization can be reached. The stabilization of gold nanoparticles is often achieved by the addition of citrate ions to the aqueous solution (Mpourmpakis and Vlachos, 2009).

Capping agents can also stabilize nanoparticles in suspensions by providing different donor atoms. Most commonly used agents are O- and S-donor types, like carboxylates and thiolates. By replacing these stabilizing agents the surface of the nanoparticles can be functionalized. The nanoparticles are then soluble in other solvents or can be functionalized with other molecules. In general, these surface modifications can be used to create different properties (e.g., surface charge, hydrophobicity) of nanoparticles that can modify their uptake behavior or circulation time in the blood.

Due to the surface modification (stabilizers, polymers, etc.) the particles can have a neutral, positive or negative net charge. Thus, the contact to a solvent (water or cell culture medium, blood) induces an association with tightly bound counter ions and

[3] PVP: poly(vinylpyrrolidone)
[4] PVA: poly(vinylalcohol)
[5] PEG: poly(ethylene glycol)

solvent molecules. This so-called Stern layer is surrounded by a loosely bound layer, the Gouy layer which is composed of free ions (both form the Helmholtz double layer). Due to the Helmholtz double layer, which is enhanced by steric and electrostatic stabilizers, an aggregation of the particles is energetically unfavorable (Christian et al., 2008).

The surface modification can also change the adsorption of proteins to the surface to nanoparticles after intravenous injection in *in vivo* studies or just after the administration in cell culture medium to cells *in vitro*. After the administration of particles via intravenous injection or the addition to serum-enriched medium in cell culture a protein corona on the particle surface is formed (Nel et al., 2009). Serum proteins such as albumin, LDL or HDL interact with the nanoparticle surface and proteins with a high content in the serum are adsorbed very rapidly to the surface. After further incubation these proteins are replaced by proteins with higher affinity to the nanoparticles (so-called 'Vroman effect' VROMAN, 1962). The protein corona which encompasses the nanoparticle additionally influences the interaction of nanoparticles and cell surfaces (Lundqvist et al., 2008; Lynch I. and Dawson, 2008; Marano et al., 2010). The possible interaction of nanoparticles and cells are summarized in Fig. 1.

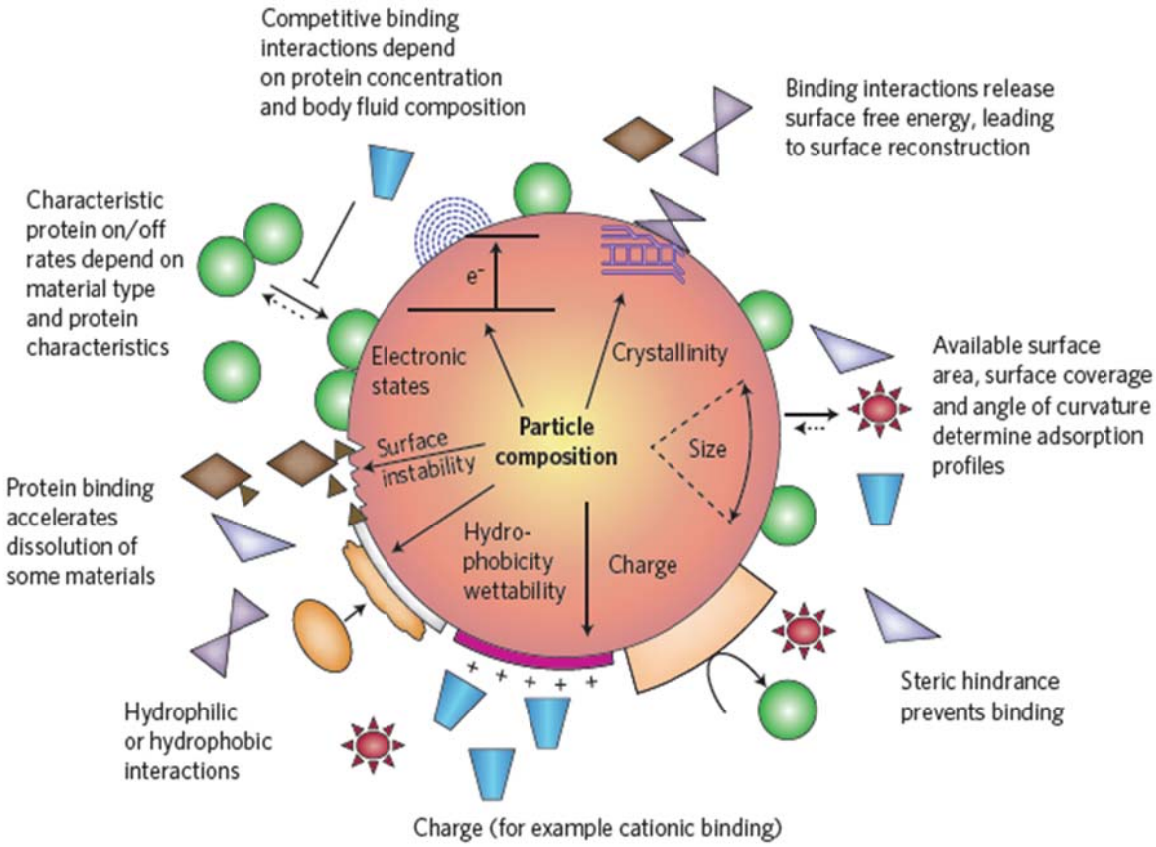

Fig. 1: Nanoparticle composition and characteristics influence the adsorption of proteins
Physicochemical characteristics of nanoparticles influence the adsorption of proteins which on their part can influence the characteristics of the nanoparticles (Nel et al., 2009).

1.2.2 Drug delivery

Different strategies to target cells, tumors and especially the brain have been investigated and improved during the last decades. Besides the novel approach of using targeted nanoparticulate carriers for drug delivery the 'traditional' strategies to target the brain have been widely studied in the past years. In Fig. 2 the traditional and new strategies are depicted.

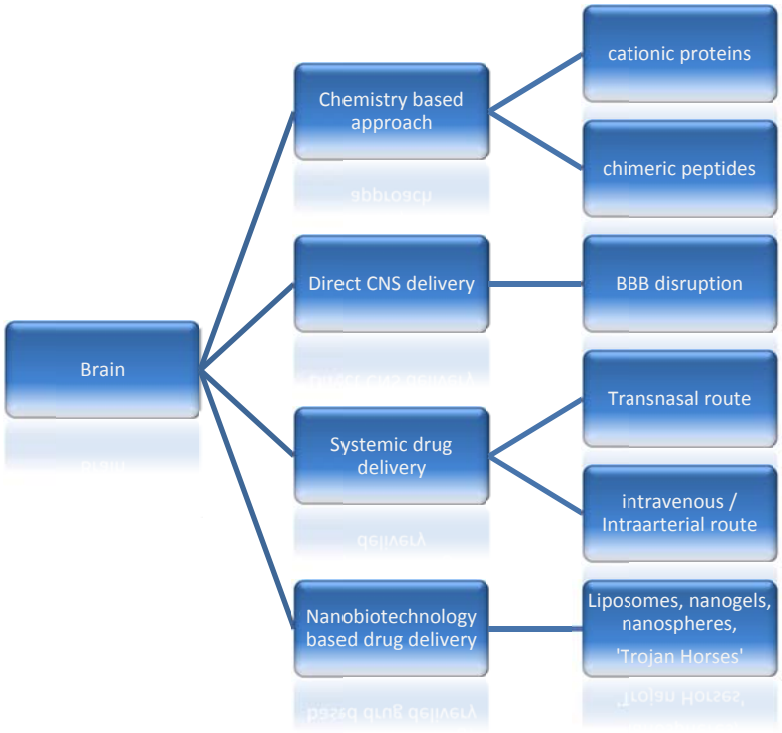

Fig. 2: Strategies for brain targeting
(modified from Alam et al., 2010)

An example for the targeting by chemistry-based strategies is the use of cationic proteins. The positively charged proteins can interact with the negatively charged cell surface and are internalized by adsorptive-mediated endocytosis (Alam et al., 2010; see Fig. 2). Chimeric peptides can be formed by the covalent coupling of the non-permeable peptide drug and a peptide (insulin, transferrin) which is known to be transported over the blood-brain barrier (Pardridge, 2001). The disadvantage of this system is that the drug peptides are not protected from enzymatic degradation. Drugs can also overcome the BBB if they exhibit similarities to proteins which are transported by specific transporters (GLUT-1 or LAT-1). Precursor proteins of dopamine (L-dopa), for example, could be delivered into the brain by using the LAT-1 transporter (large neutral amino acid carrier) (Gabathuler, 2010). In addition, the disruption of the BBB is used to transport drugs across the BBB by paracellular transport. Hypertonic solutions open the BBB by the shrinking the endothelial cells due to the high osmotic pressure (Rapoport, 2000). After loosening the tight junctions, drugs can enter the brain. However, toxic substances can also freely enter the brain and thus cause serious side effects. Intravenous and intra-arterial strategies for delivering drugs to the CNS are often used. After injection the substances should reach the brain via the blood stream. Due to the large number of capillaries in the brain the therapeutics can be taken up by the endothelial cells. The disadvantage for the administration by injection into the blood is the clearance

properties of the immune cells and the low accumulation in the brain tissue due to the active efflux transporters and the rapid clearance from the extracellular fluid (Alam et al., 2010). The non-invasive method of drug delivery through the nasal mucosa is a further strategy to target the brain. The high permeability of the nasal epithelium enables some drug delivery to the brain (Costantino et al., 2007). However, frequent usage of this administration route leads to damage of the nasal mucosa.

The new strategy using nanomaterials is a promising methodology to solve some of the problems associated with drug delivery to the brain. The advantages of the 'traditional' strategies combined with nanoparticles should result in enhanced uptake. Coupling, protection of therapeutics and functionalization with targeting molecules make nanoparticles ideal drug vectors. Due to the specific targeting, doses of therapeutics could be decreased which should also reduce peripheral side effects to other cell types and organs. Targeting tumors and/or the brain with nanostructured particles is currently the major effort under investigation. On account of the tight barrier function of the brain it is very difficult to administer drugs to treat brain diseases. To overcome these problems brain-targeted nanoparticles could enable the transport across the blood-brain barrier und could therefore be used as drug delivery systems (DDS). Nanoparticles that deliver drugs to organs are called nanocarriers. Nanocarriers can be divided into matrix-type systems (nanoparticles) and reservoir-type systems (nanocapsules).

Both nanocarriers systems should exhibit the following properties: (Olivier, 2005; Bhaskar et al., 2010):

- Non-toxic, biodegradable, biocompatible
- Stable in blood
- Should be targeted for better uptake properties
- Non-inflammatory
- No platelet aggregation
- Prolonged incubation times
- Protection of incorporated drugs
- Controlled drug release
- Resistant to transport to efflux transporters within the brain endothelial cell membranes

Several groups have investigated the delivery of different nanoparticles with various targeting molecules to tumors or the brain.

In general, polymeric nanoparticles, several nanospheres, nanosuspensions, nanogels, nanoliposomes and carbon nanotubes have been used for the purpose of crossing the BBB by various endocytotic mechanisms (Alam et al., 2010).

By conjugation of folic acid to human serum albumin (HSA) nanoparticles were shown to exhibit an increased internalization into cancer cells compared to non-targeted nanoparticles and the uptake into other cell types (Ulbrich et al., 2010). The theoretical background of this targeting effect is that folic acid binds to the cancer cells which overexpress the α-folate receptors compared to normal cells (Markert et al.; Park et al., 2005).

It has been shown that the conjugation of insulin or transferrin to HSA nanoparticles leads to enhanced drug delivery across the blood brain barrier (Ulbrich et al., 2009; Ulbrich et al., 2011). Polymers made of PBCA[6] and coated with polysorbate-80 were also able to cross the BBB (Schroeder et al., 1998; Kreuter et al., 2002). In general, the coating with polysorbate-80 enables most nanoparticles to cross the BBB (Alyautdin et al., 1997). The findings of Lück suggest that polysorbate-80 binds to apolipoprotein E (apo E) in the serum which appears to mediate the uptake of the entire complex into the brain (Lück, 1997; Kreuter, 2001). An alternative to nanoparticles made of PBCA are nanoparticles made of PLA[7] and PLGA[8] and coated with mPEG[9] which can be loaded with anti-cancer drugs such as doxorubicin for transport across the BBB (Olivier, 2005). Other nanocarriers such as glucose-derived carbon nanospheres can also overcome the BBB due to their functional similarity to dextran or polysorbate 80 (Selvi et al., 2008).

Liposomes can incorporate lipophilic and hydrophilic drugs. By coating these liposomes with proteins (human serum albumin, transferrin, insulin) a receptor-mediated endocytosis can be achieved. Cationic liposomes can be internalized by adsorptive-mediated endocytosis and thus overcome the BBB (Schnyder and Huwyler, 2005).

Short peptides sequences, with cationic or amphiphatic character which do not exceed 30 amino acids in length and are rich of arginine and/or lysine residues are used as cell penetrating peptides (CPPs). CPPs be conjugated to nanoparticles and are used for drug delivery purposes into cells. CPPs such as nuclear transcription activator Tat protein, Tat-(47–57) the regulator of expression of HIV Rev protein (HIV-1 Rev-(34–50)), the Drosophila Antennapedia protein, Antp(43–58), as well as

[6] PBCA: poly(butylcyanoacrylate)
[7] PLA: poly(lactide-co-glycolide)
[8] PLGA: poly(lactide-co-glycolide acid)
[9] mPEG:methoxypoly(ethylene glycol)

small oligoarginine, (R)n, small oligolysine, and model amphipathic peptide MAP can be used for drug delivery (Futaki, 2002; Fernández-Carneado et al., 2004; Patel et al., 2007). A new previously identified family of peptides with a Kunitz domain derived from proteins such as aprotinin and other human proteins that can cross the BBB, are the angiopeps. They consist of 19 aminoacids, are able to bind to LDL receptor-related protein and demonstrate a high transcytosis rate (Michel Demeule, 2008). Therapeutics such as paclitaxel exhibited an enhanced uptake to the brain when conjugated with angiopep-2 compared to unconjugated paclitaxel (Régina et al., 2008). In addition, it has been demonstrated that angiopep-conjugated PEG-modified poly(amidoamine) dendrimers can be used for gene delivery to the brain (Ke et al.).

As shown above, liposomes, dendrimers and polymeric nanoparticles with and without specific targeting proteins are used for gene delivery (Faraji and Wipf, 2009). Beside these nanoparticles gold nanoparticles can serve as drug delivery systems. Due to the easy fabrication of gold nanoparticles with controlled sizes (Schmid, 1992), the optical properties of gold nanoparticles for imaging purposes, the inert, non-toxic, biocompatible character of the gold core and the possibility for easy surface modifications make gold nanoparticles nearly a perfect system for drug delivery and in general for biomedical applications (Connor et al., 2005).

1.2.3 Gold nanoparticles

Properties

The general characteristics of nanoparticles were briefly summarized in chapter 1.2.1. Gold nanoparticles are of interest for many biomedical applications such as drug delivery, imaging and diagnostics due to their biocompatibility *in vitro* and *in vivo* (Hainfeld et al., 2006, 2006; Sperling et al., 2008). The synthesis of gold nanoparticles is uncomplicated and reproducible. For example, gold nanoparticles can be synthesized by reduction of $AuCl_4^-$ salts with citric acid (Turkevich et al., 1951; Frens, 1973). They exhibit a soft acid character and react with thiols (Bhattacharya and Mukherjee, 2008). The gold-thiol bond enables the gold particles to be easily modified with a variety of self-assembling monolayers made of different polymers (Love et al., 2005).

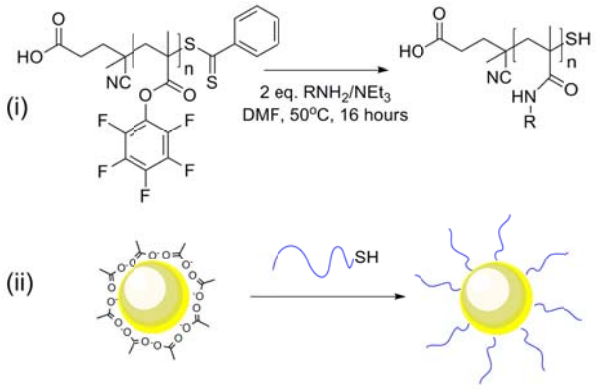

Fig. 3: Formation of polymer monolayer onto pre-formed citrate-coated gold nanoparticles
Citrate-stabilized gold nanoparticles can be coated with different polymers via thiol bonds (with permission of Matthew Gibson, University of Warwick, UK).

By changing the ratio of sodium citrate and $HAuCl_4$ the size of gold nanoparticles can be modified.

Different methods are used to generate unique shapes of gold nanoparticles such as nanorods or nanoclusters (Schmid et al., 1988; Sau and Murphy, 2004).

An important criterion for nanoparticles is that they must be non-toxic when introduced into the host. Therefore, the synthesis of nanoparticles it is important to study the potential to induce cytotoxic effects in cells. Although gold is considered to be inert, biocompatible and non-toxic, a general induced toxicity of gold nanoparticles has to be excluded. Due to the different properties of bulk and nanoparticulate materials even from the same source, makes it imperative to test for possible toxicity.

Nanotoxicology

Although using gold nanoparticles for medical applications appear to be promising due to their biological inert character and their high biocompatibility (Bhattacharya and Mukherjee, 2008) several groups have shown that toxic effects of gold nanoparticles on cells cannot be generally excluded. Gold nanoparticles can cause nephrotoxicity and cell death of erythrocytes (Sereemaspun et al., 2008; Sopjani et al., 2008) *in vivo* and 13nm-sized PEGylated gold nanoparticles have been reported to accumulate in the liver and induce inflammation and apoptosis (Cho et al., 2009). Also, studies with *Daphnia magna* (which is in general used for ecotoxicity studies) demonstrated that gold nanoparticles were toxic after Daphnia were exposed to 70µg/ml for 48 hours (Li et al., 2010b). In addition to the incubation time and the dose of gold nanoparticles, physicochemical properties, such as surface charges, surface modification, shape and size may be responsible for toxic effects. In particular, small gold nanoclusters (1.4nm in diameter) have been shown to have a

higher toxicity, independent of the tested cell type, compared to larger counterparts with a diameter of 15nm (Pan et al., 2007). The toxic effects observed with smaller gold nanoparticles are even observed when cells were exposed to a 100-fold lower concentration. In addition, the surface charge of gold nanoparticles highly influences the uptake properties in cells. Compared to anionic gold nanoparticles, cationic gold nanoparticles possess a higher attraction to the extracellular matrix compounds and / or cell membrane. Thus, the uptake potential into cells due to the attraction to the negatively-charged cell membrane increases with the higher amount of positive charges. Beside the strong propensity for internalization, positive charges of the nanoparticle surface modifications also result in an increased cytotoxicity (Hauck et al., 2008; Nel et al., 2009; Lin et al., 2010). Furthermore, all these studies reveal that although the bulk material is inert the nano-sized counterparts can lead to cytotoxicity due to the decreased size, to the surface modifications with various chemical substances or contaminants (e.g., CTAB Niidome et al., 2006).

As recently published by our group it could be demonstrated that the presence of contaminants, such as sodium citrate, on the surface of gold nanoparticles induce cytotoxicity in human type II alveolocyte (ATII)-like cell lines (A549 and NCIH441; Uboldi et al., 2009).

Beside the induction of toxicity (apoptosis (programmed cell death)) it has been shown that gold nanoparticles could cause oxidative stress, mitochondrial damage, autophagy and induce the expression of pro-inflammatory factors (Pan et al., 2009; Li et al., 2010a; Marano et al., 2010). For drug delivery purposes the induction of these events needs to be prevented. As reactive oxygen species (ROS) are well known to induce cell death and changes in the expression of pro-inflammatory and proliferative factors, the induction of these cell activities after exposure to gold nanoparticles is currently a major focus of investigations. In addition, the importance of endotoxin-free production of nanoparticles is of great importance for nanoparticles that are intended for use in medical applications. Endotoxins, which are also known as lipopolysaccharide (LPS), are known to induce the expression of pro-inflammatory cytokines and sepsis-like consequences (Vallhov et al., 2006). Therefore, *in vitro* studies which focus on the induction of pro-inflammatory mediators need to be performed with endotoxin-free samples to prevent misinterpretations in cell reactivity.

The exclusion of negative effects of nanoparticles on cells *in vitro* is the first barrier which nanoparticles for medical applications have to overcome.

Applications of gold nanoparticles

Through functionalization, gold nanoparticles are currently being used for biological and medical applications. Imaging is one of the oldest applications of gold nanoparticles in medicine and biology. Gold nanoparticles can be conjugated to antibodies which can specifically bind to antigens. By choosing antigens to for example vesicles or membrane receptors these cell compartments can be visualized by different microscopic methodologies due to the increased contrast of the gold. The gold-antibody complex is also used for time-resolved imaging using different optical techniques (Sperling et al., 2008; Boisselier and Astruc, 2009). Gold nanoparticles in contrast agents also improve X-ray tomography *in vivo* by shortening the exposure time (Kim et al., 2007).

Gold nanoparticles can also be coupled to oligonucleotides and used as biosensors for DNA sequences. The coupled oligonucleotide binds to the complementary strand of the DNA by hybridization. On account the presence of several oligonucleotides on the gold nanoparticle surface the particles aggregate and their plasmon resonance frequency changes as a result of the reduced distance between particles. This technique was improved by Mirkin's group and is used for colorimetric detection of different analytes by gold sensors (Mirkin et al., 1996; Jain et al., 2006). In diagnostic applications gold nanoparticles are used in tumor detection and treatment by targeted internalization and drug delivery.

Targeted delivery of gold nanoparticles

After functionalization with folic acid, gold nanoparticles were internalized in folate receptor-positive tumor cells which can then be detected (Dixit et al., 2006). Immunotargeting of tumor cells by gold nanoparticles was also possible by addressing the overexpressed transmembrane glycoprotein, epithelial growth factor receptor (EGFR), which was investigated by Richards-Kortum's group (Sokolov et al., 2003). In addition to the surgical removal of cancer, photothermal therapy can be used. Small gold nanoparticles can improve the therapy, which involves organic or inorganic photoabsorbers, such as indocyanine green and iron oxide, respectively. The small particles are internalized by cancer cells and have the advantage of a fast conversion of light into heat (Hirsch et al., 2003). Thus, the tumor cells can be destroyed by hyperthermia.

In addition to the above-mentioned methodologies gold nanoparticles are also used for targeted drug delivery. Cells internalize nutrients by different endocytotic pathways (see Fig. 6). Thus, targeting of cell-specific receptors by substrates (transferrin, insulin, modified lipoproteins) bound to nanoparticle surface leads to an uptake of the particles by receptor-mediated endocytosis, and this is often used for

targeted drug delivery by gold nanoparticles. The release of BODIPY, a model drug, which was coupled to functionalized gold nanoparticles, has been demonstrated (Hong et al., 2006). Also the chemotherapeutic drug, paclitaxel, has been conjugated to gold nanoparticles and used for drug delivery (Gibson et al., 2007). Large biomolecules, such as proteins or DNA, are also successfully delivered by gold nanoparticles. Plasmid DNA has been bound to the surface of gold nanoparticles. The particles prevent enzymatic degradation of the DNA which is then released by glutathione treatment (McIntosh et al., 2001; Hong et al., 2006). Thus gold nanoparticles are also suitable for gene delivery.

Additionally, the biodistribution of gold nanoparticles can be directed to the target organ or cell type (tumor cells). Gold nanoparticles without specific targeting accumulate in high amounts in the liver. Especially larger particles (5nm–200nm) can be found in the liver after administration by injection, while the accumulation of smaller particles (1.4nm) and negatively charged gold nanoparticles (2.8nm) in the liver is generally less (Hirn et al., 2010). Thus, coupling gold nanoparticles with targeting molecules can prevent the accumulation in the liver, spleen and kidneys. By preventing this unspecific accumulation unwanted effects of gold nanoparticles might be prevented.

As mentioned above, targeting the brain with therapeutics against degenerative diseases (Alzheimer's disease, Parkinson) or brain tumors is of great interest. Due to the complex structure of the neurovascular unit and the regulated transport and active efflux of various substrates, targeting the brain with drugs against brain diseases is not very efficient. For a targeted and improved administration of drugs nanotechnology is a promising tool which is currently under intensive investigation during the past few decades. The hope is that nanotechnology can help solve many problems of today's medicine, and therefore investigation of nanomaterials of relevance for drug delivery and further biomedical applications are of great interest. Their small dimensions and high cell transport properties make nanoparticles excellent candidates for targeted drug delivery into the brain. However, as success depends on overcoming the significant blood-brain barrier (BBB), the latter has become a major focus of investigation (Olivier, 2005; Alam et al., 2010).

1.3 The Blood-brain barrier

The neurovascular unit

The brain is the most powerful organ in the body. Its complex structure, the possibility to process external stimuli and to control all body activities make the brain a fascinating organ. Disorders or brain diseases mostly lead to restrictions affecting

the whole organism. The brain is located in and protected by the skull and is surrounded by the meninges that consist of three layers of thin membranes (*dura mater*, *arachnoid mater*, *pia mater*), which, in addition to protecting the brain, supply it with nutrients and oxygen. The delivery of nutrients and oxygen is guaranteed by a complex capillary system which is composed of macro- as well as of microcapillaries. To ensure the functionality of the brain and to prevent exposure to toxic substances, the microcapillaries constitute a protective unit, the so-called blood-brain barrier.

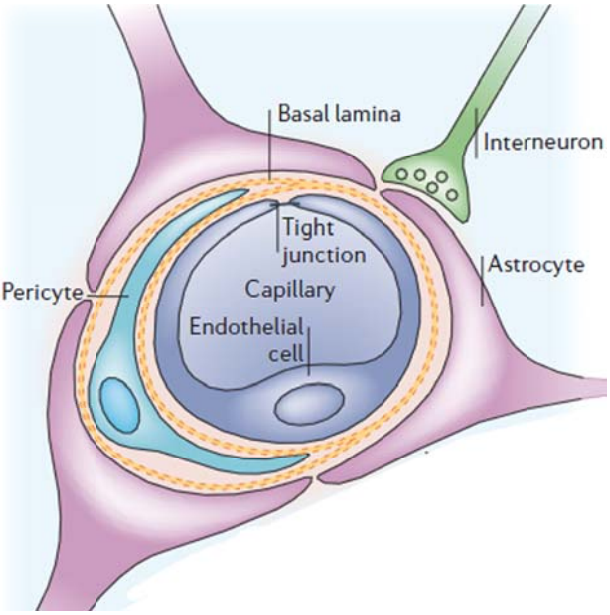

Fig. 4: Neurovascular unit of the blood-brain barrier

The blood microcapillary is lined with endothelial cells that form tight junctions. Pericytes are embedded into the basal lamina that is formed by the endothelial cells and the pericytes, and are enclosed on the abluminal side of the endothelial cells. The foot processes of the astrocytes are in contact with both cell types and ensure the cellular link to neurons (Abbott et al., 2006).

Barriers between external compartments and the brain are known as blood-neural barriers; however, the major focus of research has been directed at the blood-brain barrier (BBB) (Garcia et al., 2004). The BBB is formed by specific endothelial cells which line the inner side of the vessels and are closely connected by tight junctions, have a lack of fenestrations and exhibit less pinocytotic activity than endothelial cells from other parts of the body (Reese and Karnovsky, 1967; Stewart, 2000). Thus, paracellular transport is practically impossible under physiological conditions. Although the barrier is primarily formed by specialized endothelial cells the interaction with other cells such as astrocytes, pericytes and neurons is of great importance to ensure a tight neurovascular unit.

This barrier is highly regulated and is essential for the function and health of the central nervous system (Hawkins and Davis, 2005). In general, *in vitro* studies have shown that pericytes regulate endothelial cell proliferation, survival and vascular branching (Lai and Kuo, 2005). Also the interaction of endothelial cells and astrocytes in the neurovascular unit improve the BBB properties (Tao-Cheng and Brightman, 1988). Especially under pathological conditions the interaction of astrocytes and pericytes with endothelial cells is of great importance. Stroke,

trauma, infections or inflammatory processes, multiple sclerosis, HIV, Alzheimer's disease, epilepsy or brain tumors all influence the permeability of the BBB and thus the interaction of astrocytes and endothelial cells (Abbott et al., 2006).

Cell-cell connections by junctional proteins

A breakdown of the blood-brain barrier implies a decrease in tight junctions of the endothelial cells and increased paracellular transport. Under physiological conditions these tight junctions, which are formed by different membrane proteins such as occludin, junctional adhesion molecules (JAMs) and claudins, prevent paracellular transport (Fig. 5).

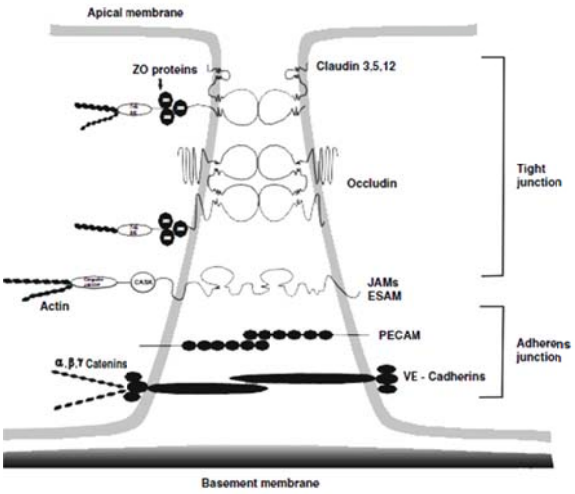

Fig. 5: Tight and adherent junctions of brain endothelial cells

The tight junctions are formed by occludin, junctional adhesion molecules (JAMs) and claudins. The tight junction-associated zonula occludens (ZO) proteins are the linker between the tight junctions and the actin filament within the cells. Adherent junctions are mainly formed by vascular endothelial cadherin (VE-cadherin) and platelet-endothelial cell adhesion molecule-1 (PECAM-1). VE-cadherin is connected with the actin filaments by the catenin proteins (Correale and Villa).

In brain endothelial cells claudin-3 and claudin-5 are expressed which form the primary tight junctions by homophilic and hetereophilic interactions (Morita et al., 1999; Nitta et al., 2003). Further tightness is enhanced by the occludins. Occludin is a 65kDa membrane protein which is expressed in lower amounts in endothelial cells from other parts of the body (Hirase et al., 1997). The homophilic binding of the four loops of two occludin proteins which are anchored in the cell membrane and connected with zonula occludens (ZO-1 - ZO-3) proteins and the actin filament over a short cytoplasmatic carboxy-terminal domain is one of the important connections in establishing functional tight junctions.

Another group of tight junction proteins are the junctional adhesion molecules (JAMs). The homophilic binding of the extracellular domain improves the tight junctions formed by claudins and occludin. The connection to the actin filaments is mediated by Ca^{2+}-dependent protein serine kinases (CASK).

Stabilization of tight junctions depends on various adherent junctional proteins (AJ proteins) such as vascular endothelial cadherin (VE-cadherin) and platelet-endothelial cell adhesion molecules (PECAM-1/CD31). VE-cadherins are connected to the cytoskeleton by α-, β-. γ-catenins acting as adapter proteins. In general, tight junctions and adherens junctions form a unit, which is highly regulated by the level of extracellular Ca^{2+} and phosphorylation of serines and threonines of various tight junction proteins. A decrease in the extracellular Ca^{2+} level leads to conformational changes of the structure of VE-cadherin and results in the dissolution of the bonds (Alexander et al., 1998). Cells treated with calcium-free media also show a redistribution of ZO-1 and occludin, this being initiated by different signaling cascades. Phosphorylation is a second way of regulating the tightness of the tight junctions. Serine and threonine phosphorylation of the tight junction proteins leads to a change in the permeability. The above-mentioned brain diseases also influence the tightness of the barrier by destroying the balance of phosphorylation changing the level of calcium by the release of inflammatory cytokines.

Transport pathways across the BBB

Due to the presence of the tight junctions a regulated transport of nutrients via different pathways across the BBB has to be ensured. The polarity of the endothelial cells is also reflected by the polarity of transporters. Energy-dependent transporters like the ATP-binding cassette- (ABC-) transporter, P-glycoprotein (P-gp) and the Na^{+}- dependent transporters are located luminally or abluminally, respectively. Transport mechanisms are summarized in Fig. 6. Drugs against brain diseases mostly enter the brain by the transcellular lipophilic pathway (b). Small water-soluble agents can overcome the BBB by a paracellular pathway (a), but due to the tight junctions a paracellular transport of larger molecules and lipophilic substances is prevented. Transport proteins like GLUT-1 (glucose transporter-1) or LAT-1 (L-system for large neutral amino acids) for the transport of glucose, amino acids and nucleosides are the third possible transport mechanism present in the blood-brain barrier (c). Some proteins like insulin and transferrin are transported via receptor-mediated transcytosis (d). Plasma proteins like albumin are internalized via adsorptive transcytosis (e). Besides route (b) drug delivery is possible via uptake routes (c) - (e) (Abbott et al., 2006).

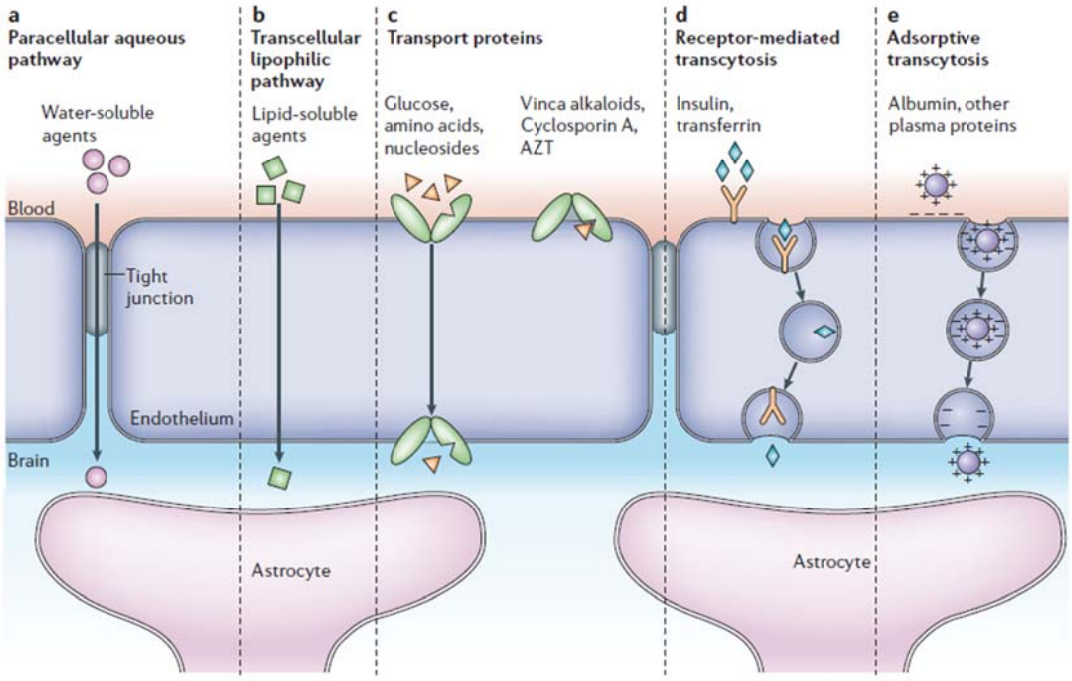

Fig. 6: Transport pathways across the brain endothelial cells

Brain endothelial cells form a tight barrier by expressing different tight junction proteins. Due to the limited paracellular transport nutrients have to be transcytosed by receptor-mediated transport systems. Only small lipid-soluble agents can overcome the barrier without transport pathways (**b**). Transport proteins (**c**), receptor-mediated transcytosis (**d**) and adsorptive transcytosis (**e**) are possible transport mechanisms. The polarity of the endothelial cells is also reflected by the polarized transport functions. Water and small water-soluble agents can overcome the barrier by intercellular transport (**a**) (Abbott et al., 2006).

Internalized drugs have to be exocytosed by endothelial cells to be transported to the brain and to fulfill their therapeutic effect. An accumulation of drugs in brain endothelial cells is often prevented by the efflux transporters that are expressed on the luminal side of the endothelial cells (Schinkel, 1999). These transporters belong to ATP-binding cassette (ABC)-transporters which are known to transport toxic substances and different kinds of xenobiotics back to the blood stream by using ATP as an energy source.

P-glycoprotein (P-gp or ABCB1, a product of the human multidrug-resistance-1 gene (*mdr1*)), multidrug-resistance (associated) protein-1 and -5 (MRP-1, MRP-5 (ABCC) and breast cancer resistance protein (BCRP, ABCG2) are the most investigated and prominent active efflux transporters in brain endothelial cells (Löscher and Potschka, 2005). P-gp transports internalized colchicine and vinblastine back to the blood stream (Drion et al., 1996). Other anti-cancer drugs like doxorubicin and antiepileptic drugs, such as phenytoin, are additional examples for the variety of P-gp substrates (Löscher and Potschka, 2005). In Fig. 7 the localization of several ABC-transporters is depicted.

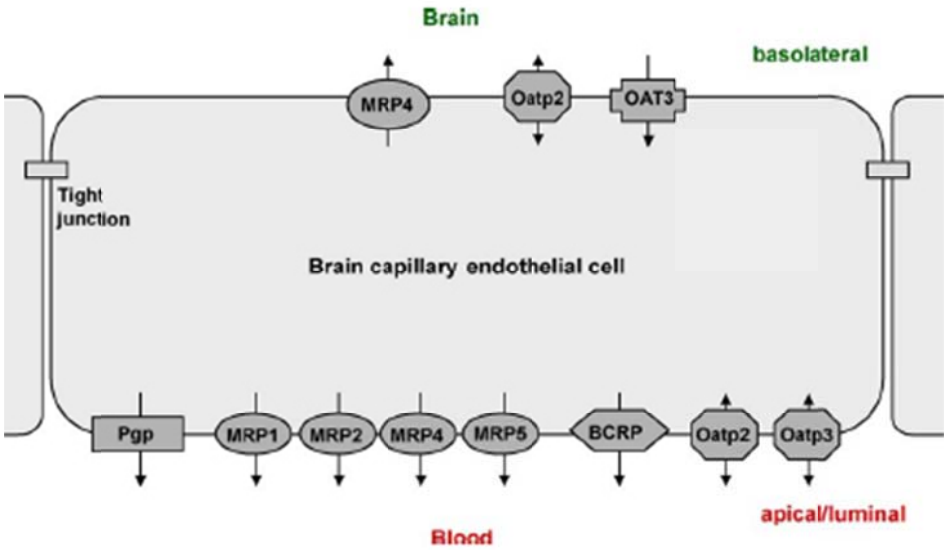

Fig. 7: Polarized location of ABC- efflux transporters in brain endothelial cells

Several efflux transporters are shown which are localized apically and basolaterally. Many other transporters are known but due to their unknown function and/or localization they are not included in this overview. Oatp2/3 are only expressed in rodent brain endothelial cells. The arrow heads represent the transport direction (Löscher and Potschka, 2005).

In vitro blood-brain barrier models

The complexity of the brain and especially of the blood-brain barrier is summarized above. For the investigation of drug delivery and possible effects on the function of the blood-brain barrier, drug transcytosis and the regulation of efflux transporters, *in vitro* model systems have been developed to determine the effects of different drugs, chemicals or nanoparticles on the barriers.

Several models of the blood-brain barrier have been generated by different groups. Gaillard et al. developed a coculture model by using primary bovine brain capillary endothelial cells (BCEC) and rat astrocytes (Gaillard et al., 2001). Coculture models with astrocytes have also been developed by the groups of Kido (Kido et al., 2002), Jeliazkova-Mecheva (Jeliazkova-Mecheva and Bobilya, 2003) and Galla (Franke et al., 2000). Instead of bovine endothelial cells the groups used primary porcine brain endothelial cells.

To be relevant the different models must demonstrate characteristics which are similar to the *in vivo* situation. By building tight junctions the endothelial cells develop a barrier that can be measured by determining the transport of different sized model drugs or the transendothelial electrical resistance (TEER). The TEER-values *in vivo* can reach 1500-2000 Ohm x cm² (Butt et al., 1990), compared to endothelial cells from other parts of the body that exhibit a resistance of approximately 3 Ohm x cm² (Crone and Christensen, 1981).

Isolated primary endothelial cells exhibit those cell properties which are needed to establish a tight barrier. Thus, they are closer to the *in vivo* situation and are therefore highly suitable to mimic the BBB *in vitro*. After isolation, the primary cells are seeded onto a permeable transwell filter membrane to build up a differentiated and polarized monolayer. The properties of the barrier can be improved by the coculture or even triple culture of endothelial cells with other cell types (Fig. 8)

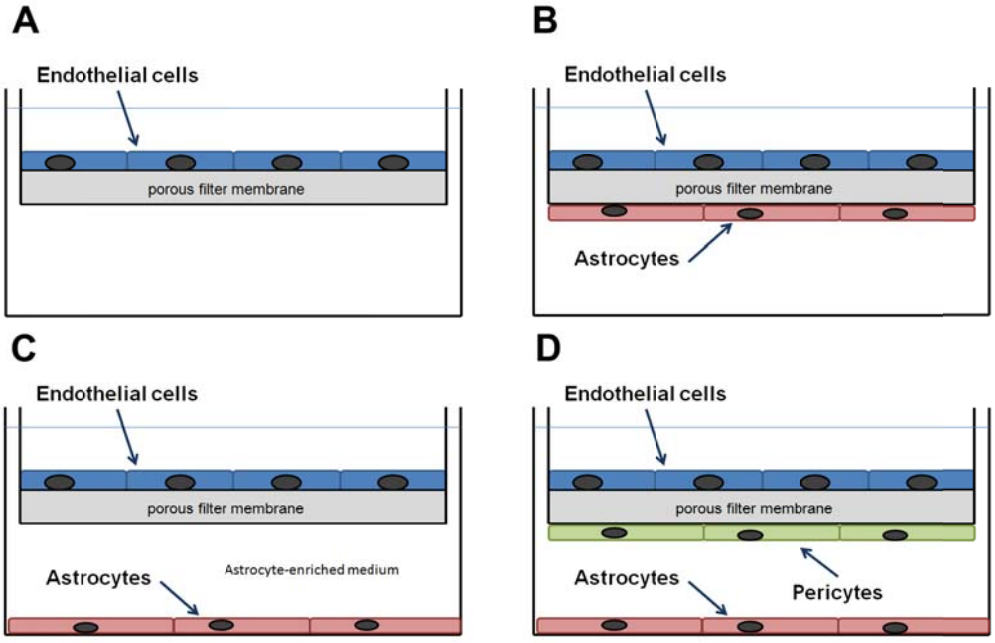

Fig. 8: Different BBB models on transwell filter membranes

(**A**) Monoculture of brain endothelial cells on transwell filter membranes (Zhang 2006). (**B**) Coculture model of brain endothelial cells and astrocytes separated by the porous filter membrane. Choosing different sizes of pores guarantees a direct contact or just a 'communication' by soluble factors (Jeliazkova-Mecheva, 2003). (**C**) Coculture model of brain endothelial cells and astrocytes. Astrocytes are seeded on the bottom of the plate and enrich the medium with factors; no direct interaction possible (Nakagawa 2007). (**D**) Triple- or coculture of brain endothelial cells, pericytes with or without astrocytes (Nakagawa et al., 2007; Thanabalasundaram et al., 2010).

Models using monocultures which exhibit a high TEER value of 300 to 550 Ohm x cm² have also been described (Zhang et al., 2006). The addition of hydrocortisone and the reduction of serum increased the tightness of the barrier (Hoheisel et al., 1998). In addition, components of the extracellular membrane/basement membrane can influence the growth of endothelial cells (Ingber, 1990). Type IV collagen, fibronectin, laminin, and SPARC (secreted protein acidic and rich in cysteine) are the components of the basement membranes (Timpl, 1989). Tilling et al. have demonstrated the influence of different basement membrane proteins in porcine brain capillary endothelial cells in primary culture. The mixture of laminin and fibronectin (1:1), type IV collagen with fibronectin (1:1), but also fibronectin coating

on its own, enhanced the resistance of the barrier compared to rat tail collagen type I coating (Thomas Tilling et al., 1998).

Despite the advantages in using primary cells the disadvantage is the time-consuming isolation. Moreover, there might be differences in the formation of a tight barrier properties from donor to donor. For this reason brain endothelial cell lines are also used to generate blood-brain barrier models. The group of Couraud immortalized a primary human brain endothelial cell type via sequential lentiviral transduction of hTERT and SV40 large T antigen. Characterization and transport studies demonstrated that hCMEC/D3 can be used to mimic the blood-brain barrier *in vitro* and may replace the usage of primary cells (Dauchy et al., 77; Weksler et al., 2005; Poller et al., 2010).

1.4 Aim of the study

Many nanoparticles are synthesized for biomedical usage. Due to the different bulk materials, different synthetic procedures as well as different physico-chemical properties (size, shape, structure, surface charge, etc.) the reactions caused in organisms or even cells have to be investigated to guarantee a biocompatibility of these nanoparticles.

Although the toxicity and uptake behavior of various gold nanoparticles have been investigated by several groups the results presented show conflicting observations in various cell types, so that and a unified conclusion with respect to toxicity, uptake behavior, biodistribution in organisms, the uptake route as well as the fate of nanoparticles in single cells cannot be postulated. Moreover, the lack of standard nanoparticles, methods which fulfill a standard operating procedure (SOP), and other discrepancies in the nanoscience community prevent the comparison of nanoparticle behavior in general.

The aim of this study is to investigate the principle reactions of various endothelial cells after exposure to gold nanoparticles which are produced by the same synthesis route but exhibit different physico-chemical properties. Besides the immune cells in the blood system, endothelial cells are the first cells that come in contact with nanoparticles which are administered by intravenous injection. Thus the reactions of these cells after exposure to nanoparticles are of great importance for medical applications. In attempting to reduce animal experiments the application of primary cells and primary cell culture models which are closer to the *in vivo* situation than cell lines is necessary and is a central goal in this study. In addition to cell toxicity, differential uptake and intracellular fate of the different gold nanoparticles are major parts of this study. The quantification of gold nanoparticles by spectroscopy to

replace quantification by images enables the uptake behavior of thousands of cells compared to the smaller number of cells that can be tested by image analyzes and facilitated the comparison of different uptake behaviors. With the help of this precise quantification method a further aim was to examine if the interaction of cells and nanoparticles which do not exhibit a specific targeting is triggered the by the physico-chemical properties of the nanoparticles, this also being critical for targeted drug delivery. In brief, this study deals with the investigation of gold nanoparticles with five different coatings and three different sizes and the examination of gold nanoparticles that differ in the presence of citrate residues on their surface. Furthermore, selected gold nanoparticles are also tested for their uptake behavior in polarized and therefore highly differentiated brain endothelial cells.

In conclusion, the aim of this study is to perform a systematic investigation of the reactivity of gold nanoparticles with different physico-chemical properties in interaction with different cell types, especially endothelial cells. This approach is necessary to assess possible applications and improvements for gold nanoparticles in medicine and biology.

2 Materials

2.1 Instruments

Table 1: Instruments

Instrument	Company
Digital Camera	Olympus, Hamburg, Germany
Genios Plus	Tecan, Männedorf, Switzerland
Hera Cell 150	Heraeus, Hanau, Germany
Hera Safe	Heraeus, Hanau, Germany
Hydro Control (Plate washer)	Tecan, Männedorf, Switzerland
NanoDrop ND-1000	NanoDrop, USA
Neubauer cell counting chamber	Marienfeld, Germany
PCR Cycler (Gene amp PCR System 9700)	Applied Biosystems, Foster City, California, USA
Real-time PCR cycler 7300	Applied Biosystems, Foster City, California, USA
Roll mixer	Karl Hecht, Sondheim, Germany
Ultramicrotome	Leica Microsystems, Germany
Unimax1010 with Incubator 1000 (plate shaker with heating unit)	Heidolph, Schwabach, Germany
UV table	Bachofer, Waiblingen, Germany

2.2 Microscopes

Table 2: Microscopes

Microscope	Type of microscope	Company
EM 410	Transmission electron microscope	Philips, Eindhoven, Netherlands
Leica DM IRBE	Light microscope with fluorescence unit	Leica, Wetzlar, Germany
Leica DMRE	Laser scanning confocal microscope	Leica, Wetzlar, Germany
Olympus IX71 with Delta Vision	Light microscope with	Applied Precision, USA

Microscope	Type of microscope	Company
	fluorescence unit	
SEM	Scanning electron microscope	Philips, Eindhoven, Netherlands

2.3 Consumables

Table 3: Consumables

Materials	Company
15ml High Clarity Polypropylene Concial Tube (17 x 120mm style)	BD Falcon, NJ, USA
50ml Cellstar Tubes	Greiner bio-one, Tuttingen, Germany
Bioreactor for 3G5 hypridoma cells	CELLine CL1000, IBSINTEGRA Biosciences, Chur, Switzerland
Cell Strainer 40 µm and 100 µm Nylon	BD Falcon, NJ, USA
Cellstar pipettes (2ml, 5ml, 10ml, 25ml)	Greiner bio-one, Tuttingen, Germany
Cover slides (24x50mm)	Menzel, Braunschweig, Germany
Cryo-tube	Nalgene, Rochester, United Kingdom
HTS Transwell 0,4µm #3378 Polyester membrane (=D: clear filters)	Costar/Corning Life sciences, Amsterdam, Netherlands
Ibidi µ-slides	Ibidi, Martinsried, Germany
LabTek II Chamber CC2-treated	Nunc, Roskilde, Denmark
Maxisorp 96-well plates	NUNC, Roskilde, Denmark
Microplates (non-sterile, flat bottom, 96-well)	Greiner bio-one, Tuttingen, Germany
Optical adhesive film (Real-time PCR)	Applied Biosystems, Foster City, California, USA
PCR reaction tubes	Applied Biosystems, Foster City, California, USA
Pipette tips (10µl, 100µl, 1000µ)	Greiner, Solingen, Germany
Pipettes (2ml, 5ml, 10ml, 25ml)	Greiner Solingen, Germany
Real-Time PCR optical 96-well plates	Applied Biosystems, Foster City, California, USA
Scalpels	Braun, Tuttingen, Germany
Thermanox cover slips (12mm)	Roth, Karlsruhe, Germany

Materials	Company
Tissue Culture Flask (12,5cm²)	BD Falcon, NJ, USA
Tissue culture flasks (25cm², 75cm²)	TPP, Trasadingen, Switzerland
Tissue culture plates (6-well, 24-well, 48-well)	TPP, Trasadingen, Switzerland
Tubes (1,5ml, 2ml)	Eppendorf, Hamburg, Deutschland

2.4 Chemicals

Table 4: Chemicals

Chemical	Company
10% Mercaptho-ethanol	Dako, Hamburg, Germany
Acetic Acid	Roth, Karlsruhe, Germany
Agar-100 resin	PLANO, Germany
Agarose	AppliChem, Darmstadt, Germany
Aqua dest.	Braun, Meslingen, Germany
Calcein-AM (1mg/ml, MW = 996g/l)	Molecular Probes, Carlsbad
DAPI (Höchst)	Sigma-Aldrich, St. Luis, USA
DMSO (Dimethylsulfoxid)	Sigma-Aldrich, Germany
dNTP mix	Qiagen, Hilden, Germany
Ethanol	AppliChem, Darmstadt, Germany
Hydrochloric acid	Merck, Darmstadt, Germany
KCl	Calbiochem, Germany
Methanol	AppliChem, Darmstadt, Germany
NaCl	Calbiochem, Germany
Nitric acid	Fisher Scientific, United Kingdom
Paraformaldehyde (3.7% in CS-buffer)	Merck, Darmstadt, Germany
Sodium hydroxide	Roth, Karlsruhe
Sulfuric acid	Merck, Darmstadt Germany
TritonX100	Sigma-Aldrich, St. Luis, USA

Chemical	Company
Tween20	Serva, Heidelberg, Germany

2.5 Buffers

Table 5: Buffers

Buffer	Composition	Used for… (company)
Blocking buffer		CAM-EIA (Roche, Karlsruhe, Germany)
Cacodylat / HCl buffer	16.06g Cacodylat 73.51mg (CaCl2 x 2 H2O 50,83mg MgCl2 x 6 H2O 400ml Aqua dest. (pH7.2 with 4M HCl)	TEM, SEM
CS-buffer	30,25g Pipes (0.1M) 0.38g EGTA (1mM) 40g Polyethylenglycol 4g NaOH adjust to 1l aqua dest.	Solvent buffer for paraformaldehyde
HEPES	(N-[2-Hydroxyethyl]piperazin-N`-[2-ethansulfonsäure])	Washing steps (Sigma, Germany)
PBS (Dulbecco's phosphate buffered saline)	Without magnesium and calcium	Cell culture (GIBCO, Germany)
PBS (Dulbecco's phosphate buffered saline)	10x, sterile solution	Isolation PBECs (Sigma-Aldrich, St. Luis, USA)
PBS (Dulbecco's phosphate buffered saline)	Stock solution (20x) 160g NaCl 4g KCl 4g KH_2HPO_4 adjust to 1l aqua dest.	Washing buffer for ELISA, Western Blot
Sodium citrate buffer (10x)	1M citric acid (24.3ml) 2M di-sodiumhydrogenphosphate (25.7ml)	CAM-EIA
TBE buffer (Tris/Borate/EDTA)	(Tris/Borate/EDTA)	DNA agarose gels (Roth, Karlsruhe, Germany)
TRIS buffer with 1% BSA	TRIS + 1% BSA fraction V (v/w)	ELISA (Roth, Karlsruhe,

Buffer	Composition	Used for… (company)
fraction V		Germany)

2.6 Solutions and cell culture media

Table 6: Solutions and cell culture media

Solution / cell culture media	Concentration	Company
Basal fibroblast growth factor (bFGF)	2,5ng/ml (Stock: 5µg/ml)	Sigma-Aldrich, St. Luis, USA
BSA (Albumine solution from bovine serum)	Stock: 35% in DPBS	Sigma-Aldrich, St. Luis, USA
BSA fraction V (Albumin solution from bovine serum)	ELISA dilutions of antibodies	Sigma-Aldrich, St. Luis, USA
Calcein-AM	Staining of cells	Molecular Probes (Invitrogen), Carlsbad, Germany
Collagen IV from human placenta	0,1mg/ml in PBS (Stock: 1mg/ml)	Sigma-Aldrich, St. Luis, USA
Collagen type I cell matrix solution	1mg/ml in 0.1% acetic acid (Stock: 3mg/ml)	MP Biomedicals, USA
DMEM	Medium for Astrocytes, pericytes	Sigma-Aldrich, St. Luis, USA
EGM-2 + supplements	Medium for endothelial cells	Lonza, Cologne, Germany
Endothelial cell growth supplement	Supplement for 500ml ECBM	PromoCell, Heidelberg, Germany
Endothelial cell basal growth medium (ECBM)	Cell culture medium for endothelial cells	PromoCell, Heidelberg, Germany
Fibronectin	1:200 in PBS (Stock: 1mg/ml)	Roche, Basel, Switzerland
Foetal Bovine Serum (FCS)	Cell culture	Sigma-Aldrich, St. Luis, USA
Gelatine	0,25% in water	Sigma-Aldrich, St. Luis, USA
Gelmount mounting media	Embedding of LabTek chambers	Biomedia

Solution / cell culture media	Concentration	Company
GlutaMAX-I	Cell culture	GIBCO, Carlsbad, Germany
Ibidi mounting medium	Pure	Ibidi, Martinsried, Germany
ITS Liquid Media Supplement (insulin, transferrin, selenic acid)	1:1000 in cell culture medium (Stock: 100x)	Sigma-Aldrich, St. Luis, USA
M-199	Medium for HUVECs	Sigma-Aldrich, St. Luis, USA
Matrigel basement membrane matrix	3D-culture – angiogenesis	Becton Dickinson Labware, Bedford, United Kingdom
MEM	Isolation PBEC	Sigma-Aldrich, St. Luis, USA
o-Phenylenediamine dihydrochloride	1 tablet is dissolved in 50ml citrate buffer and 20µl H_2O_2 was added.	Sigma-Aldrich, St. Luis, USA
Pen Strep (penicillin/streptomycin-mix)	Pen: 10,000 U/ml, Strep: 10,000µg/ml	GIBCO, Carlsbad, Germany
Percoll PLUS	Isolation of PBEC	GE Healthcare, München, Germany
Puromycin	3µg/ml (Stock: 4mg/ml)	Calbiochem, Darmstadt, Germany
Rat tail collagen I	0,1mg/ml in 0.25% acetic acid (Stock: 3,5mg/ml)	BD Biosciences, Pharmingen, Belgium
RNAsin	RNase inhibitor	Promega, Mannheim, Germany
RPMI	Medium for epithelial cells	GIBCO, Carlsbad, Germany
Sodium heparin	10µg/ml (Stock: 20mg/ml)	Sigma-Aldrich, St. Luis, USA
Substrate solution A and B	ELISA	R&D Systems, Wiesbaden, Germany
Transferrin Texas Red	150µg/ml	Molecular Probes (Invitrogen), Carlsbad, Germany

2.7 Enzymes

Table 7: Enzymes

Enzyme	Used for…	Company

Enzyme	Used for…	Company
25% trypsin/EDTA	cell culture	GIBCO, Carlsbad, Germany
Collagenase type I	Isolation of HUVEC	Worthington, Lakewood, NJ, USA
Collagenase type IV	Isolation of PBEC	CellSystems, Troisdorf, Germany
Collagenase/dispase	Isolation of PBEC	Roche, Basel, Switzerland
Dispase (2.36 U/ml)	Isolation HDMEC	GIBCO, Carlsbad, Germany
DNase	Isolation of PBEC	Sigma-Aldrich, St. Luis, USA
DNase (RNase free)	Isolation of mRNA	Qiagen, Hilden, Germany
Horseradish peroxidase (biotinylated with a streptavidin complex) 1:1000 in blocking buffer))	CAM-EIA	Amersham Pharmacia Biotech, Freiburg, Germany
Horseradish peroxidase (with streptavidin)	ELISA	R&D Systems, Wiesbaden, Germany
Trypsin (2,5% w/v)	Isolation HDMEC	Biochrom, Berlin, Germany
Verpene/Trypsin	Isolation of HDMEC	GIBCO, Carlsbad, Germany

2.8 FITC-Dextrans (FD)

Table 8: FITC-dextrans, all purchased from Sigma-Aldrich, St. Luis, USA

Solution	Size	Stock solution	End concentration
Sodium fluorescein	<4kDa	10mg/ml	10µg/ml
FD4	4kDa	250mg/ml	2,5mg/ml
FD20	20kDa	100mg/ml	2,5mg/ml
FD70	70kDa	100mg/ml	2,5mg/ml

2.9 Nanoparticles

Table 9: Nanoparticles (PDI: poly dispersity index; - : unknown)

Nanoparticle	**Composition**	**Surface modification**	**Average size (STEM/DLS)**	**PDI**	**Zeta potential**
AuS0302-RIT	Gold nanoparticle	Sodium citrate residues, while –RIT has less amount of sodium citrate (~8%) compared to –RIS-02, -RIS-04	9,79nm	0.33	-
AuS0302-RIS02	Gold nanoparticle		11,19nm	0.331	-
AuS0302-RIS04	Gold nanoparticle		25nm	0.362	-
AuNP-XX-2	Gold nanoparticle	Ethane diamine	18nm (= XX: 61); 35nm (= XX: 65); 68nm (= XX: 71)		Positive
AuNP-XX-14	Gold nanoparticle	Glucosamine			Neutral
AuNP-XX-17	Gold nanoparticle	Hydroxypropylamine			Neutral
AuNP-XX-23	Gold nanoparticle	Taurine			negative
AuNP-XX-28	Gold nanoparticle	PEG (poly ethylene glycol)			neutral

All nanoparticles were synthesized and characterized by my collaborators from Italy and the United Kingdom. Au-RIS/RIT was synthesized by Daniele Bonacchi from CERICOL – Centro di Ricerche Colorobbia, Via Pietramarina 123, 50059 Firenze, Italy (Uboldi et al., 2009), while AuNPs-XX-YY were produced by Matthew Gibson, Warwick University, United Kingdom.

The synthesis and characterization of AuNPs-XX-YY was described in Gibson et al. (Gibson et al., 2011) and Freese et al. (manuscript submitted).

2.10 Antibodies

Table 10: primary antibodies

Antibodies (from species)	**Dilution (used for…)**	**Company**
3G5	Pure (Immunostaining)	Cell culture supernatant from hypridoma 3G5
CD31 (mouse)	1:50 (Immunostaining, FACS)	Dako, Hamburg, Germany
CD34 (mouse)	1:400 (Immunostaining)	Dianova, Hamburg, Germany

Antibodies (from species)	Dilution (used for…)	Company
Claudin-5 (rabbit)	1:500 (Immunostaining)	AbCAM, Cambridge, United Kingdom
Dynabeads conjugated with antibody against CD31	8-16µl (HDMEC isolation)	Invitrogen, Carlsbad, Germany
EEA-1	1:100 (Immunostaining)	BD Biosciences, Pharmingen, Belgium
ELISA antibodies	See 'Kit systems'	R&D Systems, Wiesbaden, Germany
E-selectin (mouse monoclonal anti-human), (mouse)	1:2000 in blocking solution (CAM-EIA)	BenderMedSystems, Austria
Glial fibroblast associated protein (GFAP) (mouse)	1:200 (Immunostaining)	Sigma-Aldrich, St. Luis, USA
Ki67 (clone MIB-1), (mouse)	1 µg/ml (CAM-EIA)	DAKO, Hamburg, Germany
M-6-P-R	1:100 (Immunostaining)	Calbiochem, Darmstadt, Germany
Occludin (mouse)	1:100 (Immunostaining)	Invitrogen, Carlsbad, Germany (Zymed)
Smooth muscle actin (SMA), (mouse)	1:100 (Immunostaining)	Dako, Hamburg, Germany
VE-Cadherin (mouse)	1:100 (Immunostaining)	BD Biosciences, Pharmingen, Belgium
vWF (rabbit)	1:8000 (Immunostaining)	Dako, Hamburg, Germany
ZO-1 (rabbit)	1:200 (Immunostaining)	Invitrogen, Carlsbad, Germany (Zymed)
β-Catenin (mouse)	1:400 (Immunostaining)	BD Biosciences, Pharmingen, Belgium

Table 11: secondary antibodies

Antibody	Species (dilution)	company
Alexa 488	goat anti-mouse (1:1000)	Invitrogen, Carslbad, Germany
Alexa 488	goat anti-rat (1:1000)	Invitrogen, Carslbad, Germany
Alexa 488	donkey anti-rabbit (1:1000)	Invitrogen, Carslbad, Germany

Antibody	Species (dilution)	company
Alexa 488	donkey anti-goat (1:1000)	Invitrogen, Carslbad, Germany
Alexa 546	goat anti-mouse (1:1000)	Invitrogen, Carslbad, Germany
Alexa 546	goat anti-rabbit (1:1000)	Invitrogen, Carslbad, Germany
Alexa 594	donkey anti-rabbit (1:1000)	Invitrogen, Carslbad, Germany
Alexa 594	donkey anti-goat (1:1000)	Invitrogen, Carslbad, Germany
IgG secondary antibody	anti-mouse (1:1000 in blocking solution, CAM-EIA)	SE Healthcare, USA
ELISA antibodies	See Kit systems	R&D Systems, Wiesbaden, Germany

2.11 Standards

Table 12: Standards

Standard	Company
1kb marker (for agarose gels)	New England Biolabs, Ipswich, MA, USA
Percoll gradient density markers	GE Healthcare, München, Germany

2.12 Oligonucleotide

Table 13: Oligonucleotides (all oligonucleotides were purchased from Microsynth (www.microsynth.ch) with an annealing temperature of ~60°C)

Primer	Forward (5' – 3')	Reverse (5' – 3')
Actin	TAC GCC AAC ACA GTG CTG TCT	TGC ATC CTG TCG GCA ATG
BCRP	CAG GTC TGT TGG TCA ATC TCA CA	TCC ATA TCG TGG AAT GCT GAA G
ICAM	CGG CTG ACG TGT GCA GTA AT	CAC CTC GGT CCC TTC TGA GA
IL-6	AAT GAG GAG ACT TGC CTG GT	TTT CTG CAG GAA CTG GAT CA

Primer	Forward (5’ – 3’)	Reverse (5’ – 3’)
IL-8	TGG CAG CCT TCC TGA TTT CT	TTA GCA CTC CTT GGC AAA ACT
MCP-1	GAT GCA ATC AAT GCC CCA GTC	TTG CTT GTC CAG GTG GTC CAT
MDR-1	TAA TGC CGA ACA CAT TGG AA	AGC TGG ACC ACT GTG CTC TT
MRP-1	GCC GAA GGA GAG ATC ATC	AAC CCG AAA ACA AAA CAG G
MRP-5	CAG AGG ACA CTG CAC AGC AT	AGA AGC GTC ATC TGG CCT AA
RLP13A	CCT GGA GGA GAA GAG GAA AGA GA	TCC GTA GCC TCA TGA GCT GTT
VCAM (QT00018347)	Hs_VCAM1_1_SG QuantiTect Primer Assay	Qiagen, Hilden, Germany

2.13 Kit-Systems

Table 14: Kit-Systems

Kit	Company
CellTiter AQ_{ueous} One Solution Cell Proliferation Assay	Promega GmbH, Mannheim, Germany
CytoTox96 Non-Reactive Cytotoxicity Assay	Promega GmbH, Mannheim, Germany
Human IL-6 Duo Set ELISA	R&D Systems, Wiesbaden, Germany
Human IL-8 Duo Set ELISA	R&D Systems, Wiesbaden, Germany
Human MCP-1 Duo Set ELISA	R&D Systems, Wiesbaden, Germany
Omniscript RT PCR Kit	Qiagen, Hilden, Germany
RNeasy Mini Isolations Kit	Qiagen, Hilden, Germany
SYBR Green master mix	Applied Biosystems, Foster City, California, USA

2.14 Primary cells and cell lines

Table 15: Primary cells and cell lines

Cell type (abbreviation)	Cell type (full name)
hCMEC	Human cerebral microvascular endothelial cells (cell line, purchased from Couraud, France, see chapter 2.14.1.1)
HDMEC	Primary human microvascular dermal endothelial cells
HUVEC	Primary human umbilical vein macrovascular endothelial cells
PBEC	Primary porcine brain endothelial cells
Pericytes	Primary porcine brain pericytes
U373	Human astroglioblastoma cell line (ATCC HTB-17; purchased by LGC Promochem (Germany))
A549	Human alveolar type-II (ATII)-like cell lines A549(ATCC CCL-185,) and NCIH441 (ATCC HTB-174), purchased by LGC Promochem (Germany)
NCI H441	
3G5	Hypridoma cell line that express mAb-3G5, which recognizes 3G5 antigen on microvascular pericytes (ATCC CRL-1814 purchased by LGC Promochem (Germany))

Cell media are summarized in chapter 0.

2.14.1.1 hCMEC/D3 cell culture

The hCMEC/D3 cell type was obtained from the group of Couraud (FRANCE). This brain endothelial cell line, named hCMEC (human cerebral microvascular endothelial cells), was generated as previously described (Weksler et al., 2005). Briefly, the microvascular endothelial cells were isolated from the human brain and immortalized by sequential lentiviral transduction of hTERT and SV40 large T antigen. Subsequently, the hCMEC were characterized by several techniques, including Western blot analysis, expression of cytokine receptors and staining of endothelial cell markers, CD31, vWF, at passage 22 and 33. No change in the expression of cell markers can be observed at the latter passage compared to passage 22.

3 Methods

3.1 Isolation of primary human endothelial cells

3.1.1.1 Isolation of human macrovascular endothelial cells from the umbilical vein (HUVEC; human umbilical vein endothelial cell)

Endothelial cells from the umbilical vein were isolated from fresh umbilical cords. After cleaning the umbilical cord with 70% ethanol and removing mucosal tissue and blood the umbilical vein was cut at both ends. In both ends of the vein a plastic needle was inserted and fixed with a clamp. The umbilical vein was cleaned with HEPES buffer using moderate pressure. After the cleaning procedure the vein was filled with a collagenase type I and HEPES buffer mixture (1:2 v/v) and incubated at 37°C. After 20min the umbilical cord was softly massaged to loosen the endothelial cells. The enzyme-cell suspension was collected in a 50ml tube and PBS was added to a final volume of 50ml. The cells were then centrifuged at 1500rpm for 5 minutes, re-suspended with M-199-medium + 20% FCS + 1% penicillin/streptomycin + ECGS + sodium heparin (both 1:2000) and seeded on a 0.2% gelatine-coated T25-cell culture flask.

3.1.1.2 Isolation of human dermal microvascular endothelial cells from the foreskin (HDMEC; human dermal microvascular endothelial cells)

To isolate endothelial cells from the foreskin, the foreskin was disinfected with 70% ethanol and afterwards washed with PBS. Connective tissue was excised and the dermis was cut into 2x2mm pieces. The tissue was then digested with 5ml dispase at 4°C for 14 to 16 hours. The enzymatic reaction was stopped by the addition of 2ml FCS diluted in 5ml PBS. In the following step the epidermis was separated from the dermis and latter was digested with 5ml verpene and 80µl 2.5% trypsin at 37°C for 2h after which 40ml PBS was added. By pipetting up and down several times the pieces of the foreskin dermis were disassociated. The tissue suspension was filtered through a mesh (Cell Strainer, pore size 100 µm). After a centrifugation step at 1200rpm for 5 minutes the cells were re-suspended in ECBM + Supplement-Mix + 1% penicillin/streptomycin and seeded onto a gelatine-coated T75cm²-culture flask.

The culture medium was changed every 4 days until the cells reached confluence. The endothelial cells were purified from contaminating cells by using Dynabeads conjugated with antibody against CD31. First, 8 to 16µl of Dynabeads/CD31 solution were washed with PBS in tube fixed to a magnet. The Dynabeads/CD31 were then re-suspended in 5 ml PBS + 0.1% BSA and added to the reduced volume of cell

culture medium in the cell culture flask. The beads were incubated with the cells at 37°C for 20 min with shaking of the flask after 10 minutes and microscopic control of the binding of the beads to endothelial cells. After the incubation period the medium was discarded and the cells were detached with 1ml 25% trypsin/EDTA solution and re-suspended in PBS + 10% FBS. The cell suspension was transferred to a 15 ml tube fixed in the magnet. After 1 minute incubation cells labelled with CD31-Dynabeads were located at the side of the tube closest to the magnet. The liquid was discarded and the cells were re-suspended in 3 ml PBS+ 0.1% BSA. The cells were mixed in the tube on a roll mixer at 4°C for 10 min and afterwards put through a 40µm filter. The cells were again washed 3 times with PBS + 0.1% BSA on a roll mixer at 4°C for 10 minutes with magnetic separation and discarding the PBS + 0.1% BSA with each wash. After the washing steps the HDMEC were re-suspended in ECBM + supplement mix + 1% P/S and seeded onto a gelatine-coated cell culture flasks. The cells were grown to confluence, passaged 1:3 and 4h later a second CD31 separation was performed to purify the HDMEC a second time as described above. When HDMEC reached confluence again they can be used for experiments in ECBM + 15% FCS + 1% penicillin/streptomycin + sodium heparin (1:5000) and bFGF (1:500).

3.2 Isolation of primary porcine endothelial cells and pericytes

PBECs (**p**orcine **b**rain **e**ndothelial **c**ells) were isolated from fresh porcine brains as previously described by Unger et al. (Unger et al., 2002b). The protocol with changes is described in the following. The brain was washed with PBS and the meninges were carefully removed. The grey matter was removed from the white matter and saved to another petri dish with PBS. The grey matter tissue was minced into small pieces (1-2mm) and transferred to a 50ml tube. The isolated brain tissue was centrifuged at 1400rpm at 4°C for 10 minutes to pellet the microvascular structures. After removing the PBS the tissue pellet was re-suspended with 2ml collagenase type IV, 1ml DMEM medium and 200µl DNase and the tissue was digested for 30 minutes at 37°C. Every 10 minutes the cell suspension was pipetted up and down several times to help to disassociate the tissue. To stop the enzymatic reaction cold PBS was added to a final volume of 50ml. By centrifugation at 1400rpm at 4°C for 10 minutes the tissue was separated from the PBS and enzymes. The supernatant was discarded and the tissue was re-suspended in 20% Percoll Plus in PBS and centrifuged at 2600rpm at 4°C for 60 minutes. The upper phase of the Percoll gradient was removed and the bottom 10ml which contain the capillary fragments was left in the tube. 40ml PBS were added and the suspension was centrifuged at 1400rpm at 4°C for 10minutes. The supernatant was discarded

and the capillary fragments were digested with a collagenase/dispase mixture with 100µl DNase at 37°C. After 10 minutes the tissue was washed with PBS and centrifuged at 1400rpm at 4°C for 10 minutes. The pellet was re-suspended in 1ml PBS and put on a prepared Percoll gradient (2ml 10x PBS, 13ml PBS, 24ml Percoll Plus, 15µl of each density marker 1,05 and 1,06; centrifuged with 8500rpm for 2 hours without brake). The gradient was centrifuged for 15 minutes at 2600rpm (10°C). The cells between the 1.05 and 1.06g/ml marker were collected and washed with PBS at 1400rpm (4°C) for 10 minutes and seeded in ECBM + supplement mix + 1% penicillin/streptomycin + ITS (insulin-transferrin-selenium mixture, 1:1000) on fibronectin-coated Transwell membranes.

In most cases cells were seeded on the filters of a 24-Transwell plate (polyester membrane with a pore size of 0.4µm) in a volume of 210µl in the upper chamber. The day of isolation is day 0 (d0). The medium was supplemented with 3µg/ml puromycin for 2 days. On day 2 the concentration of puromycin was reduced to 2µg/ml. On day three the medium without puromycin was added.

To isolate porcine brain pericytes the same protocol was used. The cells were seeded on fibronectin-coated culture flasks with ECBM + supplement mix + 1% penicillin/streptomycin but were treated with puromycin for 24 hours. The next day medium was changed to ECBM + supplement mix + 1% penicillin/streptomycin. After the cells reached confluence they were sub-cultivated. After two passages the pericytes have generally overgrown the endothelial cells and were then used for further studies.

3.3 Cell culture

All cells mentioned in these studies were grown under standard cell culture conditions with 5% CO_2, 95% humidity and 37°C in Hera cell 150 incubators. For the handling of cells under sterile conditions a Hera Safe sterile bench was used.

3.3.1 Coating of culture surfaces

The coating of flasks, plates, LabTeks, transwell filter membranes and Ibidi culure dishes with extracellular membrane proteins, like gelatine, fibronectin or collagen increase and improve the adhesion of the endothelial cells to the culture surface. Additionally, it could be shown recently that the use of different coatings influences the expression of several tight junction proteins. A difference in the measured TEER values can also be observed (Tilling et al., 1998). For the coating of the culture surfaces, the flasks were incubated for 1h at 37°C with different dilutions in PBS of collagen I (1:100), collagen IV (1:10) and fibronectin (1:200).

3.3.2 Cell passage and cell seeding

Cells were grown on coated tissue culture flasks and plates. When cells reached confluence they were sub-cultivated as described below. Cell culture medium was discarded and cells were washed once with Dulbecco's phosphate buffered saline (PBS). After incubation with 0.5ml 25% trypsin/EDTA solution at 37°C for 2 minutes the cells detached from the cell culture surface. To stop the enzymatic reaction and to transfer the cells, 5ml of cell culture medium was added. In general, cells were passaged 1:3 to 1:5 in the respective cell culture medium (see Table 16). For experiments cells were counted in a Neubauer cell counting chamber and seeded at the needed cell density. In Table 16 the cell culture media for the different cell types are listed:

Table 16: Cell media for different cell types

Cell type	Medium	Dilution for passage
hCMEC	EGM + 15% FCS + 1% P/S + bFGF (1:500) + sodium heparin (1:5000)	1:4; used until passage 35
HDMEC		1:3; used until passage 3
HUVEC	M199 + 20% FCS + 1% P/S + ECGS + sodium heparin (both 1:2000)	1:3; used until passage 3
U373	MEM + 10% FCS + 1% P/S + 1% sodium pyruvate + 1% GlutaMAX-I	1:5
PBEC	EGBM + supplement mix + 1% P/S + ITS (1:1000)	
Pericytes	see PBEC, without ITS	1:3
A549	RPMI + 10% FCS + 1% P/S	1:4
NCI H441		1:3
3G5	DMEM + 10% FCS +1% P/S	6 million cells per 15ml medium

3.3.3 Freezing / defreezing of cells

To freeze cells, cell medium was discarded and cells were washed with PBS and then trypsinized with 0.5ml trypsin/EDTA until the cells detached. The enzymatic reaction was stopped by the addition of cell culture medium supplemented with FCS. For pelleting the cells were transferred to a centrifuge tube and centrifuged at 1200rpm for 5 minutes. Cells were then re-suspended in FCS including 10% DMSO

(Sigma-Aldrich, Germany) and 1.8ml of the cell suspension was transferred to a cryo-tube. The cryo-tube was put into the -80°C freezer and transferred to the fluid nitrogen tank to guarantee the best store conditions the next day.

For thawing cells were warmed in a water bath and transferred with fresh medium into a coated culture flask (see 3.3.1). Medium was changed after cells attached onto the culture surface.

3.3.4 Angiogenesis

Collagen type I gel matrix

Endothelial cells can be characterized by immunostaining and PCR analysis. Additionally, endothelial cells can be induced to form microvessel-like structures. Endothelial cells were grown on a fibronectin-coated 24-well plate until confluence. The medium was discarded and the cells were covered with 400µl collagen type I cell matrix solution. After an incubation of 30 minutes at 37°C a gel formed and this was carefully covered with 1ml cell culture medium. After 24 hours the angiogenesis of the 3-D culture can be documented by phase contrast microscopy (Leica IBRE). In addition, cells can be stained with Calcein-AM (see 3.5.1).

Matrigel

The Matrigel was thawed on ice and was diluted 1:2 with cold ECBM + 15% FCS + 1% P/S + supplements. 50µl of the mixture was added to a well of a 96-well-plate. The plate was incubated at 37°C for 30 minutes. After the polymerization of the gel 50000 cells were seeded in 200µl medium on the top of the gel. Cells were cultured in the incubator for 24 hours and microscopic images were taken with a Leica IBRE microscope equipped with a digital camera.

3.3.5 Determination of transendothelial electrical resistance (TEER)

The **t**rans**e**ndothelial **e**lectrical **r**esistance (TEER) is measured with an electrode coupled to a millivolt – ohm – meter (EVOM). The TEER value is given in Ohm x cm². The surface area of the filter membrane is 0.33cm². To calculate the appropriate resistance the measured resistance has to be multiplied with 0.33. The formula below summarizes the calculation of the TEER:

$$\text{TEER} = \text{measured resistance} \times \text{surface area [Ohm} \times \text{cm}^2\text{]}$$

The higher the TEER value the lower the permeability through the barrier and the tighter the barrier-model system.

3.3.6 Permeability studies with sodium fluorescein and FITC-Dextrans

The barrier tightness of cells growing on a transwell system can be characterized by permeability studies of different sized FITC-dextrans as well as the measurement of the transendothelial electrical resistance (TEER, see chapter 3.3.5). Cells were grown on fibronectin-coated filters until the TEER values increased to 200 Ohm x cm² (PBEC) or 40 ohm x cm² (hCMEC). To start the transport study the medium of the upper chamber was replaced by 210µl medium + 10µg/ml sodium fluorescein (Na-FITC) or 210µl medium + 2,5mg/ml FITC-Dextran (FD) suspensions. Cells were incubated at 37°C. Every 30 minutes the TEER-value was measured and 50µl of the lower chamber was transferred to a 96-well plate in which 50µl of 1mM NaOH was added. After a total incubation time of 180 minutes the experiment was stopped.

Dilutions of the stock solution starting with 1/10 of the used concentration of every FITC Dextran were used to set up a standard curve (50µl of each dilution in triplicate was added to 50µl of 1mM NaOH, further dilutions 1/2). The fluorescence was measured in the fluorescence reader with an excitation wavelength of λ=480nm and an emission wavelength of λ=585nm. After the calculation of the standard curve the concentration of the FITC dextrans in the downer chamber could be determined and the permeability coefficient could be calculated by using the formula:

$$P_{app} = \frac{V_A}{A \times c_D} \times \frac{dc_A}{dt} \; [cm \times s^{-1}] \,,$$

in which:

V_A : volume of the acceptor compartment [cm³]

A : contact area of the membrane which is in contact to the donor solution [cm²]

c_D : concentration of donor solution [µg/ml]

dc_A / dt: increasing concentration of the acceptor solution over time [µg/ml x s^{-1}]

P_{app} : permeability coefficient (‘k_p –value’) [cm x s^{-1}]

This formula is derived by using the Fick’s laws of diffusion under consideration of infinite-dose conditions. For details see Moderne Pharmazeutische Technologie, 2010, chapter 4.6. A low permeability coefficient characterizes a low drug transport over a membrane and thus a tight barrier.

3.3.7 Generation of mAb-3G5 by 3G5 hybridoma cells in a bioreactor

The cells were grown in a bioreactor in 15ml fresh DMEM + 10% FCS + 1% P/S as recommended by the manufacturer (CELLine classic). Sub-cultivation was done twice a week. Cell suspension was centrifuged and the supernatant was directly

used for immunostaining or stored at 4°C. Cells were seeded in a concentration of 1 x 10^6 cells /ml. The lifetime of the bioreactor was about 3-4 months.

3.4 Treatment with gold nanoparticles and detection methods

3.4.1 Incubation with transferrin-Texas Red

Cells were grown to confluence on coated cell culture plates as described in chapter 3.3. Cells were incubated with fresh medium (ECBM + 1% BSA) and 150µg/ml Transferrin Texas Red at 37°C. After 30 minutes cells were washed with HEPES + 1% BSA and fixed with 3.7% paraformaledhyde. The staining of the cell compartments were done as described in chapter 3.7.2.

3.4.2 Incubation with nanoparticles

Cells were grown to confluence on coated cell culture plates or Thermanox (electron microscopy) as described in chapter 3.3. The medium was discarded and nanoparticle suspensions with different concentrations of nanoparticles were added to the cells. Nanoparticles were diluted in ECBM + 15% FCS + 1% P/S + sodium heparin + bFGF. After the incubation for 4h, 24h, 48h or 72h at 37°C, cells were washed with HEPES + 0.2% BSA (3x) and were fixed for further investigations.

3.4.3 Detection of gold nanoparticles by microscopy and spectroscopy

3.4.3.1 Light / Fluorescence microscopy

After fixation with 3.7% paraformaldehyde and the staining of different cellular structures (see chapter 3.7.2.) cells were examined by light and fluorescence microscopy. Agglomerations / aggregates of gold nanoparticles can be detected by the Olympus/Delta Vision microscope using the DIC filter.

3.4.4 Transmission electron microscopy (TEM)

All the samples for the transmission electron microscope were fixed with glutaraldehyde in cacodylate buffer (1:10; pH 7.2) for 20 minutes at RT. After washing the samples with cacodylate buffer they were stored at 4°C or immediately processed as follows.

Samples were placed in 1% (w/v) osmium tetroxide for 2 hours and and followed by dehydration in ethanol. Samples were then passaged through a propylene oxide solution and embedded in agar-100 resin (PLANO, Germany) and polymerized at 60°C for 48 hours. Ultrathin sections were cut with an ultramicrotome (Leica Microsystems, Germany), placed onto copper grids and stained with 1% (w/v) uranyl

acetate in alcoholic solution and lead citrate. Ultra-structural analysis was performed with a transmission electron microscope EM 410 (Philips; Eindhoven, Netherlands).

3.4.5 Scanning electron microscopy (SEM)

Samples were fixed as described in 3.4.4. The samples were washed with cacodylate/HCl buffer and post-fixed in 2% osmium tetraoxide for 2h. After dehydration through concentration gradients of ethanol from 50 to 100% for 15 minutes each step the samples were dried in HMDS in two steps each for 20 minutes. Afterwards the samples were dried and mounted onto a holder for gold coating in a sputter coater and analyzed by the scanning electron microscope.

3.4.6 Quantification of gold nanoparticles using inductively coupled plasma atomic emission spectroscopy (ICP-AES)

(the quantification by ICP-AES was done by Dr. Matthew I. Gibson at the Warwick University, UK)

50000 cells were seeded on fibronectin-coated 24well plates. After reaching confluence the medium was replaced by the nanoparticle suspension (10µg/ml). After the treatment for 4h and 24h the cells were washed with HEPES + 0.2% BSA, were detached by trypsin incubation and transferred after the addition of 0.9ml PBS to microcentrifuge tubes. The cell suspension was stored at -20°C and was sent to Warwick at room temperature. To the cell lysate solution 0.15ml of aqua regia (3:1 Hydrochloric acid : Nitric acid was added. After incubation overnight, the samples were further diluted to 5ml using milliQ water to give a total sample volume of 5ml. These samples were then analysed for total gold content by inductively coupled plasma atomic emission spectroscopy (ICP-AES). Three different measurements were carried out with each sample.

3.5 Cytotoxicity assays

3.5.1 Calcein-AM cell viability assay

To determine cell viability, the cell culture medium was removed and replaced with 1mM Calcein-AM solution (500µl medium + 2µl Calcein-AM). After incubation at 37°C for 20 minutes viable cells can be detected by fluorescence microscopy. Viable cells hydrolyze the internalized Calcein-AM by an endogenous esterase into a fluorescent calcein and this remains in cells with an intact membrane, i.e. viable cells. The fluorescence was monitored using Leica microscope (Leica DM IBRE) with a 485nm excitation filter and 530nm emission filter system.

3.5.2 Viability test (MTS-Assay)

The MTS-Assay (CellTiter AQ_{ueous} One Solution Cell Proliferation Assay) was used as described by the manufacturer (Promega, Mannheim, Germany).

The tetrazolium component (3-(4,5-dimethylthiazol)-5-(3-carboxymethoxyphenyl)-2-(4-sulfophenyl)-2H-tetrazolium) of the MTS-assay is enzymatically oxidized by dehydrogenases of metabolic active cells. The formazan product can be quantified by the absorption of light at a monochromatic wavelength of λ=490nm. The absorption is proportional to the number of living cells.

10000 cells were seeded onto fibronectin-coated wells of a 96-well plate and grown until 90% confluence. After the exposure to nanoparticles the cell culture medium was removed and stored at -20°C (for LDH detection, see chapter 3.5.5.). The cells were washed twice with a HEPES buffer supplemented with 0.2% BSA. 120µl MTS-medium solution (100µl medium and 20µl MTS stock solution) were added to each well and then incubated at 37°C. After 45-60 minutes 100µl of the solution was transferred to a new 96-well plate and the absorption was measured as described above. For the calculation of the percent viability the blank (no cells with medium and MTS stock solution) was subtracted from all measured values. The mean of the measured absorption of the untreated control cells were set to 100%.

The cells were washed twice with HEPES buffer with 0.2% BSA and fixed with 60µl Ethanol-Methanol mixture (1:2) at room temperature for 20 minutes. After fixation, the cells were washed with PBS, stored in PBS at 4°C and used for the proliferation assay (3.5.3).

3.5.3 Proliferation assay (Ki-67)

The nuclear protein Ki-67 can be detected in cells which are in the G1-, S-, G2- und M-phase of the cell cycle (Sasaki et al., 1987; Morita et al., 1999; NanoCare Consortium, 2009). In resting cells (G_0-Phase) the protein cannot be detected (Gerdes et al., 1984). Thus, the detection of the Ki-67 can be used for determining the proliferation rate of the cells (Scholzen and Gerdes, 2000).

The cells fixed during the MTS assay (chapter 3.5.2) were also used for the detection of Ki-67.

After the cells were washed with PBS + 0.05% Tween 20, 100µl of 0.1% Triton X-100 in PBS was added and incubated at room temperature for 5 minutes to permeabilize the cells. After an additional washing step cells were incubated with the blocking solution and 1% H_2O_2 for 30 minutes to block endogenous peroxidases. Cells were washed again and incubated with 50µl primary anti-human Ki-67 antibody (1:80) at 37°C for 1 hour. After sufficient washing with PBS, 50µl

secondary antibody, coupled with horseradish peroxidase (HRP, 1:400), was added to the cells and incubated at 37°C for a further 45 minutes.

After an additional washing with PBS, 170µl substrate solution (o-phenylenediamine dihydrochloride) in citrate buffer was added to the cells and incubated at 37°C for 15 minutes. 160µl of the substrate solution was transferred to a new 96-well plate and 50µl 3M HCl was added. The absorption of the solution at λ=490nm was measured while the mean absorption of the controls was set to 100%.

3.5.4 Crystal violet staining

The cells used for the MTS and Ki-67 proliferation assay were also used for the crystal violet staining. In this assay the total protein concentration can be determined.

The cells were stained with 50µl 0.1% crystal violet solution at room temperature for 20 min. After washing the cells with water they were air-dried overnight. The next day 100µl acetic acid (33%) was added for 10 minutes. The supernatant was transferred to a new 96-well plate and the absorption was measured at λ=600 nm. The mean of the measured absorptions of the controls were set to 100%.

3.5.5 Cytotoxicity assay (release of lactate dehydrogenase (LDH))

The release of the lactate dehydrogenase by cells into the cell medium is an indicator of cell cytotoxicity. The CytoTox96 Non-Reactive Cytotoxicity Assay is used to detect the released lactate dehydrogenases (LDH). LDH catalyzes the substrate lactate to pyruvate and NADH + H^+. NADH + H^+ reduce tetrazolium salt to formazan. The absorption of formazan was then measured at a wavelength of λ=490nm.

The release of LDH of untreated cells was used as a control and the LDH activity of lysed cells was set to 100%. [(Absorption sample – absorption of Au-NP) / Absorption 100% lysis] x 100 = % of cytotoxicity

3.6 Molecular biology

3.6.1 Cell characterization by polymerase chain reaction

After cells were grown to confluence the cell supernatant was discarded. The cells were washed with PBS and detached by the addition of RLT buffer with 10% mercaptho-ethanol. The RNA was isolated as described in 3.6.2 and translated to cDNA as described in 3.6.3. Cell and gene-specific primers were used for the characterization of cells by polymerase chain reaction (see 3.6.4).

3.6.2 Isolation and quantification of RNA

The RNA isolation was performed with the RNeasy Mini assay from Qiagen. The assay was used as recommended by the manufacturer. The elution of the RNA was done with 17µl RNase-free H_2O.

The quantification of the RNA concentration was photometrically determined using the NanoDrop ND1000 spectrophotometer. 1µl of the eluted RNA-solution was used to determine the RNA concentration. The absorption at the wavelength λ = 260nm and λ = 280nm was measured to investigate the purity of the samples. Purified RNA has an absorption quotient ($absorption_{260nm}$ / $absorption_{280nm}$) of 2.0. Water was used as a blank and to synchronize the NanoDrop system. The concentration of the RNA was calculated by the NanoDrop software as follows:

$$c \left[\frac{\mu g}{ml} \right] = OD_{260nm} \times \text{dilution factor} \times \text{extinction coefficient}$$

The molar extinction coefficient of RNA is 40. The RNA was used for the synthesis of cDNA and stored at -80°C.

3.6.3 cDNA-synthesis: reverse transcription polymerase chain reaction (RT-PCR)

1µg RNA and the Omni-Script RT-PCR Kit was used as recommended by the manufacturer for cDNA synthesis. The pipetting scheme is depicted in Table 17. After the RT-PCR the samples were stored at -20°C.

Table 17: Pipetting scheme and PCR program

Pipetting scheme	RT-PCR program
x µl RNA (1µg)	
2µl 10x buffer	
2µl dNTP mix (5mM each dNTP)	
2µl oligo dT Primer (10µM)	37°C for 1 hour, storage at -20°C
1µl RNAse Inhibitor (10U/µl)	
1µl Omniscript	
adjust to 20µl RNAse free water	

3.6.4 Polymerase chain reaction (PCR)

After the isolation of the RNA (3.6.2) and the synthesis of the cDNA (3.6.3) the investigation of the expression of different genes in various cell types was carried out by the polymerase chain reaction (PCR). Different gene specific oligomers (primers, diluted 1:10 in water) designed with a tool on the genescript.com

homepage, checked by BLAST/NCBI and purchased from Microsynth (www.microsynth.ch) were used in combination with the Taq PCR core kit. The primers are listed in Table 13. The pipetting scheme and the PCR program used is depicted in Table 18:

Table 18: PCR pipetting scheme and PCR programm

Pipetting scheme	PCR program
2µl Template (diluted 1:20 in water)	94°C, 2min
2.5µl 10x buffer	94°C, 30s*
0.5µl dNTP mix (5mM each dNTP)	60°C, 30s*
0.5 Forward primer (1:10)	72°C, 30s*
2.5µl Reverse primer (1:10)	72°C, 10min
0.125µl Taq Polymerase (10U/µl)	4°C until use or storage at -20°C
14.875µl water	(* = 35 cycles)

After the amplification by PCR the reaction was diluted with sample buffer and run on a 2% agarose gel + 0.02% ethidium bromide to separate the DNA by length using gel electrophoresis (80 Volt for 1h in 1% TBE-buffer). To determine the size of the DNA fragments a 1kb marker was used. Due to the intercalation of ethidium bromide into the DNA double helix the different bands can be visualized and monitored by UV-light. Images were obtained with an Olympus digitial camera and colors were inverted by Adobe Photoshop CS3 or CS5.

3.6.5 Quantitative real-time PCR

The PCR can also be used for the semi-quantification of the PCR products. This method is called quantitative real-time PCR. A fluorescent dye (SYBR green I) is used for the quantification process. For each sample 4µl cDNA (1ng/µl), 12.5µl SYBR green master mix, 0.25µl of each primer (forward and reverse) and 8µl water were used. Real-time PCR was done in triplicate for each cDNA. The following cycler program was used: 95°C 10min, (95°C 15s, 60°C 30s) x 40 cycles, dissociation step: 95°C 15s, 60°C 1min and 95°C 60s.

After each PCR cycle the amount of SYBR green intercalated into the double helix of the DNA is measured and plotted. Ribosomal protein 13A (RPL13A) was taken as an endogenous standard and the relative gene expression was determined using the ΔΔCt method. Gene expression of the untreated controls was set to the reference value 1.

3.7 Protein biochemical methods

3.7.1 ELISA

The enzyme-linked immunosorbent assay was used to analyze cytokines released into the cell culture supernatants by cells. Cells were grown on fibronectin-coated 96-well or 24-well plates and stimulated with nanoparticles in different concentrations. The supernatant was collected and stored at -80°C.

To quantify the amount of released cytokines into the cell culture supernatant, NUNC Maxisorp 96-well plates (NUNC, Roskilde, Denmark) were coated with the primary capture antibody (R&D Systems, Germany) at room temperature on a shaker (50rpm) overnight. The antibodies were used as recommended by the manufacturer. The plates were washed and blocked with 100µl PBSA (1% fraction V, Roth, Karlsruhe) at RT for 1h. The plates were washed with PBS + 0.05% Tween20. 100µl of the diluted supernatants (1:3 diluted in PBSA or TRIS + 1% BSA (IL-8)) of the stimulated cells were added. The plates were incubated at 37°C for 2h. Standards were diluted and also transferred to the prepared plates for 2 hours. The standard dilutions are listed in Table 19.

Table 19: Cytokine standard dilutions

Cytokine	Stock solution of standard	First dilution	Dilution steps	Number of dilutions	Diluted in…
ICAM	70ng/ml	1000pg/ml	1:2	8	PBSA (1%)
IL-6	35ng/ml	600pg/ml	1:2	8	PBSA (1%)
IL-8	110ng/ml	2000pg/ml	1:2	8	TRIS + 1% BSA
MCP-1	70ng/ml	1000pg/ml	1:2	8	PBSA (1%)
VCAM	70ng/ml	1000pg/ml	1:2	8	PBSA (1%)

After the 2 hours of incubation the plates were washed 3 times with PBS + 0.05% Tween20. The respective secondary antibodies (R&D Systems, Wiesbaden) were diluted in PBSA (1%) and TRIS + 1% BSA for IL-6, ICAM, VCAM and IL-8, respectively. 100µl of the antibodies were added to each well and incubated for 2 hours. After washing the cells (3x), 100µl streptavidin-HRP (R&D Systems, Wiesbaden, diluted 1:200 in the same buffers as was used to dilute the antibodies was added to the wells and incubated at room temperature for 20 minutes. Cells

were washed with PBS + 0.05% Tween20 and incubated with a mixture (1:2) of substrate reagent A and substrate reagent B (R&D Systems, Wiesbaden). The reaction at room temperature was stopped by the addition of 50µl 2N H_2SO_4 after 20 minutes and the absorption was measured at λ = 450nm. Based on the dilutions of the supernatants and the standard curves the concentrations of the different cytokines could be calculated.

3.7.2 Staining of cell compartments and cell membrane proteins

Cells were grown on fibronectin-coated culture flasks, 6-well plates, Ibidi µ-slides or LabTeck chambers.

Afterwards cells were fixed with 3.7% paraformaldehyde in CS buffer, permeabilized by the addition of TritonX100 in PBS and stained with different antibodies. Species specific fluorescent secondary antibodies were used for the detection. In addition, cell nuclei were stained with DAPI and the samples were embedded with Fluoro Mount or Ibidi mounting medium and covered with a 24mm x 50mm cover slip. Fluorescence microscope and laser scanning confocal microscope (Leica DMRE) were used for the detection and image capture.

4 Results

4.1 Characterization of human cerebral microvascular endothelial cells (hCMEC)

The **h**uman **c**erebral **m**icrovascular **e**ndothelial **c**ell line, hCMEC, was received from the group of Dr. Pierre-Oliver Couraud (Institut Cochin, Centre National de la Recherche Scientifique UMR 8104, Institut National de la Santé et de la Recherche Médicale (INSERM) U567, Université René Descartes, Paris, France). In Weksler et al. (2005) the cell line was described and characterized using several methods. By microscopic investigation of cell morphology and of special endothelial junctional cell markers (PECAM-1 and VE-Cadherin) as well as junction-associated proteins (β-catenin, γ-catenin, ZO-1, JAM-A, and claudin-5) and Western Blot analysis of the expression of brain-specific ABC transporters (P-glycoprotein) hCMEC were characterized as brain microvascular endothelial cells with typical brain endothelial cell characteristics. Also the barrier function of the hCMEC was confirmed by transport studies with different-sized FITC-dextrans and determination of the permeability coefficient. After receipt of the hCMEC cell line, a re-characterization was performed to confirm the findings of Weksler and Förster (Weksler et al., 2005; Forster et al., 2008). In Fig. 9 the morphology of hCMEC in passage 27 is shown. The cells showed an endothelial-like, contact-inhibited morphology (A). Additionally, hCMEC were able to form vascular-like structures in Matrigel after 24 hours following seeding (B).

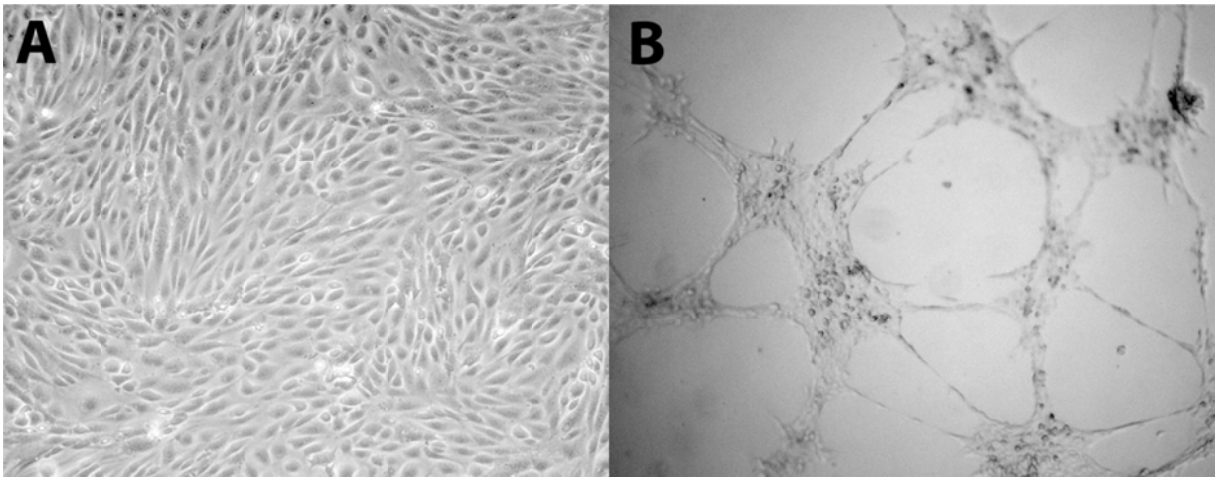

Fig. 9: Morphology and formation of vascular-like structures of hCMEC in passage 27

(A) Cells were grown on fibronectin-coated cell culture flasks in PC-medium. A confluent cell layer of hCMEC with a specific endothelial-like morphology could be detected (Phase contrast microscopy, 10x). (B) After 24 hours of seeding hCMEC on Matrigel, vascular-like structures could be demonstrated (Leica DM IRBE, 5x).

In Fig. 10 the staining of von Willebrandt factor and the adherens junction proteins, PECAM-1 and VE-Cadherin, in hCMEC and HDMEC is shown. The comparison of images of hCMEC and HDMEC indicates that hCMEC expresses typical endothelial cell marker proteins. HDMEC were characterized as cells with typically endothelial cell characteristics (Unger et al., 2002a). Compared to the data and images published by Weksler and group, hCMEC exhibit the same cell markers after staining with specific antibodies and counter-staining with Alexa 594-coupled secondary antibody.

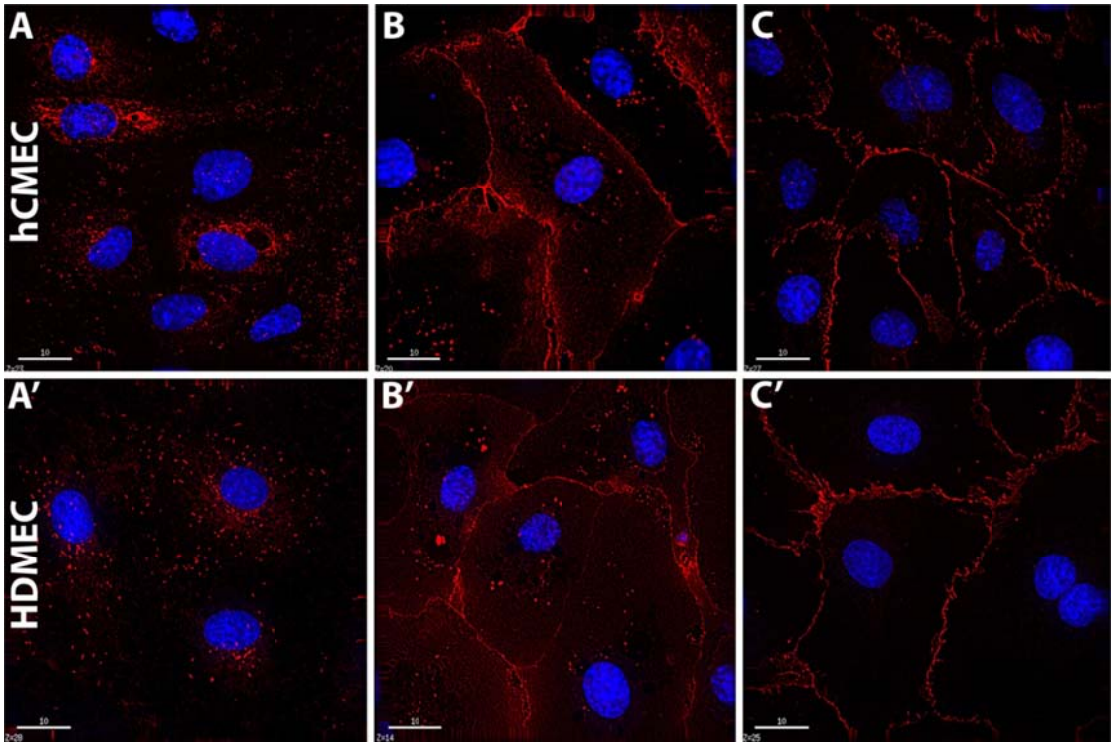

Fig. 10: Expression of endothelial cell markers in hCMEC and HDMEC

hCMEC and HDMEC were grown on fibronectin-coated LabTek chambers and fixed with paraformaldehyde. Cells were stained for von Willebrandt factor (**A, A'**), PECAM-1 (**B, B'**) and VE-cadherin (**C, C'**) (all in red). Nuclei were stained with Hoechst. (fluorescence microscopy (Delta Vision), 60x).

In Fig. 11 the adherens correlated protein, beta-catenin, and the tight junction proteins, claudin-5 and ZO-1, in hCMEC were stained. The results show that hCMEC form typical tight junctions which are important in the formation of a tight BBB.

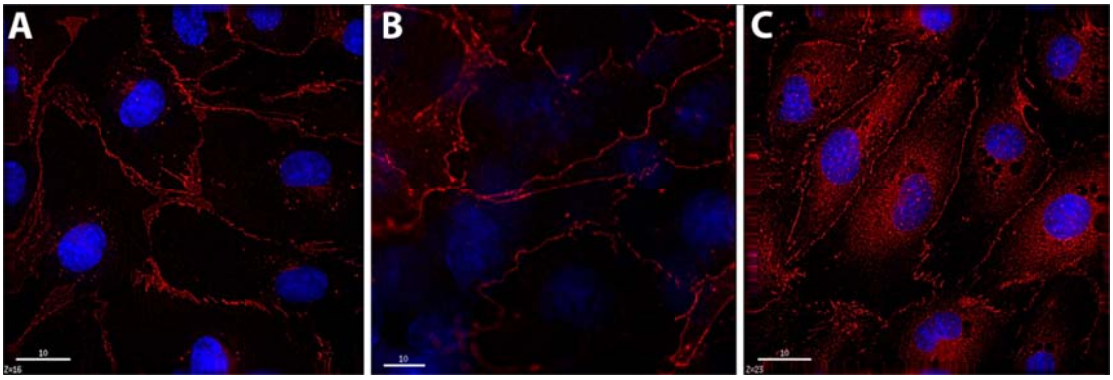

Fig. 11: Expression of AJ- and TJ-proteins in hCMEC

hCMEC were grown on fibronectin-coated LabTek chambers (B, C) and fixed with paraformaldehyde. Cells were stained for β-catenin (**A**), claudin-5 (**B**) and ZO-1 (**C**) (all in red). Nuclei were stained with Hoechst. (fluorescence microscopy (Delta Vision), 60x).

After the isolation of hCMEC RNA and reverse transcription to cDNA the gene expression of different ATP binding cassette (ABC) transporters in hCMEC were determined. HDMEC and HUVEC cDNA was also investigated by using the specific primer pairs listed in Table 13. In Fig. 12 the results of the PCR amplification of hCMECs, HDMEC and HUVEC cDNA with different primers is shown. The comparison of the gene expression of multidrug resistance protein-1 (MRP-1), MRP-5 and breast cancer resistance protein (BCRP) indicated that all three transporters were expressed in endothelial cells. Different results in the gene expression could be observed by using the specific primers for the ABC-transporter P-glycoprotein (P-gp/ *mdr-1 gene*). Although MRP-1, MRP-5 and BCRP were expressed to some extent in all the examined endothelial cell types, MDR-1 was present only in hCMEC. The results were similar to those which were published by Dauchy (Dauchy et al., 77) and support the brain endothelial characteristics of hCMECs.

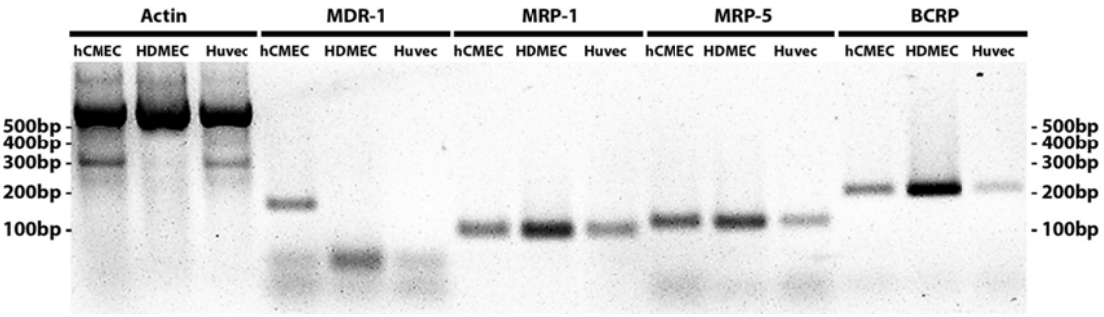

Fig. 12: Analysis of ABC-transporter gene expression in hCMEC, HDMEC and HUVEC by PCR

The comparison of the gene expression of ABC-transporters in different endothelial cells is shown. Cells were grown to confluence and lysed by RLT-buffer with mercapthoethanol. RNA was isolated and transcribed to cDNA. By using specific primers for different ABC transporters and analyzing the results of the gene expression by electrophoresis on a 1% agarose gel differences in the expression can be observed.

4.2 Characterization of primary porcine brain microvascular endothelial cells (PBEC) and pericytes

The PBECs (**p**orcine **b**rain **e**ndothelial **c**ells) were isolated from freshly obtained porcine brains. After the isolation process the small microvessels were directly seeded into transwells or examined for morphology and staining experiments after culture on cell culture plates. After several days the endothelial cells started to grow out of the microvessels. The process of outgrowth is depicted in Fig. 13.

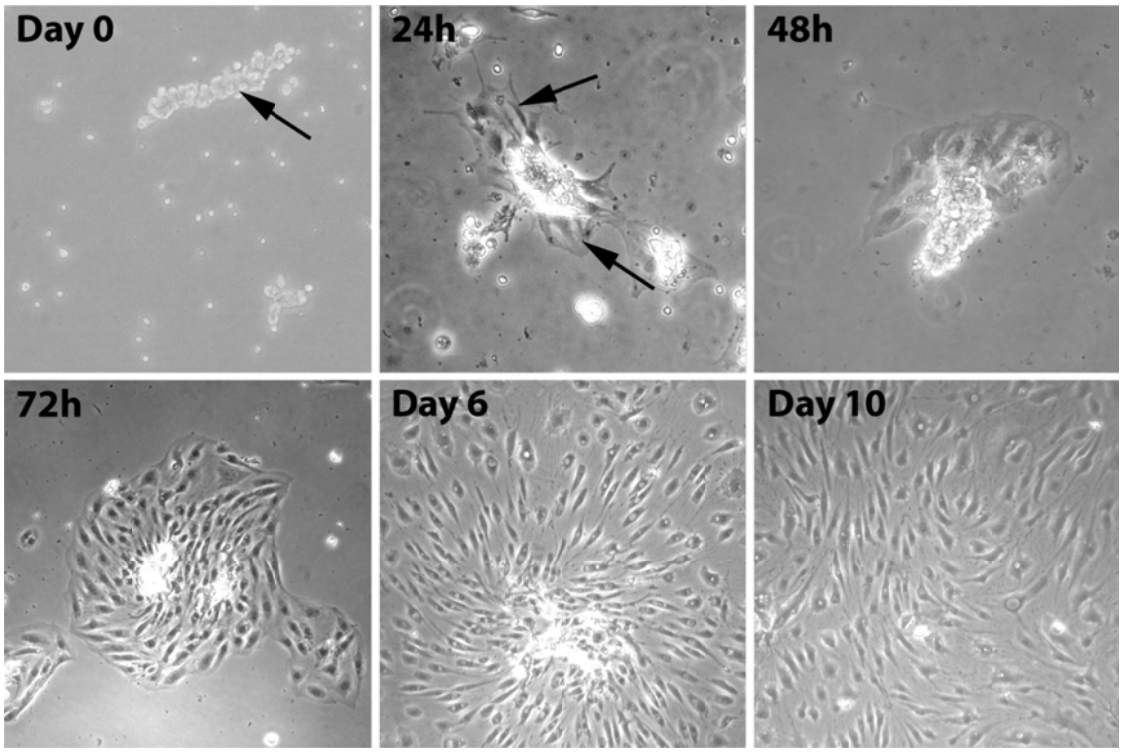

Fig. 13: Outgrowth of primary porcine brain endothelial cells after isolation

After the isolation process small microvessels were seeded on cell culture plates. **Day0** shows a capillary fragment (arrow) shortly after isolation. After 24 hours the first cells can be seen growing out of the capillaries (**24h**; arrow). The proliferation of cells over the next days is presented in **48h** to **Day10**. After day 10 a confluent cell layer has developed. Images were made by phase contrast microscopy (Leica, DM RE; 5x, 10x or 20x) after different time points.

Using the same isolation protocol two different cell types can be isolated. In Fig. 14, isolated porcine endothelial cells and pericytes are shown. The PBEC have an endothelial-like cell morphology. After an extended cultivation the cells exhibit many large vacuoles especially in the perinuclear region (data not shown). The PBEC cell morphology initially exhibited round and swollen cells (see Fig. 14 (A, arrow head)). In contrast to the endothelial cells, pericytes have a long and spindle cell morphology which was also observed *in vivo* where one cell covered several endothelial cells. In Fig. 14 C endothelial cells form tube-like structures after seeding

in a collagen type I gel. The viability of the cells was checked by the Calcein-AM assay (Fig. 14 D).

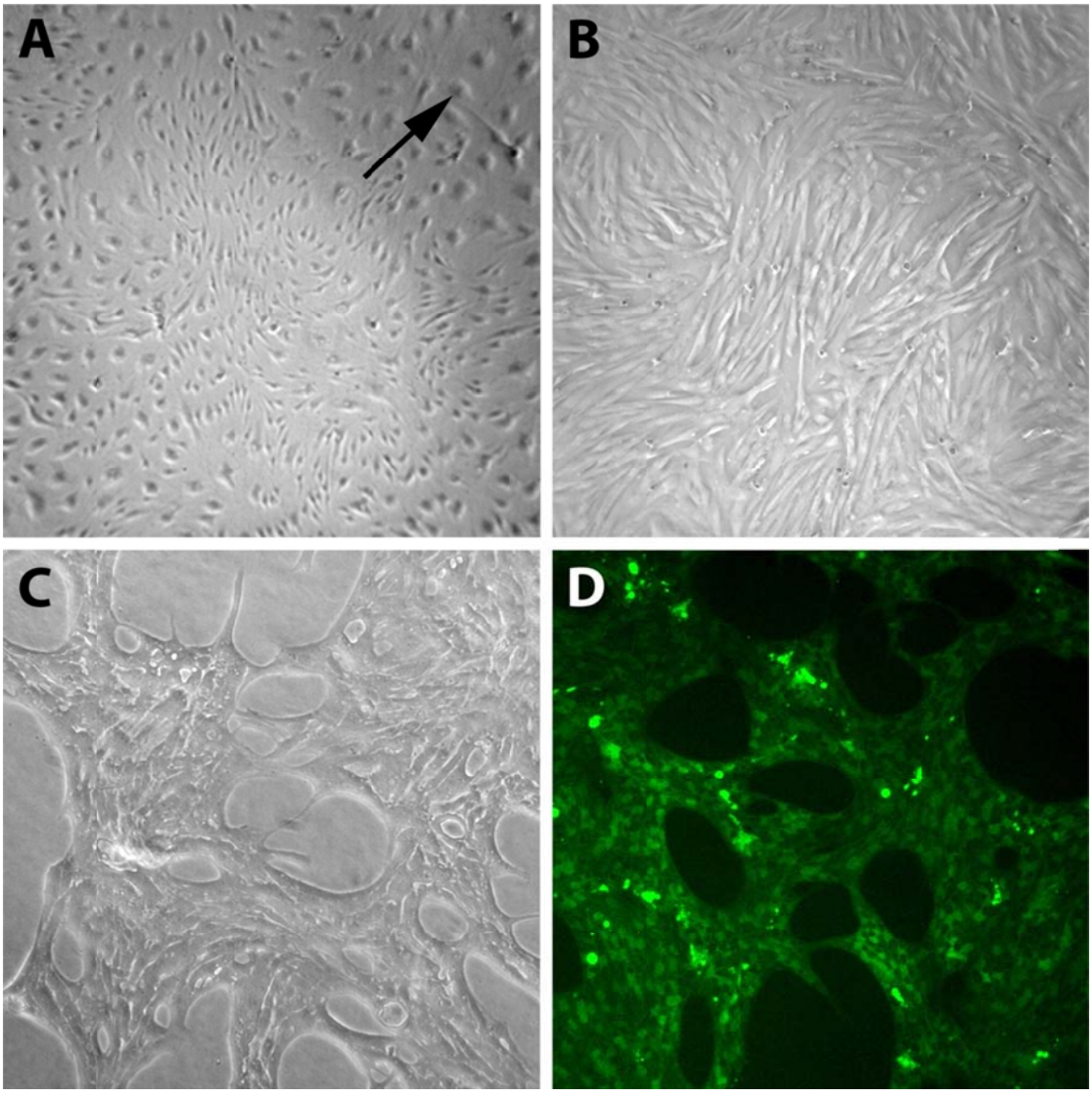

Fig. 14: Morphology of PBECs and primary porcine brain pericytes (PPBPs) and vascularization of PBECs in collagen type I gel.

The different morphologies of PBECs and pericytes are shown in (**A**) and (**B**), respectively. In (**C**) tube-like structures of PBECs could be detected after growing the cells in collagen type I gel. In (**D**) the cells were stained with calcein-AM to show that they were still viable. (Leica DM IBRE, 5x, 10x).

The PBECs were further characterized by FACS analysis (data not shown) and immunofluorescent staining. In Fig. 15 the staining of endothelial-specific cell markers are shown. In Fig. 15 A and B the staining of tight junction-associated protein *zonula occludens* (ZO-1) and of the tight junction protein occludin is shown, respectively. Fig. 15 C to E depict the expression of the adherens junction proteins, beta-catenin, VE-Cadherin, and PECAM-1 (CD31). The staining for alpha actin in the brain endothelial cells was negative (data not shown). However, freshly isolated

pericytes express alpha smooth muscle actin (Fig. 15 F), but were negative for endothelial cell markers, such as CD31 (data not shown).

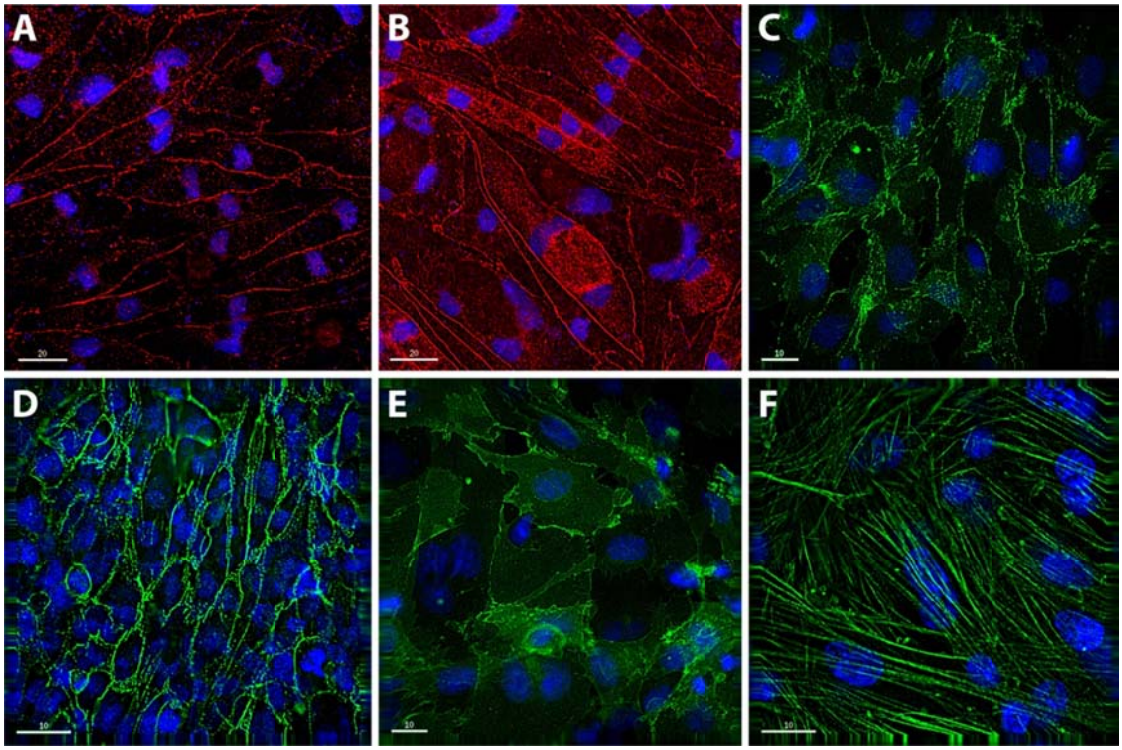

Fig. 15: Expression of tight junction and adherens junction proteins in PBEC and smooth muscle actin expression in pericytes

After fixation of cells with 3.7% paraformaldehyd PBECs were stained for tight and adherens junction proteins. In (**A**) the staining of ZO-1 (red) is shown. The following images represent the staining of occludin (red, **B**), beta-catenin (**C**), VE-Cadherin (**D**) and CD31 (**E**). In (**F**) the staining of alpha actin in porcine brain pericytes is shown. Nuclei are stained in blue (Hoechst). (Delta Vision, fluorescence microscope (40x and 60x).

A specific marker of microvascular pericytes was developed by Nayak and coworkers in 1988 (Nayak et al., 1988). A hybridoma cell line 3G5 was developed (see chapter 3.3.7) and the mAB produced was shown to specifically react with porcine pericytes in monoculture (data not shown). Additionally, the pericytes were stained with mAB 3G5 in a triculture with hCMEC and U373 (astroglioma cell line). The indirect immunostaining shows that the pericytes (green) lined the microcapillaries generated by endothelial cells (red) but are not directly co-localized with the specific cell marker of endothelial cells (Fig. 16 A). The staining of pericytes was also successful in thin human brain sections (Fig. 16 B). The 3G5-positive cells were also located around the microcapillaries but not in the periphery between the microvasculature. The results presented in Fig. 16 demonstrate that mAB 3G5 can be used for the specific immunostaining of primary porcine brain pericytes.

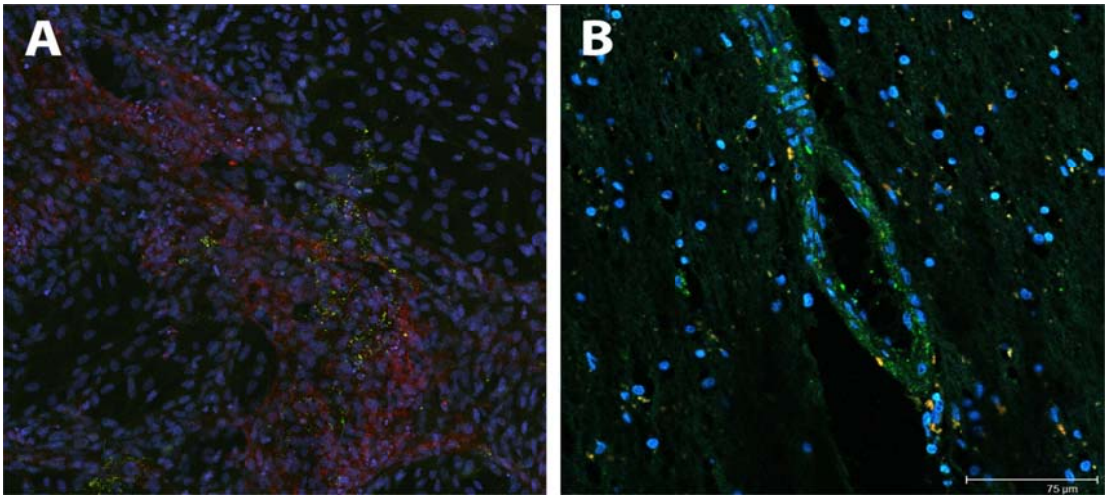

Fig. 16: Staining of porcine pericytes with mAb 3G5

(**A**) Porcine pericytes were cultured with hCMEC/D3 and astroglia cells (U373) for several days. hCMEC/D3 were stained with anti-CD31 antibody (red) while pericytes were counter-stained with mAB 3G5 (green). The localization of the green fluorescence is obviously located in the regions in which the CD31-positive endothelial cells are also present. (**B**) Human brain was fixed and cut into thin sections. Afterwards mAB 3G5 was used to identify microvascular pericytes (green). The pericytes were found on the microcapillaries, while in other regions no positive staining of pericytes could be detected. Nuclei are stained with Hoechst dye (blue), (Confocal microcopy, 40x).

4.3 Establishment of BBB-Models: Monocultures

4.3.1 Blood-brain barrier formation by PBEC

The isolation of porcine brain endothelial cells is described in chapter 3.2. To set-up a blood-brain barrier model using the isolated endothelial cells, numerous individual factors, i.e., transwell filter systems, culture medium, transwell filter coating, cell densities etc., were evaluated to find the best culture conditions. A summary of different evaluations is as follows: 24-well-transwell filter membranes with a pore size of 0.4µm and made of polyester coated with fibronectin appear to be the best culture surface for porcine brain endothelial cells to generate a tight barrier. Polycarbonate filter membranes as well as collagen I (rat tail) and collagen IV (human placenta) coatings were less successful for barrier formation. Investigations with different cell culture media and supplements were also performed. Seeding the PBECs isolated and cultured in 24-well transwells using ECGM, the purchased supplemental kit, supplemented with ITS (1:1000) and 3µg/ml puromycin for the first three days and changing the medium to ECGM, the purchased supplemental kit, supplemented with ITS (1:1000) without puromycin lead to the tightest barrier, as measured by TEER. A co-culture with astrocytes and/or pericytes did not increase the barrier tightness. Further studies will be made to enable the generation of a coculture or even triculture model of the BBB.

After the successful isolation and characterization of porcine endothelial cells the next step was to generate a cell-culture model that exhibit characteristics of the blood-brain barrier. Isolated microvessels were directly seeded onto fibronectin-coated transwell filter membranes. After the successful purification of the cells by the use of the antibiotic puromycin the outgrowing endothelial cells proliferated and started to build up a barrier. This process was followed by measuring the transendothelial electrical resistance (TEER) with time in culture (see Fig. 17).

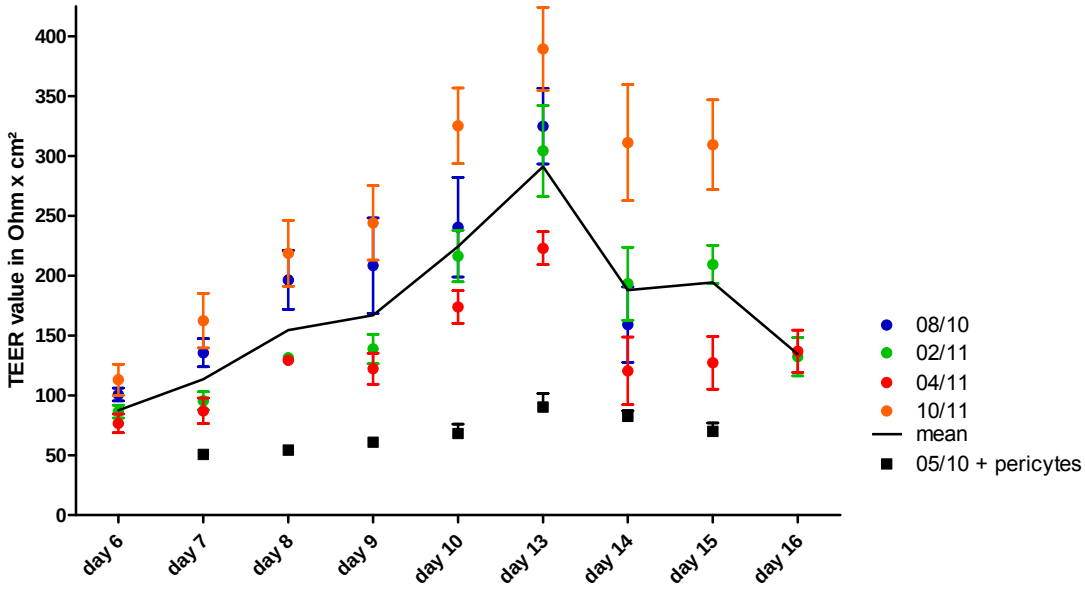

Fig. 17: Increasing transendothelial electrical resistance (TEER) of PBECs cultured on transwell filter membranes

Isolated microvessels from various donors were seeded on transwell filter membranes. Porcine brain endothelial cells started to grow out of the microvessel and build up a barrier. The tightness of the barrier increased until day 13 detected by measuring the TEER values. Each data point represents the mean resistance of PBECs cultured on 20-23 filter membranes ± standard deviation (SD) measured on the corresponding day. The mean TEER-values of the four experiments are presented as line diagram. In contrast to the high TEER values of PEBC monocultures, PBEC cultured with pericytes exhibit a resistance of only ~75 Ωxcm² at day 13. The TEER value of a filter membrane without cells possess a resistance of around 30 Ohm x cm².

Four individual experiments are plotted in Fig. 17. The mean of the experiments is shown as line curve (black). The mean TEER value increased from day 6 to day 13 up to 291 Ohm x cm². After day 13 the TEER value started to decrease. The highest TEER values could also be reached one or two days earlier by increasing the number of isolated microvessels and the seeding density. With a higher seeding density a TEER value of 231 Ohm x cm² (SD ±13 Ohm x cm²) could be reached even on day 7 (data not shown). The coculture of PBEC with primary porcine pericytes resulted in an overall decrease in the resistance (see Fig. 17 05/10 +

pericytes). Therefore, further studies on the formation and effects on barrier characteristics were carried out with PBECs in monoculture seeded on filter membranes.

The tightness of the barrier could also be examined by the determination of the permeability coefficient by the paracellular transport of FITC-dextrans with defined sizes. As explained in chapter 3.3.6 a low permeability coefficient characterizes a tight barrier.

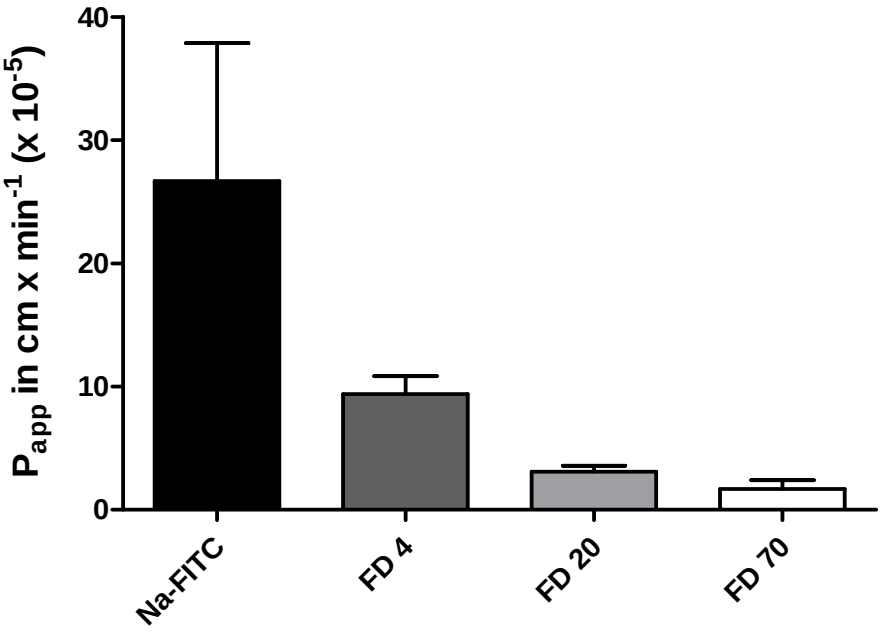

Fig. 18: Determination of the permeability coefficient (P_{app}) of PBECs cultured on filter membranes

Isolated microvessels were seeded on transwell filter membranes. Porcine brain endothelial cells grew to a monolayer and with time developed a barrier exhibited by increased TEER values. By detecting the paracellular transport of different sized FITC-dextrans (FD) the tightness of the barrier was determined. PBECs were exposed to FD for 120min. Each column represents the mean P_{app} of two individual experiments measured in duplicate (± SD).

As shown in Fig. 18 the permeability of the porcine endothelial cell layer decreases with the increased sizes of FITC-dextrans. Na-FITC as smallest 'particle' can cross the barrier best (P_{app}= 26.7 x 10^{-5} cm/min), while the largest FITC-dextran (FD 70) has a very low permeability coefficient of 1.7 x 10^{-5} cm/min.

These low permeability coefficients can be explained by the morphology of PBECs detected by SEM. The microscopic images indicated that the endothelial cells form cell-cell contacts when grown in a monolayer. In addition the tight junctions between the cells could be detected by transmission electron microscopy (TEM; Fig. 19).

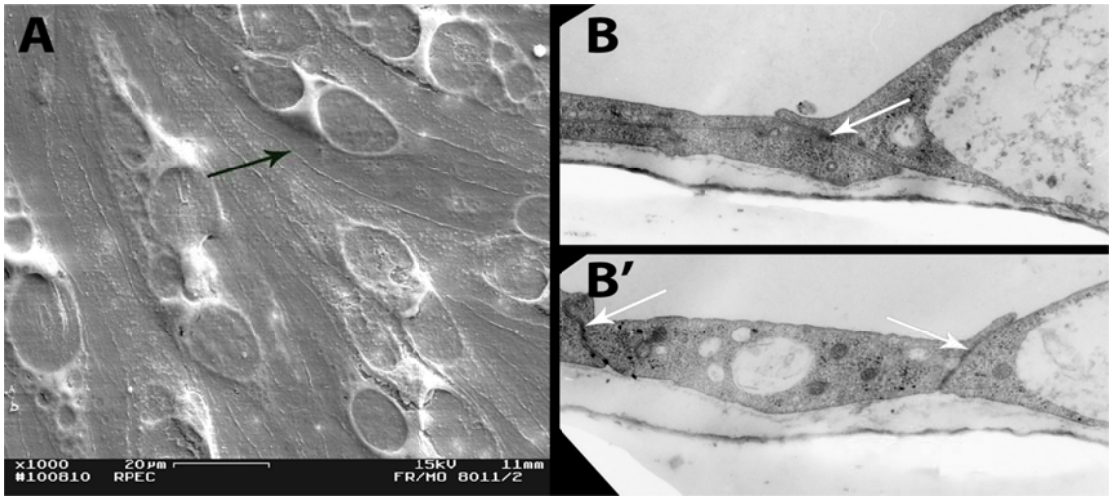

Fig. 19: Electron microscopy images of a PBEC layer on transwell filter membranes

Images of cells used for permeability studies were fixed with glutaraldehyde in cacodylate buffer and were then examined by scanning electron microscopy (**A**) and transmission electron microscopy (**B** and **B'**). The PBECs built up a dense cell layer with strong cell-cell contacts (black arrow). The tight junctions between the individual endothelial cells could also be detected by TEM (white arrows).

In summary, the isolated porcine brain endothelial cells exhibited characteristics observed *in vivo* under culture conditions *in vitro*. A tight monolayer was generated which was characterized by the formation of tight junctions. The high TEER value and the low permeability coefficient confirmed these observations.

4.3.2 Improvement and additional characterization of the blood-brain barrier model formed by hCMEC/D3

hCMEC/D3 were characterized and confirmed to exhibit characteristics of brain endothelial cells by several methods (see 4.1). Due to the observed characteristics, hCMECs are an immortalized cell line which can be used to establish an *in vitro* model of the blood-brain barrier. This was described in detail by Weksler and her group (Weksler et al., 2005) and confirmed by our culture conditions. Using hCMEC to develop an *in vitro* model of the blood-brain barrier could be of advantage on account of the human origin of the cells and the stable cell characteristics, which are not subject to the influence of different donors. Therefore, using a human brain endothelial cell line might be effective for the investigation of drug transport and drug delivery across the human BBB in an *in vitro* model system especially for high-throughput screenings.

The establishment of this model as described and developed by Weksler did not compare or confirm whether a barrier developed with the cell line is as tight as barrier models in which primary endothelial cells are used. The lack of high TEER values (30 - 40 Ohm x cm²) and the absence of electron microscopic images

necessitated further studies. Therefore, the improvements of the model as well as a better characterization of the cells growing on filter membranes were performed and are summarized in the following sections.

4.3.2.1 Morphology of hCMEC on transwell filter membranes

The expression of relevant proteins which are involved in the formation of a tight blood-brain barrier, i.e., ZO-1, occludin, claudin-5, was examined by immunofluorescent staining (see 4.1). In addition to the morphology and growth, characteristics of hCMEC were investigated. In Fig. 20 electron microscopy images of hCMEC cultured on a transwell filter membrane are shown. Individual hCMECs start to grow over one another with time. In addition, certain areas of the culture membrane are populated by a single layer of endothelial cells. In these areas, hCMECs develop a tight cell layer (Fig. 20A' – black arrow). The tight junctions between the cells can also been observed on TEM in Fig. 20B' (white arrow). Cells were closely connected and this is a requirement for the formation of a tight blood-brain barrier *in vitro* as well as *in vivo*. In areas in which cells overgrew each other these tight junctions did not exist (Fig. 20B).

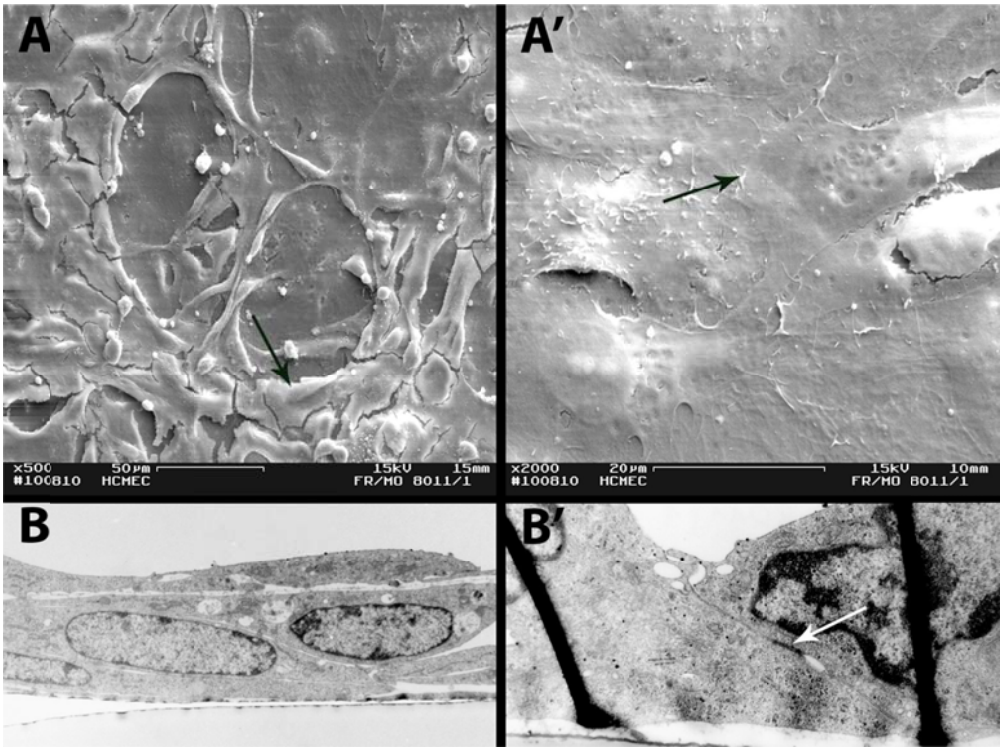

Fig. 20: Electron microscopy images of a hCMEC layer on transwell filter membranes

After the determination of the permeability coefficient by transport studies with FITC-dextrans hCMEC were fixed with glutaraldehyde in cacodylate buffer and then examined by scanning electron microscopy (**A** and **A'**) and transmission electron microscopy (**B** and **B'**). The cell layer built by hCMEC was not homogeneous. The cells initially developed a dense layer (**A'** black arrow) but after further cultivation cells began to overgrow the first monolayer (**A** – black arrow). By TEM analysis the tight

junctions between cells could be detected. In addition, the multiple layers of cells can be visualized by analyzing cross-sections of the transwell filters cultured with hCMEC (**B**).

In summary, hCMEC do not appear to be contact inhibited. The formation of multilayers of cells might lead to an endothelial barrier; however, this is not structurally similar to the BBB in vivo. In addition, the barrier and cell junctions were not characteristic of the single cell monolayer exhibited by PBEC *in vitro* (see chapter 4.3.1). These findings were confirmed by measuring the TEER values of hCMEC cells on transwell membrane filters. Values of 30 Ohm x cm² were measured (data not shown), although the cells were grown on different membrane materials (polyethylene or polycarbonate membranes), in various cell culture media with supplements, and on different surface coatings (fibronectin, gelatin, human collagen IV, rat tail collagen I) for up to 14 days.

4.3.2.2 Determination of hCMEC barrier characteristics by transport studies with FITC-dextrans

Despite the results presented in section 4.3.2.1 the transport of FITC-dextrans with different defined sizes (see 2.8) were investigated. The permeability coefficients of the different dextrans for an exposure time of 120 minutes are shown in Fig. 21. Dextrans of 70kDa revealed a low permeability coefficient (3.7 x 10^{-5} cm/min) compared to smaller dextrans with sizes of 20kDa, 4kDa and less than 4kDa (Na-FITC). Thus, the paracellular transport of FITC-dextrans was size-dependent and also comparable to those permeability coefficients which were published by Weksler and her group (Weksler et al., 2005).

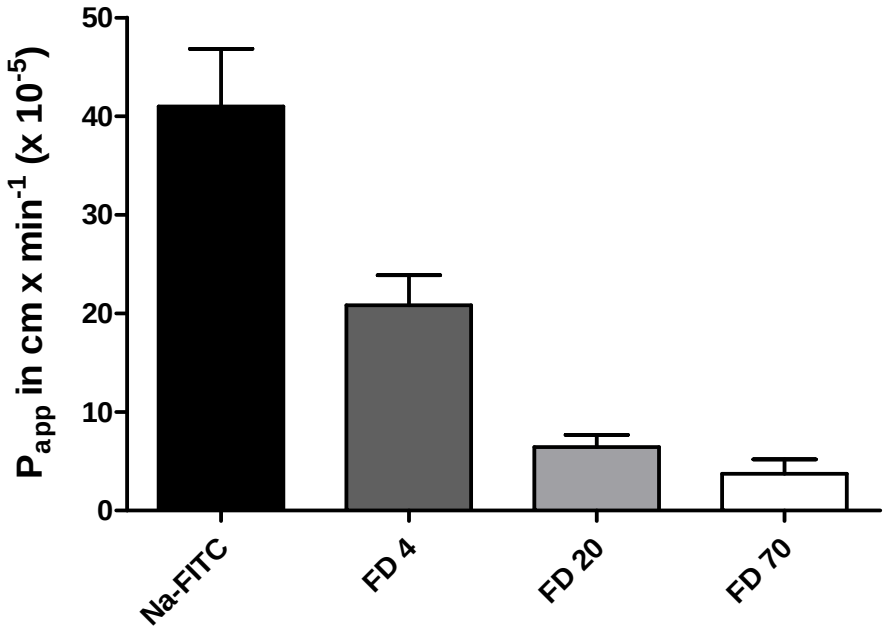

Fig. 21: Determination of the permeability coefficient (P_{app}) of hCMEC cultured on filter membranes

hCMECs were seeded on transwell filter membranes. After 8 days of hCMEC cultivation the confluence of cells were evaluated microscopically. By determining the paracellular transport of different sized FITC-dextrans (FD) the tightness of the barrier can be quantified. hCMECs were exposed to FITC-dextrans for 120min. Each column represents the mean P_{app} of two individual experiments measured in duplicate (± SD).

4.4 Adhesion and internalization of nano-structured materials in different human endothelial and epithelial cell types

As described in the introduction, nanoparticles are characterized by sizes of less than 100nm. The surface topography, surface composition, surface charge, size and additional characteristics may influence the adhesion and internalization of nanoparticles, but might also exhibit different toxic effects. Although gold bulk material appears to be non-toxic and inert the characteristics of small particles made of the same material may affect cells in a completely different fashion. In addition, surface modifications, such as coatings made by chemical modifications, can cause cell toxicity. To exclude cell toxicity caused by nano-structured material, cell viability assays, proliferation assays and cytotoxicity assays were performed. Possible cytotoxicity and uptake of gold nanoparticles of different sizes with various surface modifications are presented in the following sections and the effects of these nanoparticles on two different endothelial cell types are compared.

4.4.1 Exposure of different human endothelial and epithelial cells to gold nanoparticles with different amounts of sodium citrate

4.4.1.1 Cytotoxic effects of human endothelial cells caused by the exposure to gold nanoparticles

The effect of different sizes and the presence of varying amounts of sodium citrate residues bound to gold nanoparticle surfaces on the cytotoxicity of alveolar type-II-like cell lines A549 and NCIH441 has recently been published by our group (Uboldi et al., 2009). In the following the cytotoxic effects of these gold nanoparticles on human endothelial cells will be investigated.

In section 2.9 and Table 20 the properties of AuS03-02-RIT, AuS0302-RIS-02 and AuS0302-RIS-04 are described.

Table 20: Properties of RIT/RIS gold nanoparticles (for details see 2.9)

Sample	Size (TEM)	Sodium citrate concentration
AuS0302-RIT	10nm	Less amount of sodium citrate compared to RIS-02 and RIS-04 (~8%)
AuS0302-RIS-02	11nm	Sodium citrate
AuS0302-RIS-04	25nm	Sodium citrate

To determine the cytotoxicity of human dermal microvascular endothelial cells (HDMEC) and human cerebral microvascular endothelial cells (hCMEC/D3), cells were exposed to different concentrations (50/100/500/1000µM) of gold nanoparticles for 4-48 hours.

The cell viability and cell proliferation rate was measured using the MTS assay and Ki-67 CAM-EIA, respectively. Untreated cells were used as a control and were set to 100%. In Fig. 22 the results of the MTS assay and Ki-67 CAM-EIA are depicted. Fig. 22 demonstrates that the cell viability decreased when gold nanoparticle concentrations were above 500µM. Especially after exposure to 1mM AuS0302-RIS02 and AuS0302-RIS04 the cell viability of HDMEC decreased from 100% to 78% and 84%, respectively. In contrast to the gold nanoparticles with an excess of sodium citrate on their surface, AuS0302-RIT with a reduced sodium citrate concentration did not induce a decrease in cell viability after 48 hours of incubation. Interestingly, the cell viability of hCMEC/D3 even after exposure to 1mM AuS0302-RIS02 and AuS0302-RIS04 only decreased slightly as demonstrated in Fig. 22 A

(90% / 93%). In addition, no influence on the viability of hCMEC could be detected after exposure to AuS0302-RIT.

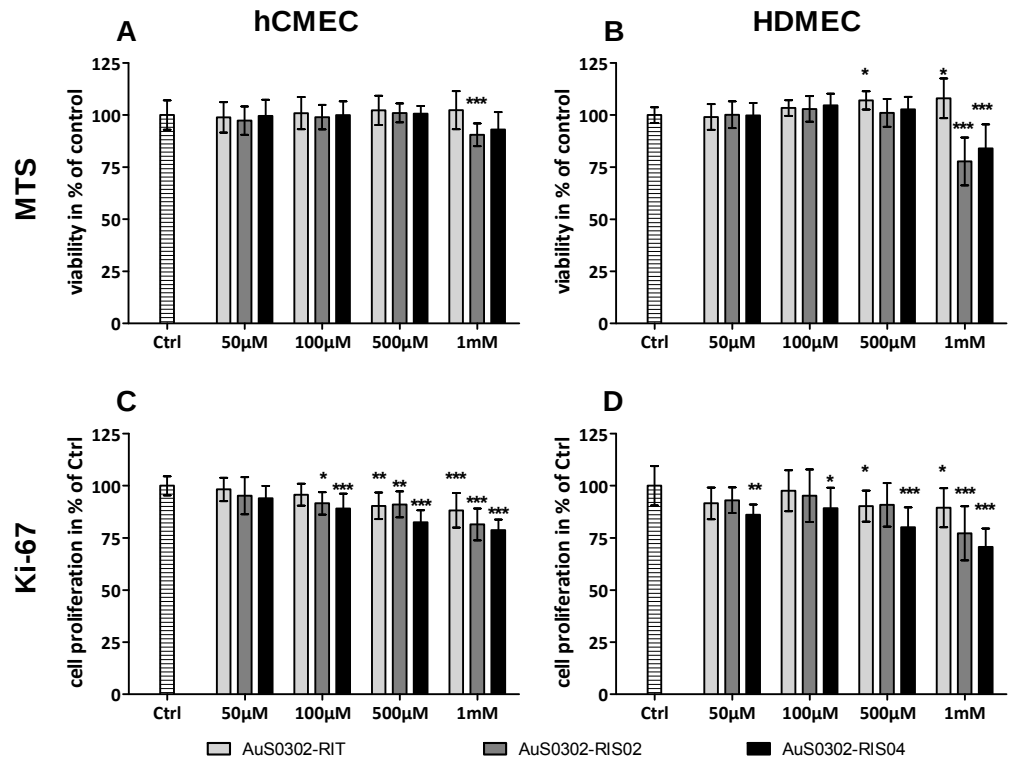

Fig. 22: Cell viability and proliferation rate of endothelial cells measured after exposure to gold nanoparticles

The endothelial cells HDMEC (**B**, **D**) and hCMEC (**A**, **C**) were exposed to different amounts of gold nanoparticles (50µM - 1mM) for 48 hours. Cell viability was measured by the MTS assay. Proliferation was detected by the quantification of the proliferation factor Ki-67 by CAM-EIA. The viability and proliferation rate of untreated cells (Ctrl) were set to 100%. Each column represents the mean ± standard deviation of four independent experiments which were performed at least in triplicate.

To identify a possible negative impact of gold nanoparticles on the proliferation capacity of cells the amount of Ki-67 of both endothelial cell types after exposure to different concentrations of all tested gold nanoparticles was determined. In both endothelial cell lines a dose-dependent decrease in the proliferation rate could be detected (Fig. 22 (Ki-67)). Exposure to 50µM and 100µM gold nanoparticles did not influence the expression of the proliferation factor Ki-67. In contrast, after exposure to 500µM of AuS0302-RIS-04 a decrease of the proliferation factor to 80% in HDMEC and 82% in hCMEC could be observed. After the exposure to 1mM AuS0302-RIS04 the proliferation decreased further to 70% (HDMEC) and 79% (hCMEC). The smaller gold nanoparticles AuS0302-RIS02 induced a milder reduction of Ki-67. After exposure to 1mM AuS0302-RIS02 the expression of Ki-67 decreased to 77% in HDMEC and 81% in hCMEC. The expression of Ki-67 after

exposure to AuS0302-RIT decreased only slightly to 90% (SD ± 8%) in both endothelial cell types.

The induction of cytotoxicity after incubation with gold nanoparticles was measured by detecting the amount of released lactate dehydrogenase (LDH) into the supernatant. Fig. 23 indicates that the release of LDH increased, depending on the concentration of the gold nanoparticles.

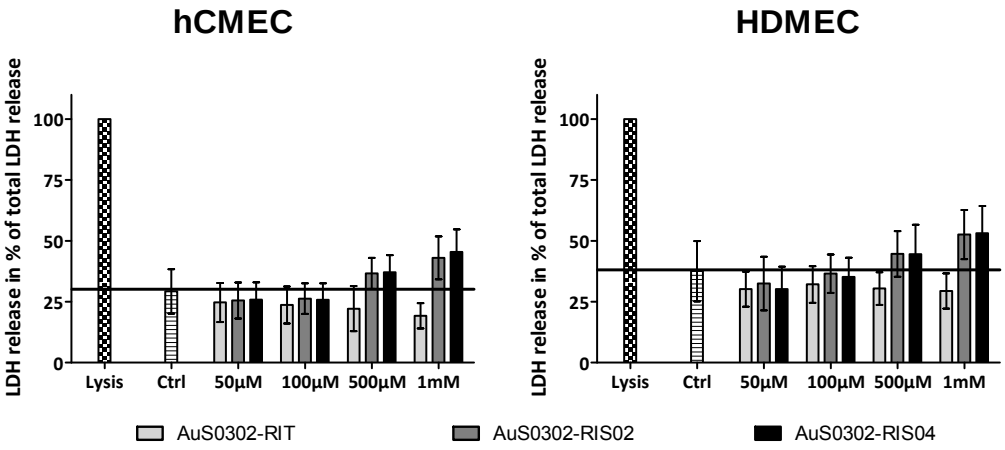

Fig. 23: Cytotoxicity of endothelial cells measured after exposure to gold nanoparticles

After 48h of exposure of HDMEC and hCMEC to various concentrations of gold nanoparticles cytotoxicity was detected by the LDH release assay. As positive control lysed cells were used and set to 100% (Lysis). Each column represents the mean ± standard deviation of four independent experiments which were performed at least in triplicate.

Gold nanoparticle concentrations up to 100µM demonstrated no induction of cytotoxicity. Furthermore, AuS0302-RIT did not influence cell toxicity in either of the cell types even after stimulation with 1mM gold nanoparticles for 48 hours. A slight increase of LDH release (7%) into the supernatant compared to the spontaneous release by the untreated cells could be determined after stimulation of HDMEC and hCMEC/D3 with 500µM AuS0302-RIS02 and AuS0302-RIS04. The exposure to 1mM of AuS0302-RIS02 and AuS0302-RIS04 led to an increase in LDH release of ~15% in both endothelial cell types compared to the spontaneous release of their appropriate untreated control cells.

In summary, hCMEC were less influenced to the exposure of AuS0302-RIS-02 and –RIS-04 compared to primary HDMECs. Gold nanoparticles with lower amounts of sodium citrate on the surface (AuS0302-RIT) did not exert a cytotoxic effect. Thus, AuS0302-RIT appeared to be more biocompatible compared to AuS0302-RIS-02 and –RIS-04.

4.4.1.2 Internalization of gold nanoparticles in human endothelial cells

To investigate the uptake of AuS0302-RIT, -RIS02 and -RIS04 both endothelial cell types were incubated with a non-toxic dose of the gold nanoparticles (300µM) for 24 hours. The internalization of the particles by the cells was confirmed by transmission electron microscopy (TEM) analysis. In Uboldi et al. the uptake of all three particles into lung epithelial cells was demonstrated after incubation for 3 hours (Uboldi et al., 2009). In this study it could also be shown that the amount of internalized gold nanoparticles increased markedly after an incubation time of 24 hours. In Fig. 24 the images showed that all gold nanoparticles were internalized by the cell types and were stored in vesicles mostly located in the perinuclear region. In addition, no particles could be detected in the cytosol or in other cell compartments, e.g., nuclei and mitochondria.

It was not possible by TEM analysis to detect different amounts of dissimilar gold nanoparticles taken up in the individual single cell types which could be attributed to the presence of different amounts of surface-bound sodium citrate or size. However, it could be seen that the vesicles/vacuoles of epithelial cells in which the nanoparticles were located were filled with a higher amount compared to those of endothelial cells. Differences in the amount of gold nanoparticles internalized by the different epithelial cells could not be clearly determined by image analysis. For the exact quantification of gold that was internalized by the different cell types the concentrations of gold in exposed cell populations was analyzed by inductively coupled plasma and atomic emission spectroscopy (ICP-AES) in addition to the TEM images (see chapter 4.4.1.3).

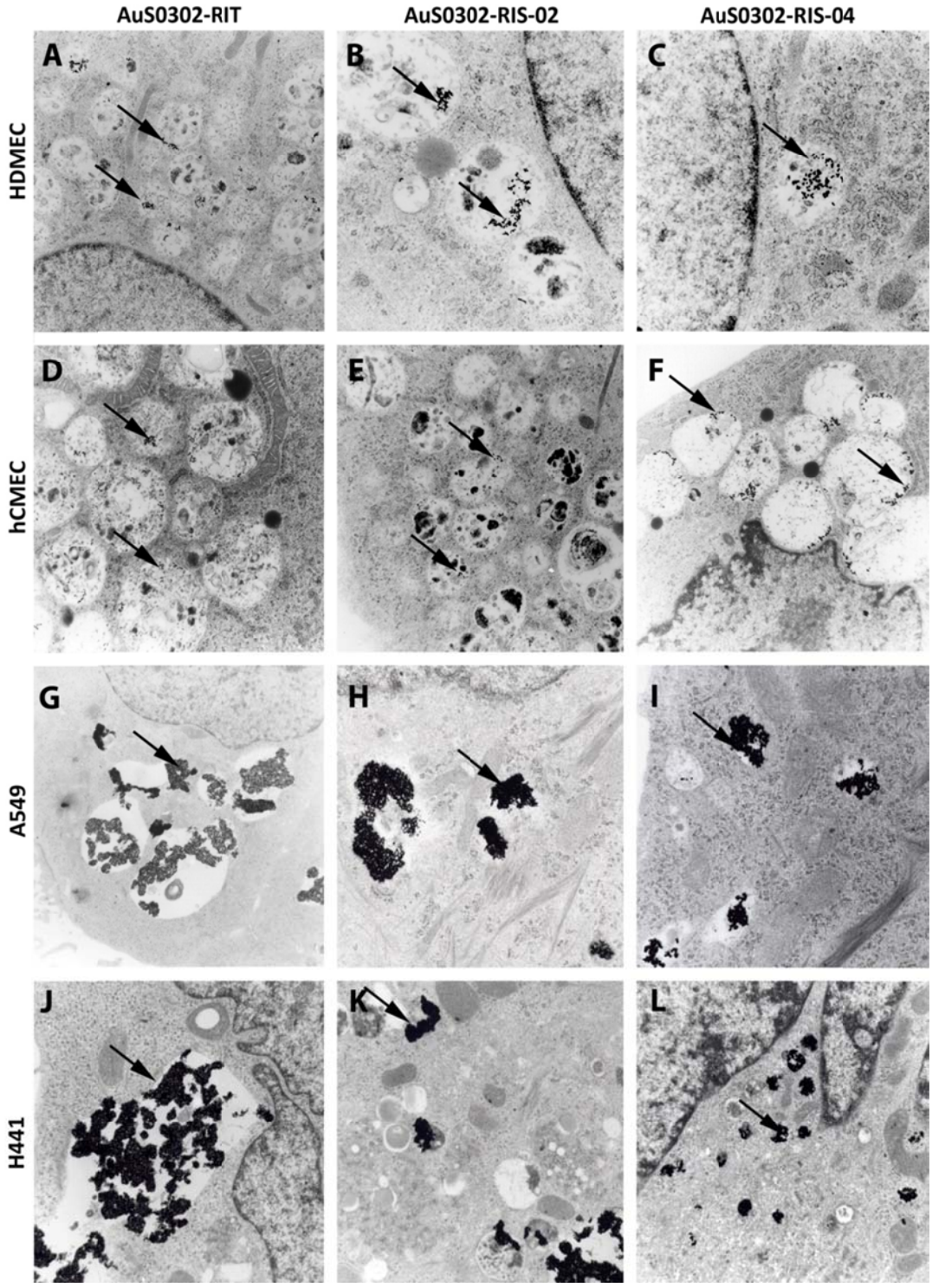

Fig. 24: Internalization of gold nanoparticles into endothelial and epithelial cells after an exposure time of 24 hours.

All cell types were incubated with 300µM gold nanoparticles at 37°C for 24 hours. Cells were extensively washed, fixed and analyzed by transmission electron microscopy (TEM). All gold nanoparticles (indicated by black arrows) were found in intracellular vesicles mostly located in the perinuclear region. None of the nanoparticles could be found in the nuclei or free in the cytoplasm. In the perinuclear vesicles of the lung epithelial cells, A549 (**G**-**I**) and H441 (**J**-**L**) the amount of gold was higher compared to the vacuoles of the endothelial cells, HDMEC (**A**-**C**) and hCMEC (**D**-**F**). Differences

in the amount of the various gold nanoparticles within the cells could not be demonstrated by TEM analysis (Magnifications: 3500 – 4400x).

4.4.1.3 Quantification and comparison of the internalized gold nanoparticles by human endothelial and epithelial cells

The confirmation of the uptake of AuS0302-RIT, -RIS-02, -RIS-04 by human endothelial and epithelial cells is shown by transmission electron microscopy in Fig. 24 (chapter 4.4.1.2) and in the publication of Uboldi et al. (Uboldi et al., 2009), respectively.

The comparison of the amount of internalized gold nanoparticles could not be performed sufficiently by image analysis but could be determined by inductively coupled plasma and atomic emission spectroscopy (ICP-AES), which is the more sensitive and quantitative method compared to image analysis. By ICP-AES differences in the amount of gold nanoparticles in the magnitude of parts per billion can be quantified. Besides the high sensitivity of the method a high number of cells can be analyzed simultaneously compared to image analysis, in which each image shows the uptake in a few cells.

In Fig. 25 the amount of gold nanoparticles taken up in the different cell types is presented. Due to the low initial concentration of 50µM the visualization and occurrence within the cells is in general low. However, the tendency of uptake behavior of the different cell types observed in TEM analysis could also be confirmed by ICP-AES. It could be demonstrated that both epithelial cell types internalized a higher amount of all types of gold nanoparticles compared to the endothelial cells. In addition, it could be shown that a slight but not significant difference in the absorption of smaller sized gold nanoparticles (AuS0302-RIT/-RIS-02) compared to their bigger counterparts (AuS0302-RIS-04) could be detected. The smaller sized gold nanoparticles were taken up in a higher amount. A difference in the quantity of internalized gold nanoparticles between the two epithelial cell types could also be demonstrated. The most prominent difference was detected after the exposure to AuS0302-RIT. The amount of AuS0302-RIT within A549 was more than two-fold higher than in H441 cells (145ppb ± 58ppb (H441) and 276ppb ± 114ppb (A549).

The main outcome of these studies was that epithelial cells internalized a substantially higher amount of all gold nanoparticles after 24 hours compared to endothelial cells. In addition, the size of the particles appeared to be a characteristic which also influences the amount of gold nanoparticles internalized. In addition, the amount of sodium citrate on the particle surfaces did not influence the uptake by different cell types.

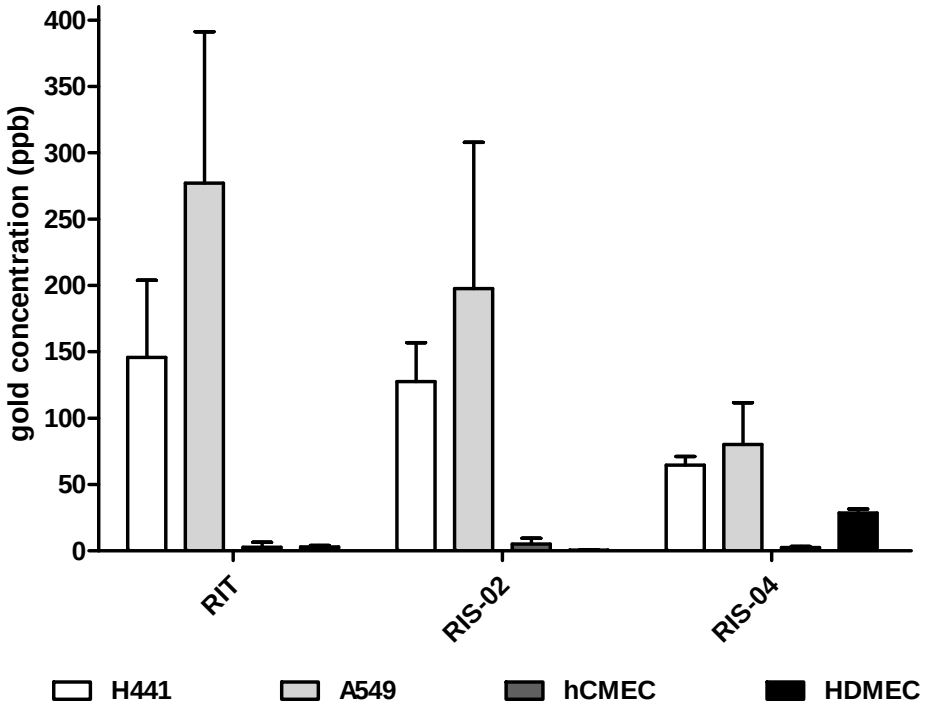

Fig. 25: Quantification of internalized gold nanoparticles in different cell types by ICP-AES
Cells were incubated with 50µM of the different gold nanoparticles for 24 hours. Cells from three individual wells were pooled and the gold concentrations (parts per billion (ppb)) were determined by ICP-AES (n>6; at least of two different experiments). The means ± SD are depicted for every cell type and for each gold nanoparticle. Untreated cells (Ctrl) were used as controls. The experiment was repeated at least twice.

4.4.2 Exposure of human microvascular endothelial cells to gold nanoparticles with different sizes and various surface modifications

In addition to the investigations of gold nanoparticles which differ in the amount of sodium citrate bound to the nanoparticle surface, studies of gold nanoparticles with different sizes and various surface modifications were also examined and are presented in the next sections. All of these nanoparticles were synthesized by the same reduction method described in chapter 2.9. The gold nanoparticles were subsequently coated with polymers which exhibited different physico-chemical properties. The properties of the gold nanoparticles are summarized in Table 9. To simplify the identification of the nanoparticles with different sizes and the substance that was used as surface modification, a coding is used in most of the figures. The first number (61-XX, 65-XX or 71-XX) stands for the different sizes/diameter of the gold nanoparticles, while 61 stands for a diameter of 18nm, 65 for a diameter of

35nm and 71 for a diameter of 65nm. The '-XX' is a code for the different surface modifications. The codes are summarized in the following table.

Table 21: Codings of gold nanoparticles (`YY': stands for the different sizes)

Code	Surface modification
YY-2	Ethanediamine
YY-14	Glucosamine
YY-17	Hydroxypropylamine
YY-23	Taurine
YY-28	PEG (polyethylenglycol)

Uptake behavior, nanotoxicology and the induction of the expression of pro-inflammatory mediators were investigated in the different endothelial cell types, HDMEC and hCMEC, after exposure to the various nanoparticles.

4.4.2.1 Investigation of cell viability after exposure to different gold nanoparticles

HDMEC and hCMEC were incubated with increasing amounts of gold nanoparticles for 4, 24 and 48 hours. The MTS assay was used to examine cell viability in response to the exposure to different gold nanoparticles.

Even after exposure for 48 hours and the incubation with high concentrations (100µg/ml and 250µg/ml) no decrease in the cell viability of hCMEC and also of the primary HDMEC could be detected (Fig. 26). Additionally, no influence on cell viability was observed after treatment with nanoparticles which have different surface properties and size. In summary, the gold nanoparticles examined which differ in size, surface modification and surface net charge, did not influence the cell viability of hCMEC and HDMEC even at high concentrations and for incubation times up to 48 hours.

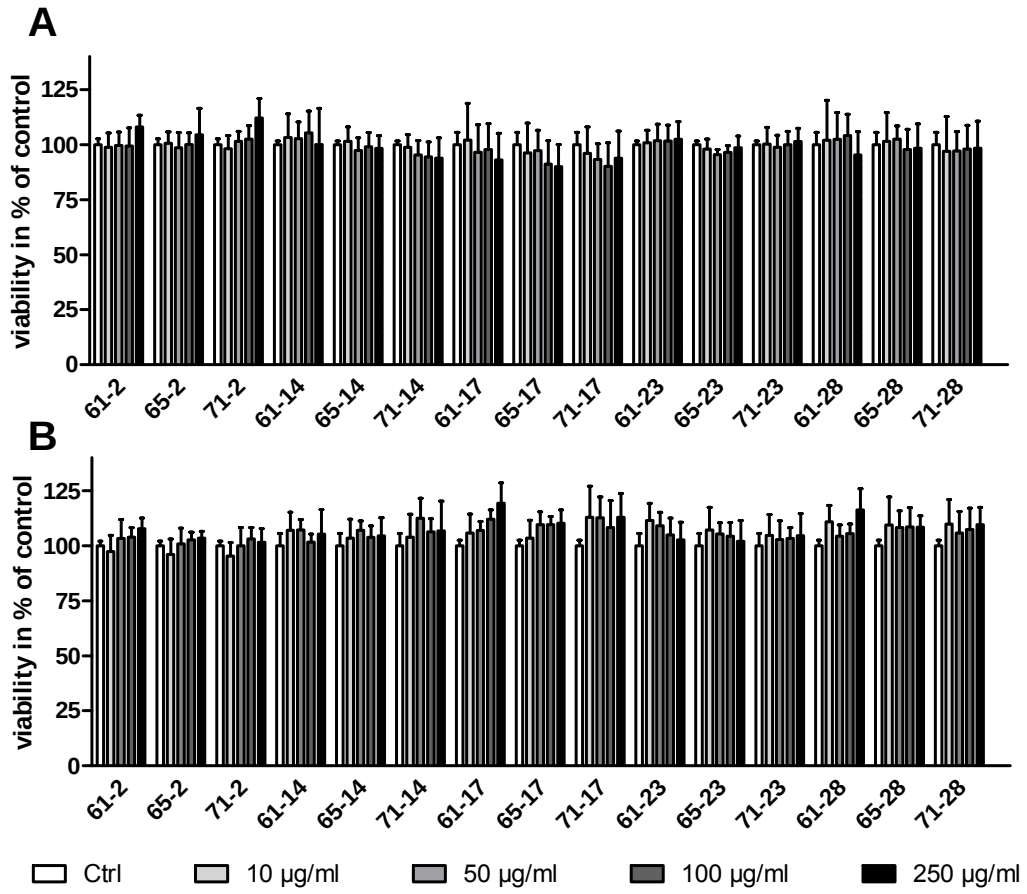

Fig. 26: Cell viability of hCMEC and HDMEC after exposure to various gold nanoparticles for 48 hours

The endothelial cells hCMEC (**A**) and HDMEC (**B**) were exposed to different concentrations of gold nanoparticles (10, 50, 100, 250µg/ml) for 48 hours. Cell viability was measured by the MTS assay. The cell viability of untreated cells (Ctrl) was set to 100%. Each column represents the mean ± standard deviation of three independent experiments; each of these was performed at least in triplicate.

In addition, no cell toxicity was observed after exposure to the different gold nanoparticle concentrations for 48 hours (determined by the release of lactate dehydrogenase into the supernatant after exposure to the nanoparticles; data not shown).

4.4.2.2 Uptake of gold nanoparticles by human endothelial cells

To determine if the gold nanoparticles were internalized by HDMEC and hCMEC, cells were treated with 100µg/ml gold nanoparticles for 24 hours. The cell membranes were identified by antibody staining of the membrane-integrated CD31 protein. In Fig. 27 and Fig. 28 the uptake of the different sized and surface modified gold nanoparticles (black dots) in hCMEC and HDMEC is shown. Interestingly, the differences in the amounts of the various gold nanoparticles within the cells could be detected by optical microscopy. Less uptake of PEGylated gold nanoparticles (-28)

was observed compared to the extremely high uptake of ethanediamine modified particles (-2), which exhibit a positive surface charge. A moderate uptake could be detected after exposure to glucosamine- (-14) and hydroxypropylamine- (-17) modified gold nanoparticles while the uptake of the smallest and the largest taurine (-23) -modified gold nanoparticles was lower.

A comparison of the amount of internalized gold nanoparticles by both cell types by using the microscopic images was not possible, since the amount of gold nanoparticles taken up per cell in both cell types was not homogeneous. However, an overall difference in the uptake of the various nanoparticles was clearly shown without the need to perform quantitative studies.

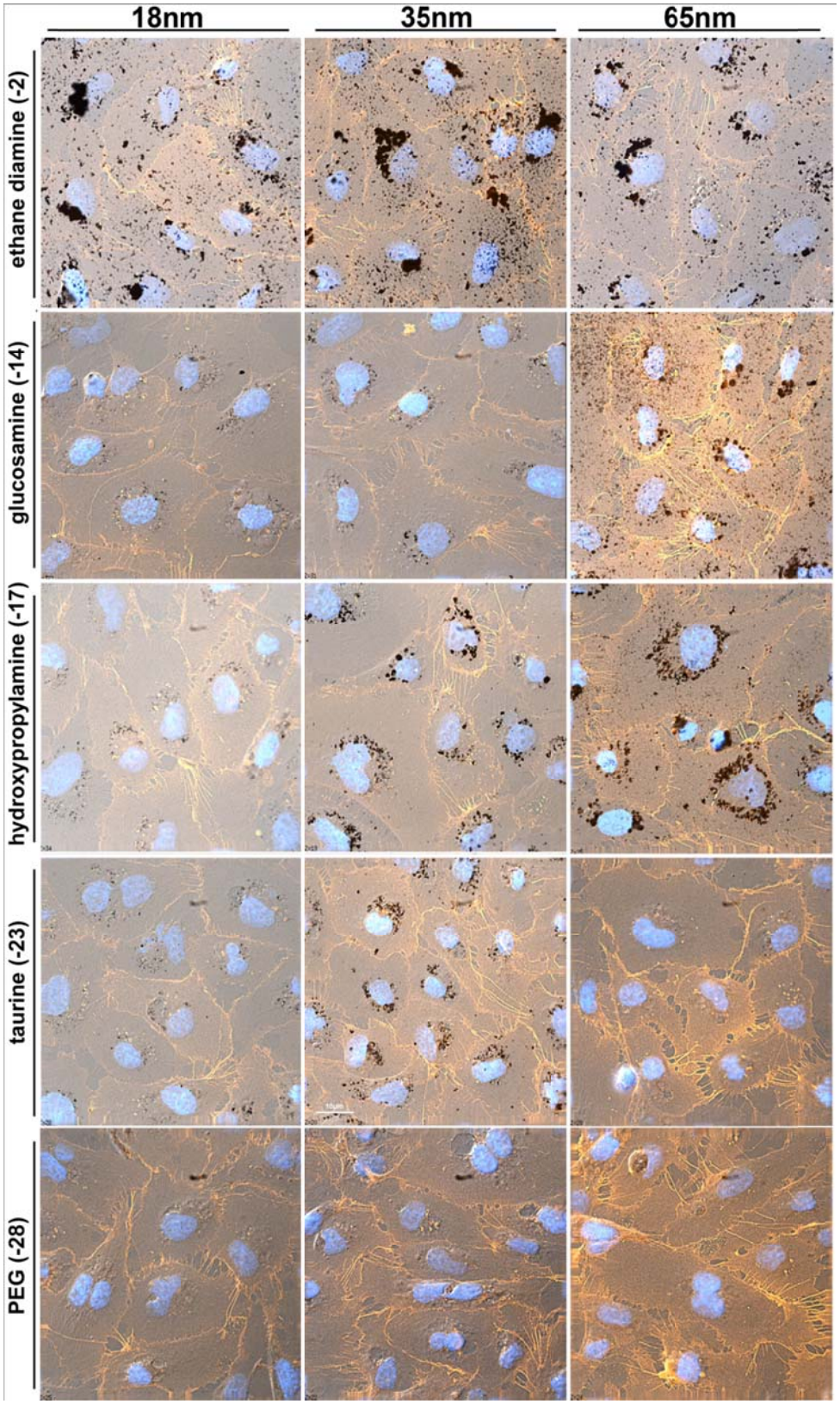

Fig. 27: Uptake of various gold nanoparticles by hCMEC after 24 hours of exposure

hCMEC were treated with 100µg/ml gold nanoparticles at 37°C for 24 hours. Cells were washed, fixed with paraformaldehyde and cell membranes were stained with anti-CD31 antibody and the corresponding secondary antibody (red-yellow). Nuclei were stained with Hoechst (blue). Aggregations of gold nanoparticles can be detected as black dots (optical/fluorescence microscopy, Delta Vision, 60x; scale bar = 10µm).

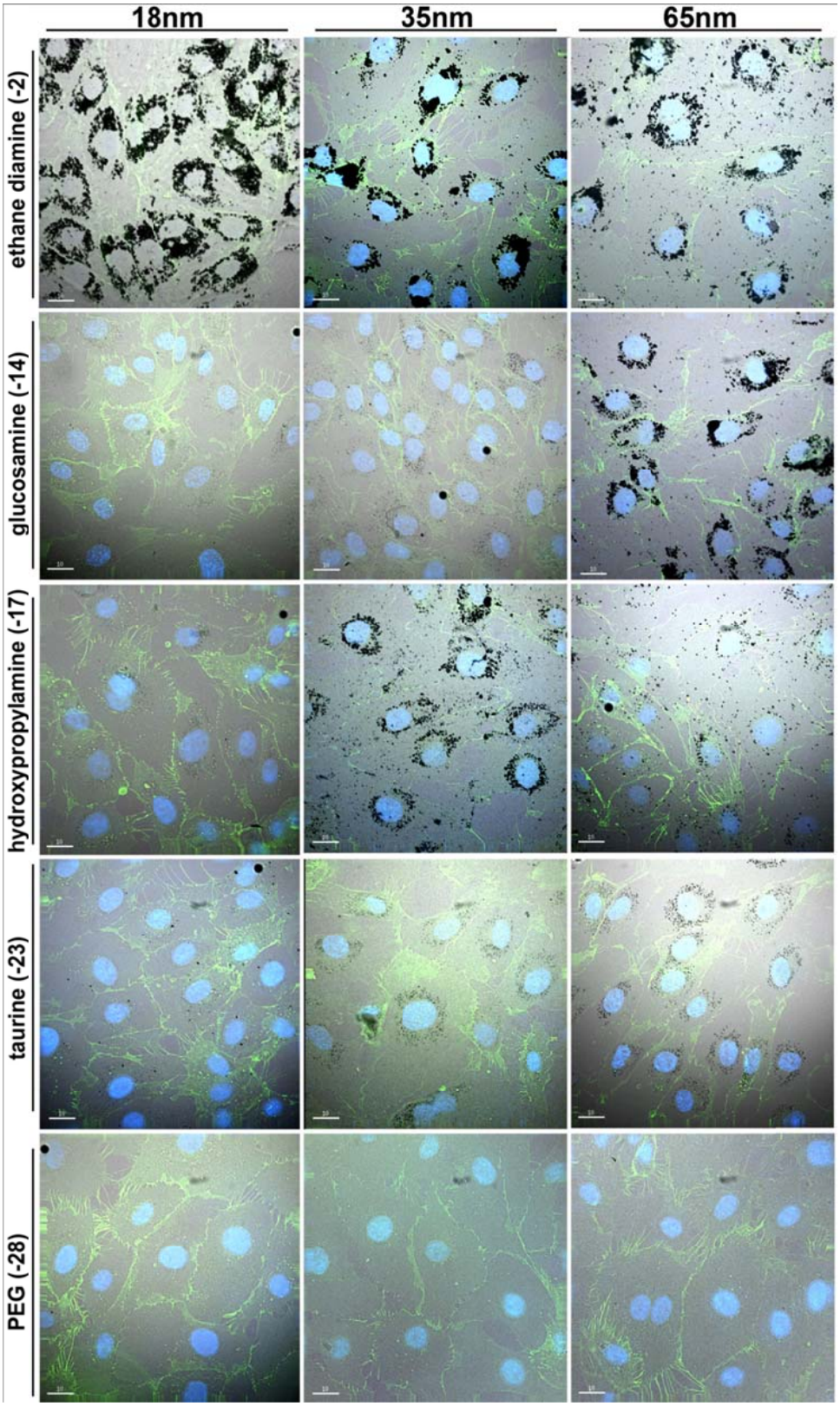

Fig. 28: Uptake of various gold nanoparticles in HDMEC after 24 hours of exposure

HDMEC were treated with 100µg/ml gold nanoparticles at 37°C for 24 hours. Cells were washed, fixed with paraformaldehyde and cell membranes were stained with anti-CD31 antibody and the corresponding secondary antibody (green). Nuclei were stained with Hoechst (blue). Aggregations of gold nanoparticles can be detected as black dots (optical/fluorescence microscopy, Delta Vision, 40x, scale bar = 10µm).

The internalization of all gold nanoparticles in hCMEC and HDMEC was confirmed by transmission electron microscopy (TEM) analysis (Fig. 29).

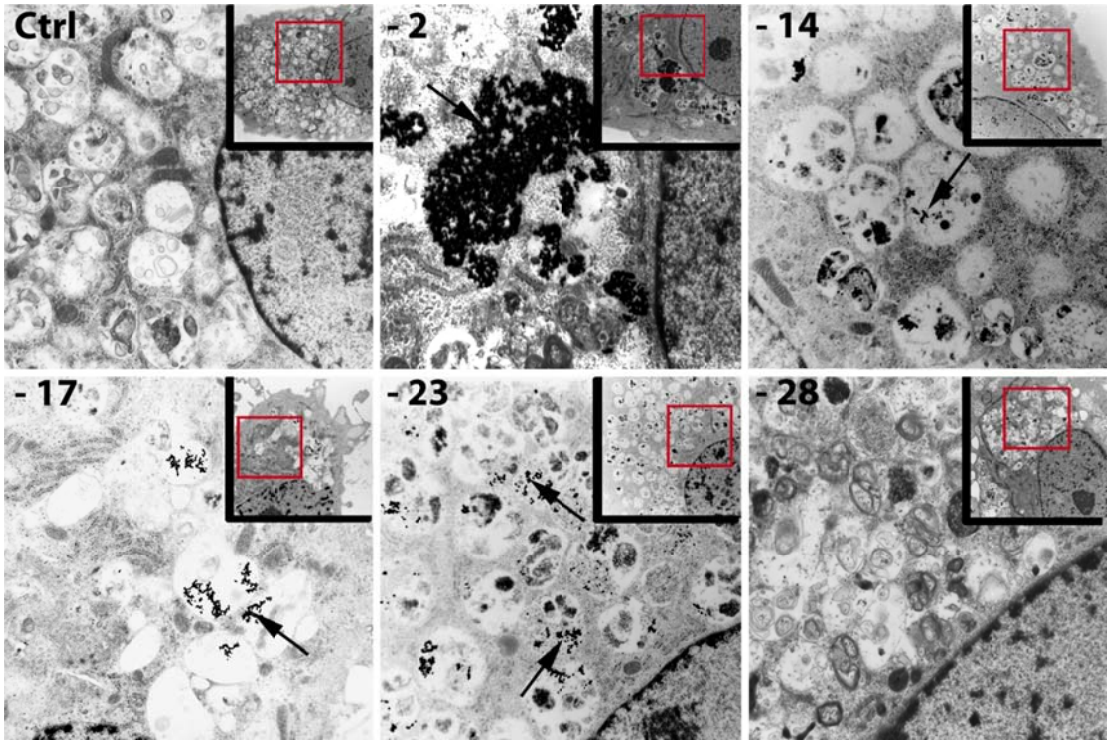

Fig. 29: TEM analysis of the internalization of 35nm-sized gold nanoparticles with different surface modifications in HDMEC after 24 hours.

HDMEC were treated with 100µg/ml gold nanoparticles for 24 hours. Cells were extensively washed, fixed with glutaraldehyde and prepared for TEM microscopy. All gold nanoparticles (indicated by black arrows) were found in intracellular vesicles. Images in the upper right-hand corners with the red perimeter represent the overview (1650x) of the magnified main image (3500x). Ctrl: no gold treatment; -2: ethanediamine AuNPs; -14: glucosamine; -17: hydroxypropylamine; -23: taurine; -28: PEG.

Due to the high resolution of the transmission electron microscope single particles could be detected. All nanoparticles were located in vesicles. After increasing the incubation time the particles were mostly located in the perinuclear region (Fig. 29). None of the TEM images demonstrated how the gold nanoparticles were internalized. Thus, it was not possible to determine the mechanism of uptake by TEM analysis. A co-localization within intracellular vesicles associated with different uptake routes was examined by immunostaining of the vesicles after exposure to gold nanoparticles using antibodies against typical vesicle markers, such as clathrin or caveolin (shown for 65-17 in section 4.4.2.5). Due to the low resolution of the light microscope only agglomerations of gold nanoparticles could be visualized. Therefore, a co-localization with the stained uptake vesicles could not be detected. In section 4.4.2.5 the storage of the gold nanoparticles in vesicles which were located in the perinuclear region was demonstrated using antibodies against flotillin-1 and flotillin-2.

4.4.2.3 Quantification of internalized gold nanoparticles by ICP-AES

An analysis of an image of a few single cells was not sufficient to quantify the amount of internalized nanoparticles within a cell or an entire population of cells. To examine the uptake of nanoparticles in an entire population of cells, inductively coupled plasma and atomic emission spectroscopy (ICP-AES) was used. This method is highly sensitive in quantifying the amount of gold atoms present in a solution. An overview of the amount of internalized gold nanoparticles can be seen in Fig. 30. The quantification of gold was determined by two different methods. First, the uptake of gold nanoparticles per single cell was calculated by examining the amount of gold atoms present in a cell extract produced from a known number of cells exposed to the gold nanoparticles. The average number of atoms present in a nanoparticle of a defined size is known and based on this the approximate number of nanoparticles present in the extract could be calculated and related to the number of nanoparticles per cell. The second method calculated the percentage of nanoparticles taken up by the cells compared to the quantity of nanoparticles to which the cells were exposed.

In general, the quantification data presented in Fig. 30 illustrate that the uptake in both cell types is time-dependent.

Besides the images in Fig. 27 and Fig. 28 the quantification of the internalized gold nanoparticles shows that the particles with the net positive charge (-2) were internalized best in both cell types. Nearly all of the gold nanoparticles were taken up after 4 hours, although the number increased after an incubation time of 24 hours.

The number of the smallest gold nanoparticles with an ethanediamine surface modification is extremely high, although only ~ 25% of the total nanoparticles in the suspension are internalized (Fig. 30 B and D). This amount is significantly increased compared to the medium sized and the largest sized gold nanoparticles with the same surface modification after exposure for 4 and 24 hours. HDMEC internalized a significantly higher amount of 61-2 compared to hCMEC even after 4 hours of incubation (Fig. 30 A and C).

Compared to the ethanediamine-modified gold nanoparticles the amount of other internalized particles is less. A significant difference in internalized nanoparticles with different sizes could be detected for nanoparticles with a glucosamine surface modification only after an exposure for 4 hours (-14; see Fig. 30 A). In addition, a significant difference in the uptake regarding different sizes could also be detected for the hydroxypropylamine-coated nanoparticles. In comparison to the glucosamine-coated particles the differences in the number of various sized

hydroxypropylamine-coated nanoparticles is not as dramatic, but approximately 50% of the largest hydroxypropylamine coated nanoparticles are taken up compared to around 3% of the smallest ones after incubation for 24 hours. Further differences in the quantity of glucosamine- and hydroxypropylamine-coated gold nanoparticles are presented in Fig. 30 and Fig. 31.

PEGylated gold nanoparticles (-28) were taken up in small amounts. After 4 hours of incubation the uptake of the negatively charged taurine-coated nanoparticles in both cell types was quite low (~ 3% of the total nanoparticles in suspension). The uptake increased to ~20% (35nm) after a further 20 hours of incubation. The largest gold nanoparticles with taurine coating were not taken up even after 24 hours of incubation.

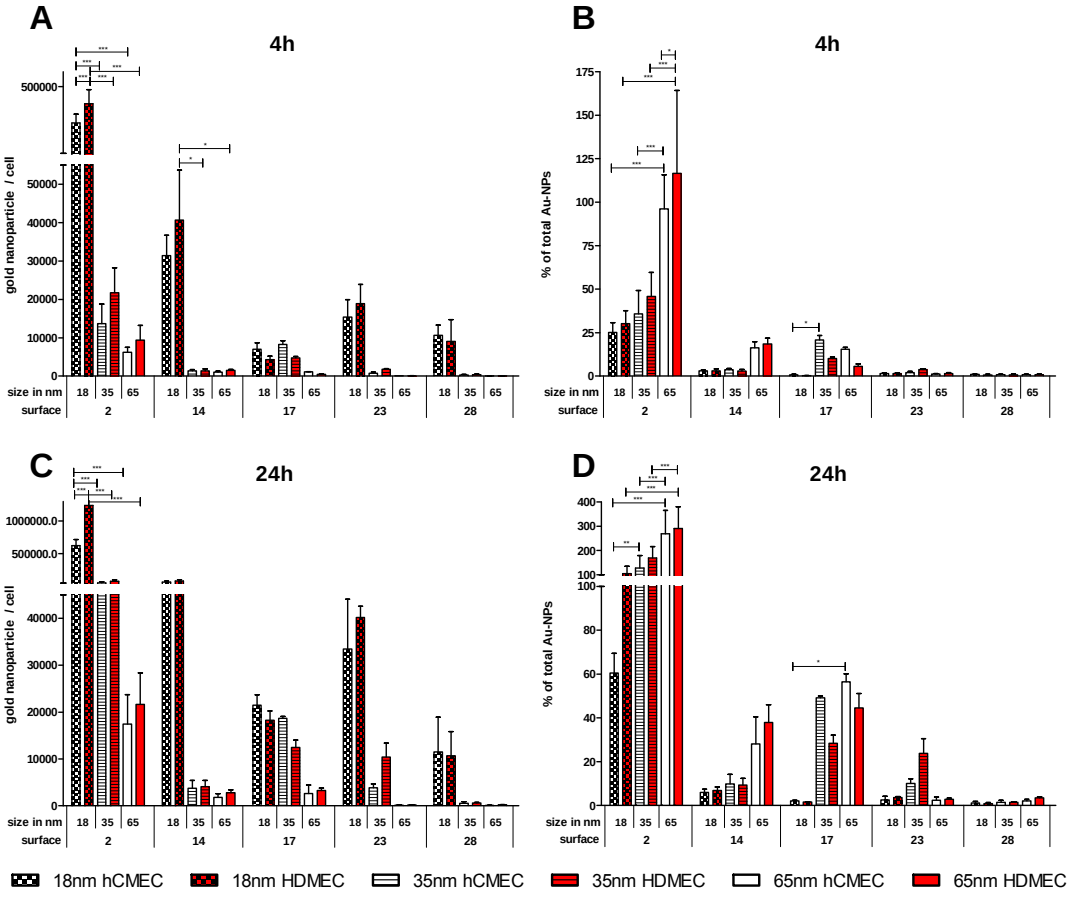

Fig. 30: Quantification of internalized gold nanoparticles in HDMEC and hCMEC by ICP-AES

After the exposure of HDMEC and hCMEC to different sizes of gold nanoparticles with various surface modifications for 4 (**A** and **B**) and 24 hours (**C** and **D**) the amount of gold within the cells was quantified by ICP-AES. In (**A**) and (**C**) the uptake of gold nanoparticles per cell is presented while in (**B**) and (**D**) the percentage of the initial/total amount of gold nanoparticles in suspension is depicted. The different surface modifications are named by the coding (-2, -14, -17, -23 and -28; for details see Table 9, chapter 2.9). 18, 35 and 65 represent the different sizes which are additionally symbolized by different

fillings of the bars. All results of hCMEC and HDMEC are presented in white and red bars, respectively. (n = 4; two-way ANOVA with Bonferroni posttests; *: $p < 0.05$; *: $p < 0.005$; ***: $p < 0.001$).

In summary, the data presented in Fig. 30 demonstrates that the positive- and neutral-charged gold nanoparticles are preferentially taken up while the negative-charged particles (taurine, -23) were internalized in a lower amount, without showing differences in the uptake with respect to various sizes and cell types. However, the positive-charged ethanediamine-coated gold nanoparticles (-2) are internalized in such a high amount that the ICP-AES comes to its limit. In addition, the ethandiamine-coated nanoparticles were more sensitive regarding the storage compared to the other gold nanoparticles. Therefore, the focus of the investigation was directed to the neutral-charged gold nanoparticles and is presented in the next section. Although the amount of absorbed PEGylated gold nanoparticles is low these particles were used as control particles for the two variants of neutrally charged gold nanoparticles.

Comparison of the uptake of gold nanoparticles with neutrally charged surface modifications

The results of the quantification of the neutrally charged gold nanoparticles that were presented in Fig. 30 are depicted in Fig. 31 in more detail. By re-calculation of significant differences in the quantity of internalized gold nanoparticles without considering the results of the ethanediamine-coated nanoparticles a comparison of the amount of internalized neutrally charged nanoparticles was performed.

It is obvious that 18nm gold nanoparticles with a glucosamine surface modification (-14) were internalized in a high amount. Even after 4 hours 30000 and 40000 nanoparticles per cell were taken up by hCMEC and HDMEC, respectively. Despite the high standard deviation more of these nanoparticles were internalized by HDMEC compared to the number that was found in hCMEC. After 24 hours of incubation the difference between this two cell types was still present and significant (see Fig. 31 C). In comparison, the larger particles with a diameter of 35nm and 65nm were internalized in a significantly lower amount. Despite the high number of nanoparticles per cell the percentage of gold nanoparticles within the cells compared to the total number of particles present in the suspension was very low. Only around 3% of the 18nm sized glucosamine coated particles (-14) were internalized after 4 hours, while after 24 hours the percentage increased to around 6% in both cell types (see Fig. 31 B and D).

In contrast to the high number of glucosamine-coated nanoparticles within the cells almost no PEGylated gold nanoparticles were taken up. The percentages of particles that were internalized were around 2% in both hCMEC and HDMEC even

after 24 hours of incubation. Additionally, the number of nanoparticles per cell was very low. Only around 70 nanoparticles per cell with a diameter of 65nm were taken up in either of the cell types. The number of 18nm nanoparticles internalized was also less (around 10000 per cell) compared to the 18nm nanoparticles with a glucosamine coating (60000 to 80000 particles per cell, described earlier).

Interestingly, the nanoparticles with a hydroxypropylamine coating did not show such a drastic size effect for internalization as was observed with the PEGylated and glucosamine-coated nanoparticles. Both the 18nm-sized and the 35nm-sized gold nanoparticles were internalized to almost the same extent even after 24 hours (Fig. 31 A and C). Moreover, the percentage of internalized nanoparticles with the medium diameter (35nm) was higher than the percentage of internalization of the largest particles (65nm). This was different from the results that were observed with the other gold nanoparticles. In addition, differences between the uptake properties by the different cell types could be observed. Based on these interesting results, the hydroxypropylamine gold nanoparticles were used for further studies and the results are presented in section 4.4.2.5.

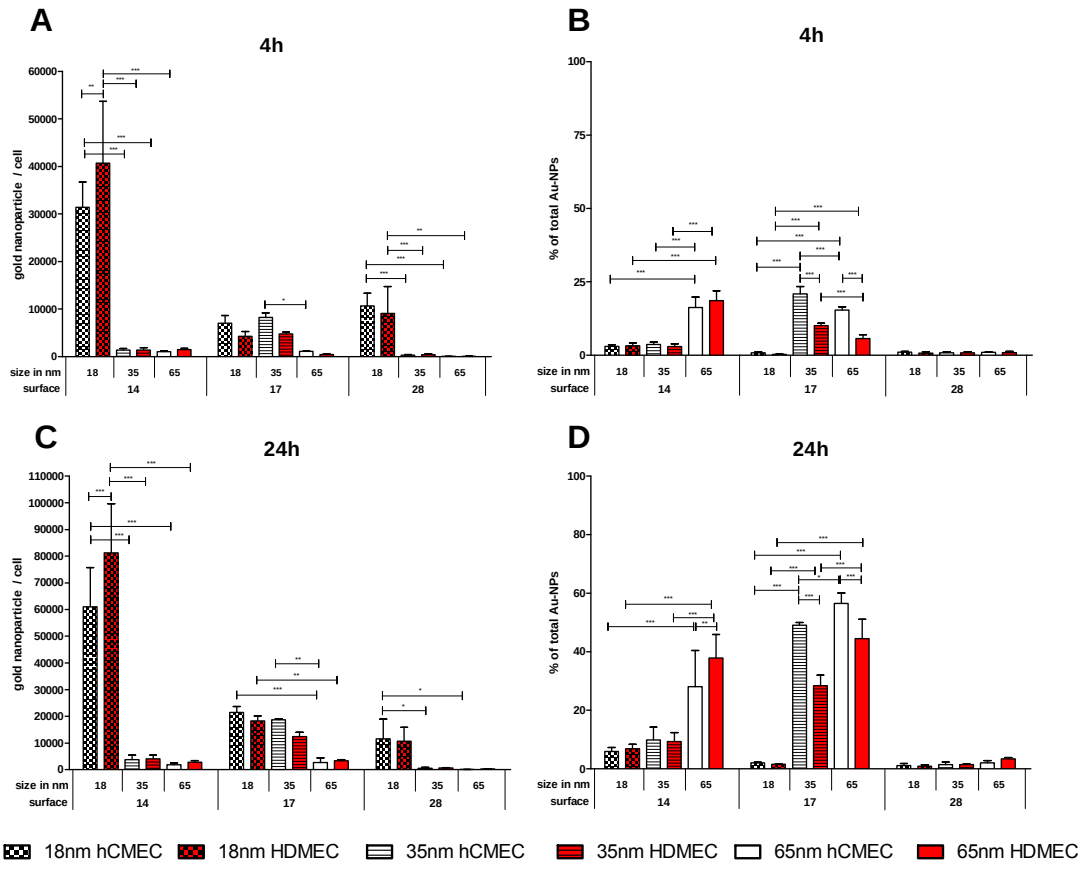

Fig. 31: Quantification of internalized gold nanoparticles in HDMEC and hCMEC by ICP-AES

After the exposure of HDMEC and hCMEC to different sizes of gold nanoparticles with various surface modifications for 4 (**A** and **B**) and 24 hours (**C** and **D**) the amount of gold within the cells were

quantified by ICP-AES. In (**A**) and (**C**) the uptake of gold nanoparticles per cell is presented while in (**B**) and (**D**) the percentage of the total amount of gold nanoparticles in suspension is depicted. The different surface modifications are named by the coding (-14, -17 and -28; for details see Table 9, chapter 2.9). 18, 35 and 65 represent the different sizes which are additionally symbolized by different fillings of the bars. All results of hCMEC and HDMEC are presented in white and red bars, respectively. (n = 4; two-way ANOVA with Bonferroni posttests; *: $p < 0.05$; *: $p < 0.005$; ***: $p < 0.001$).

4.4.2.4 Expression of pro-inflammatory mediators after exposure of endothelial cells to gold nanoparticles

The expression of pro-inflammatory mediators (MCP-1, IL-6, IL-8, MCP-1, ICAM and VCAM) was investigated by ELISA after the exposure of hCMEC to gold nanoparticles for different incubation times (4-72 hours). The stimulation of the cells with TNFα (300U) was used as a positive control for the expression of the different pro-inflammatory mediators. As depicted in Fig. 32 the exposure to different gold nanoparticles (concentration: 150µg/ml) led to an altered expression of the investigated pro-inflammatory mediators. Furthermore, various incubation times resulted in different expression patterns. After an exposure of 4 hours no increase in the expression of IL-6, IL-8, VCAM and ICAM could be detected. A slight increase in the expression of MCP-1 was detected after exposure to some of the gold nanoparticles (61-14, 65-17) for 4 hours. Compared to the 4 hour results, the expression of the pro-inflammatory mediators increased significantly after 24 hours of incubation with several of the gold nanoparticles. IL-6 expression after 24 hours of exposure to 61-14, 61-17, 65-14 was slightly increased compared to the untreated control, while a major increase in expression could be detected after exposure of the cells to the gold nanoparticles 65-14 and 71-14 (Fig. 32 A). The same results were observed after an incubation time of 48 and 72 hours, while the slight increase of IL-6 expression after 24 hours (55pg/ml) of exposure to 65-14 changed more dramatically with a higher IL-6 concentration (~150pg/ml).

In addition to changes in IL-6 expression, the expression of IL-8 after exposure to different sized gold nanoparticles with various surface modifications also varied and ranged from nearly 0pg/ml (4h) to over 1000pg/ml (72h). No differences in the expression of IL-8 could be observed after 4 hours of exposure to the different gold nanoparticles. After 24 hours the expression patterns of IL-8 increased after exposure to 61-14, 61-17, 65-14, 65-17 and 71-14. Interestingly the expression of IL-8 after exposure to 61-17 for 72 hours decreased to a normal expression pattern compared to the untreated control. However, the expression of IL-8 after exposure to 61-14, 65-14, 65-17 and 71-14 exhibited further increases. In addition, the expression of IL-8 increased only after exposure to 71-28 for 72 hours. Compared to

the untreated control cellular expression of IL-8 was unchanged after incubation times of 4, 24 and 48 hours.

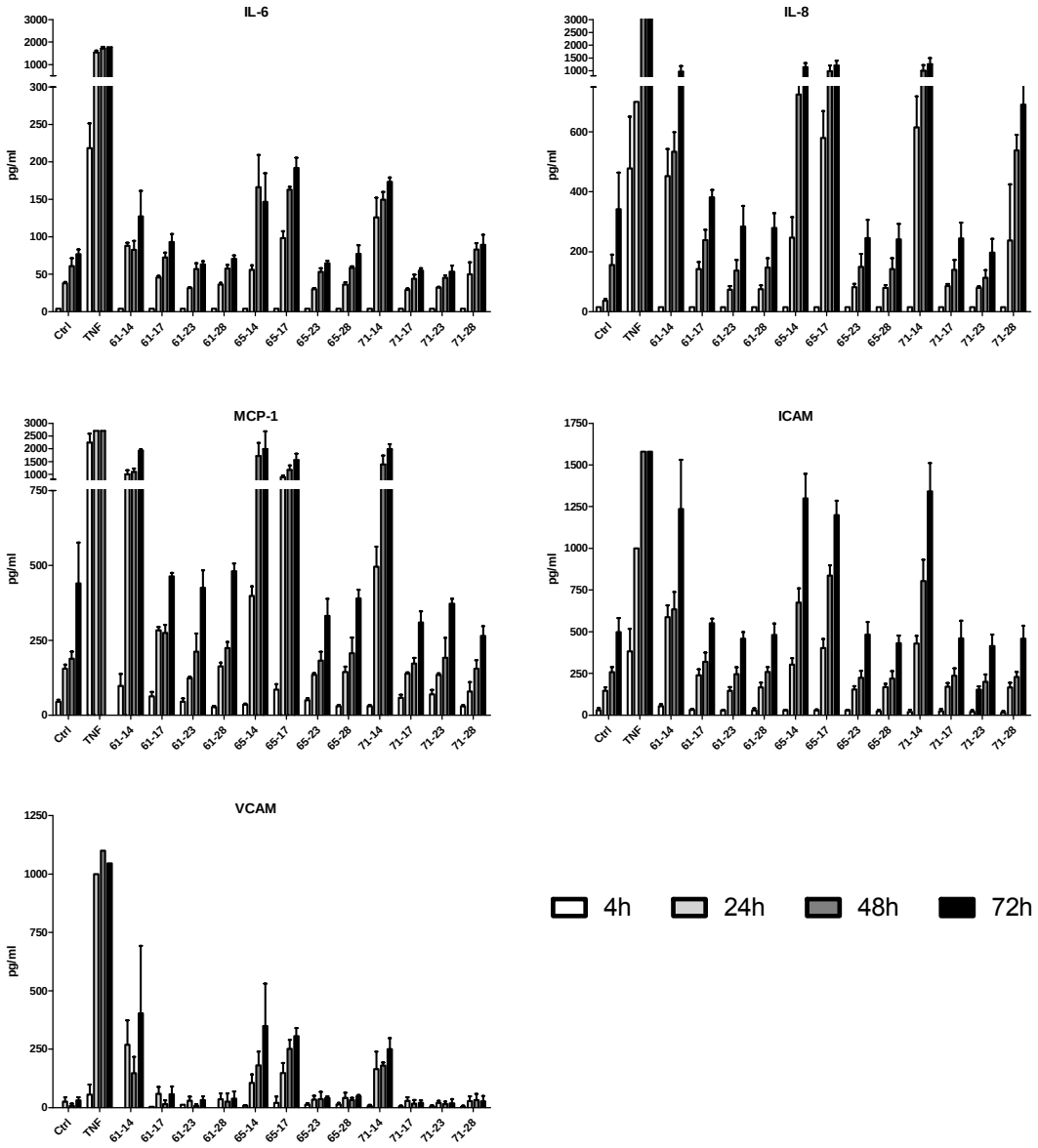

Fig. 32: Cytokine expression of hCMEC after stimulation with different gold nanoparticles

hCMECs were treated with 150µg/ml gold nanoparticles with different sizes and surface modifications. The concentrations of pro-inflammatory mediators were determined using ELISA after 4h, 24h, 48h and 72h. As positive control cells were stimulated with TNFα (300U/ml). Details are described in the text (means ± SD, n=6).

Comparison of the MCP-1 expression pattern was similar to that observed for IL-8. Stimulation of the hCMEC with 61-14, 65-14, 65-17 and 71-14 led to a dramatic increase in MCP-1 expression after 24, 48 and 72 hours. In addition, the expression of the cell adhesion molecules, ICAM and VCAM, showed a similar pattern. In conclusion, the gold nanoparticles with surface modifications with glucosamine

resulted in an increase of expression of the pro-inflammatory mediators, MCP-1, IL-6, IL-8, VCAM and ICAM. Moreover, the medium-sized gold nanoparticle (35nm) with a hydroxypropylamine (-17)-modified surface resulted in an induction and an increased expression of the pro-inflammatory mediators. In summary, the expression of these mediators increased after exposure to the gold nanoparticles after 24 hours or more exposure time, whereas little change in expression was observed after incubation with nanoparticles for 4 hours.

4.4.2.5 Size effect of hydroxypropylamine-coated gold nanoparticles

Cell viability and cytotoxicity

Based on the results observed with the neutral-charged gold nanoparticles that were coated with hydroxypropylamine further studies with these nanoparticles were carried out. In addition to the effects on cell viability (see chapter 4.4.2) cytotoxic effects on human endothelial cells were determined (Fig. 33).

HDMEC and hCMEC were incubated with increasing amounts of hydroxypropylamine-coated gold nanoparticles for 24 hours. Cell viability and cytotoxicity in response to the exposure with the hydroxypropylamine-coated nanoparticles was determined by MTS and LDH assay, respectively. The results presented in Fig. 33 (A and B) indicate that the gold nanoparticles had no influence on the cell viability of HDMEC and hCMEC even at higher concentrations up to 250µg/ml. In addition, no differences in cell viability could be detected after treatment with the different-sized gold nanoparticles. Furthermore, continued incubation for up to 48 hours exhibited no effects on cell viability (data not shown).

A low level of cytotoxicity was observed in both cell types as measured by the enzymatic activity of released LDH (Fig. 33 C and D). The control revealed that the basal release of LDH in the two cell types differed. The total LDH amount of lyzed cells was set to 100%. The cytotoxic effect of the gold nanoparticles appeared to be concentration-dependent in both cell types and even after the treatment with higher concentrations (250µg/ml) only a slight increase in LDH release could be detected. Thus, the gold nanoparticles appeared to have little cytotoxic effect. Interestingly, the gold nanoparticles appeared to have a higher cytotoxic effect on the primary cells (HDMEC) compared to the brain endothelial cell line (hCMEC, Fig. 33 C and D, respectively), especially at higher concentrations of nanoparticles. Furthermore, the higher standard deviation of LDH released after exposure of nanoparticles to HDMEC compared to hCMEC may be due to the variability of endothelial cells obtained from different donors. Even after 48 hours of exposure to the nanoparticles

no major changes in cell toxicity or cell viability could be observed in both cell types compared to the controls (data not shown).

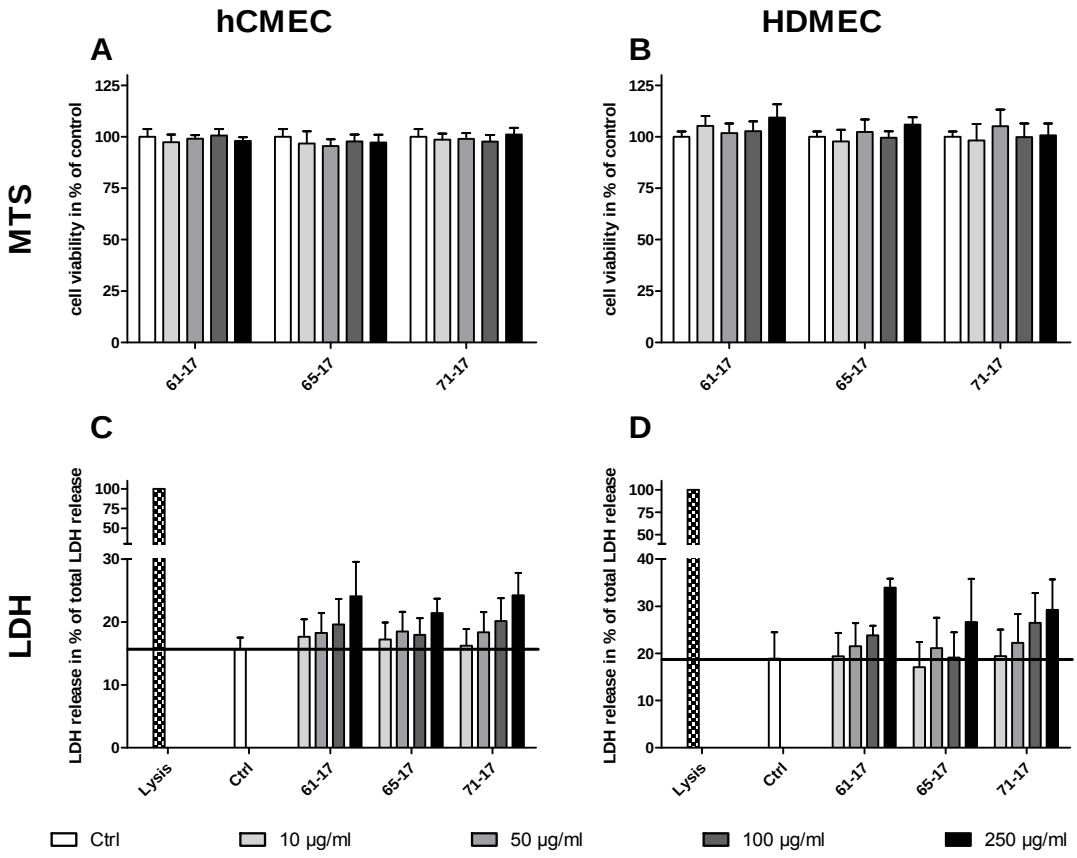

Fig. 33: Cell viability and cytotoxicity of endothelial cells after exposure to hydroxypropylamine-coated gold nanoparticles of different sizes

hCMEC and HDMEC were treated with various amounts of three different sizes of gold nanoparticles for 24 hours. Cell viability was measured by the MTS assay (**A** and **B**). The effect on cytotoxicity was analyzed by the quantification of lactate dehydrogenase released into the supernatants (**C** and **D**). Lysed cells were used to determine 100% LDH release. The cell viability of untreated cells (Ctrl) was set to 100%. Each result represents the mean ± standard deviation of three independent experiments; each of these was performed at least in triplicate.

Internalization of hydroxypropylamine-coated gold nanoparticles

hCMEC and HDMEC were exposed to three different sizes of hydroxypropylamine-coated gold nanoparticles (18nm, 35nm, 65nm). The internalization of these gold nanoparticles was analyzed by optical microscopy and by TEM. As shown in Fig. 34 and Fig. 35, differences in the amount of internalized gold nanoparticles could be detected by optical microscopy after 4 hours of exposure. The black dots represent agglomerations or possible aggregations of gold nanoparticles. Cell membranes were counter-stained to visualize the endothelial cell borders (CD31 staining, green and red-yellow). As shown in Fig. 34 high numbers of the gold nanoparticles were internalized into both cell types after 4 hours of exposure. Differences in the uptake

of the various sized gold nanoparticles were evident. The medium-sized gold nanoparticles (65-17; 35nm) were taken up to a higher extent compared to much lower quantities for the 61-17 (18nm) particles and the largest gold nanoparticles (71-17, 65nm). Some of particles were located in the perinuclear region of the cells after 4 hours of incubation (see arrows in Fig. 34).

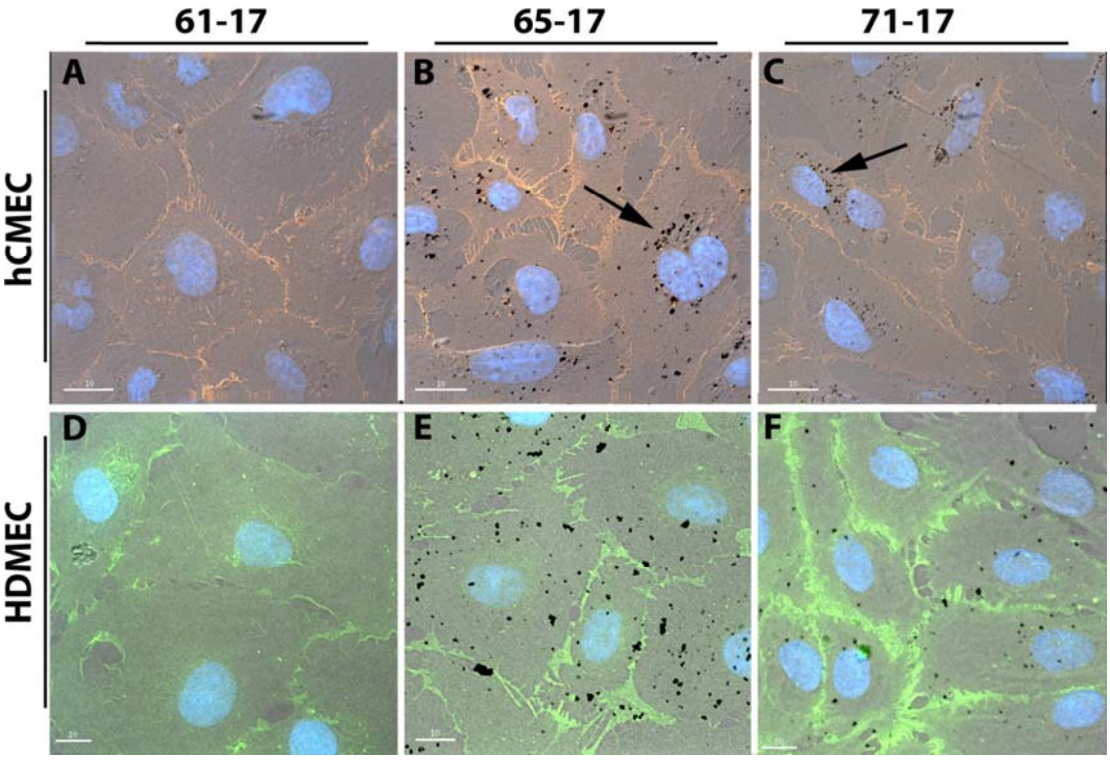

Fig. 34: Optical microscopy of internalized hydroxypropylamine-coated gold nanoparticles in hCMEC and HDMEC after 4h of incubation

hCMEC (**A**-**C**) and HDMEC (**D**-**F**) were incubated with 100µg/ml gold nanoparticles at 37°C for 4h. Cell membranes were stained by immunostaining of the membrane-integrated CD31 (red-yellow/green). Cell nuclei were stained with Hoechst dye (blue). Agglomerations of gold nanoparticles can be detected as black dots Optical/fluorescence microscopy (60x).

In Fig. 35 the uptake of the gold nanoparticles after incubation for 24 hours is depicted. Compared to the 4 hour exposure (see Fig. 34) a higher amount of nanoparticles could be detected after 24 hours of exposure. At this time point the smallest particles (61-17) as well as the larger particles (71-17) were observed in cells by optical microscopy. In addition, more particles were located in the perinuclear region. Deleterious changes in cell morphology could not be detected.

Since the resolution using optical microscopy is limited no single particles could be visualized. Therefore, an exact comparison of the quantity of internalized gold nanoparticles in HDMEC and hCMEC could not be performed. In addition, the heterogeneous uptake by single cells within the monolayers of both cell types made a comparison of the exact amount of internalized gold nanoparticles of the two cell types difficult.

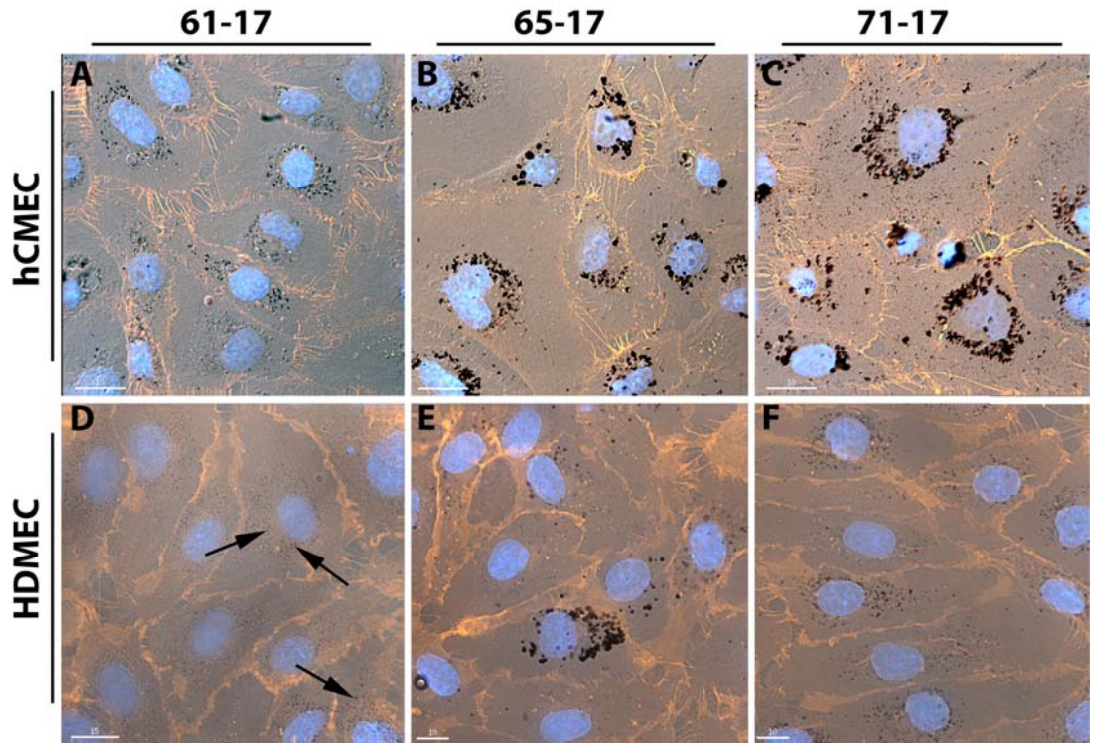

Fig. 35: Detection of hydroxypropylamine-coated gold nanoparticles in HDMEC and hCMEC by optical microscopy after 24 hours exposure

hCMEC (**A**-**C**) and HDMEC (**D**-**E**) were treated with 100µg/ml gold nanoparticles at 37°C for 24 hours. After washing and fixation cell membranes were stained with anti-CD31 antibody and the corresponding secondary antibody (red-yellow). Nuclei were stained with Hoechst dye (blue). Agglomerations of gold nanoparticles can be detected as black dots. In (**D**) aggregations are quite small as indicated by black arrows (optical/fluorescence microscopy, Delta Vision, 60x).

The internalization of the nanoparticles was demonstrated by transmission electron microscopy (TEM). The images in Fig. 36 confirmed the uptake of gold nanoparticles by cells and the storage of the gold nanoparticles in the perinuclear region within the cells. By TEM it was possible to detect single gold nanoparticles and it could be demonstrated that gold nanoparticles were stored in vesicular-like structures. None of the nanoparticles were detected in the cytoplasm, in mitochondria or in the nucleus. Representative images of the uptake of the different sized gold nanoparticles in HDMEC and hCMEC are presented in Fig. 36. In Fig. 36 the uptake of the different sized hydroxypropylamine-coated gold nanoparticles is shown after 4 hours of incubation. The comparison with Fig. 37 indicates that after a 24 hour incubation period more nanoparticles were internalized in the latter case.

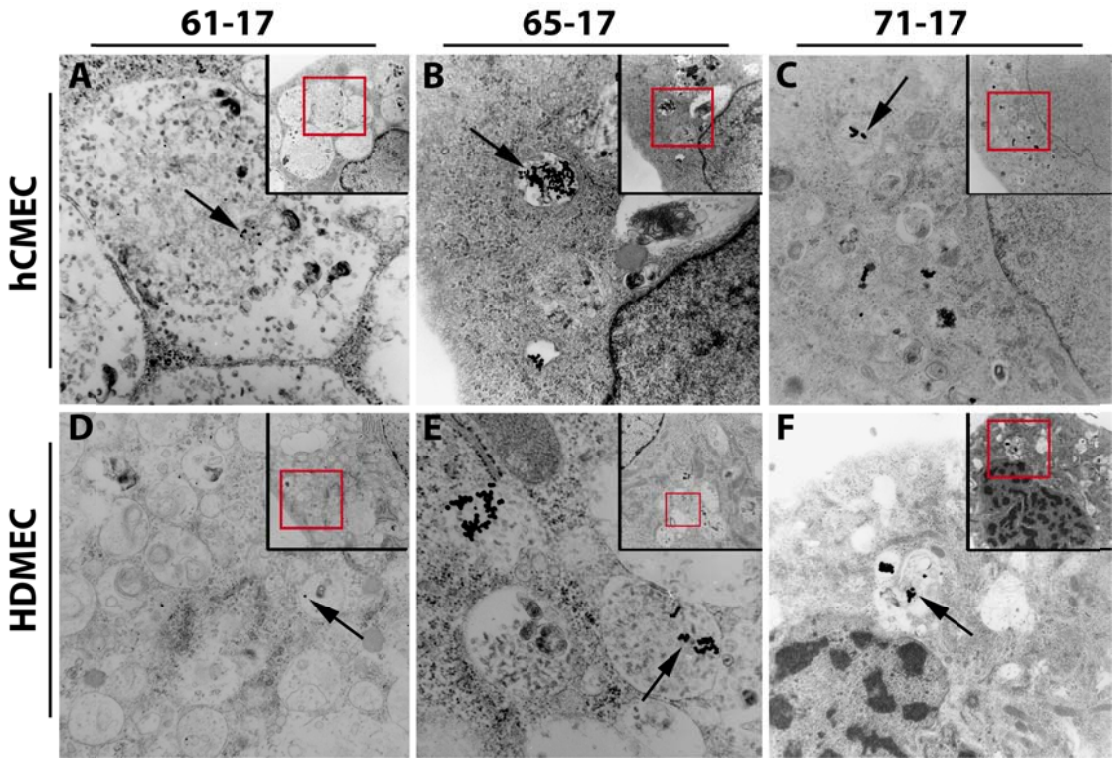

Fig. 36: TEM images of hCMEC and HDMEC after treatment with different sized hydroxypropylamine-coated gold nanoparticles for 4 hours

hCMEC (**A**-**C**) and HDMEC (**D**-**E**) were treated with 10µg/ml gold nanoparticles, fixed with glutaraldehyde and prepared for TEM microscopy. Arrows indicate the gold nanoparticles within the cells. Images in the upper right-hand corners with the red perimeter represent the overview of the magnified main image (Images 3500x; small images 2100x (**A**-**C** and **F**); 890x (**E**)).

In addition to the time-dependent difference in the amount of internalized gold nanoparticles, the medium sized gold nanoparticles (65-17, 35nm) appeared to be internalized more effectively compared to the smaller and larger gold nanoparticles (18nm and 65nm, respectively) in both cell types.

None of the TEM images showed gold nanoparticles at the surface of the cells. Thus, it was not possible to delineate the absorption or uptake mechanisms by TEM analysis. In conclusion, single particles within the cells could be visualized by TEM analysis and a storage in vesicles arranged around the nuclei was observed.

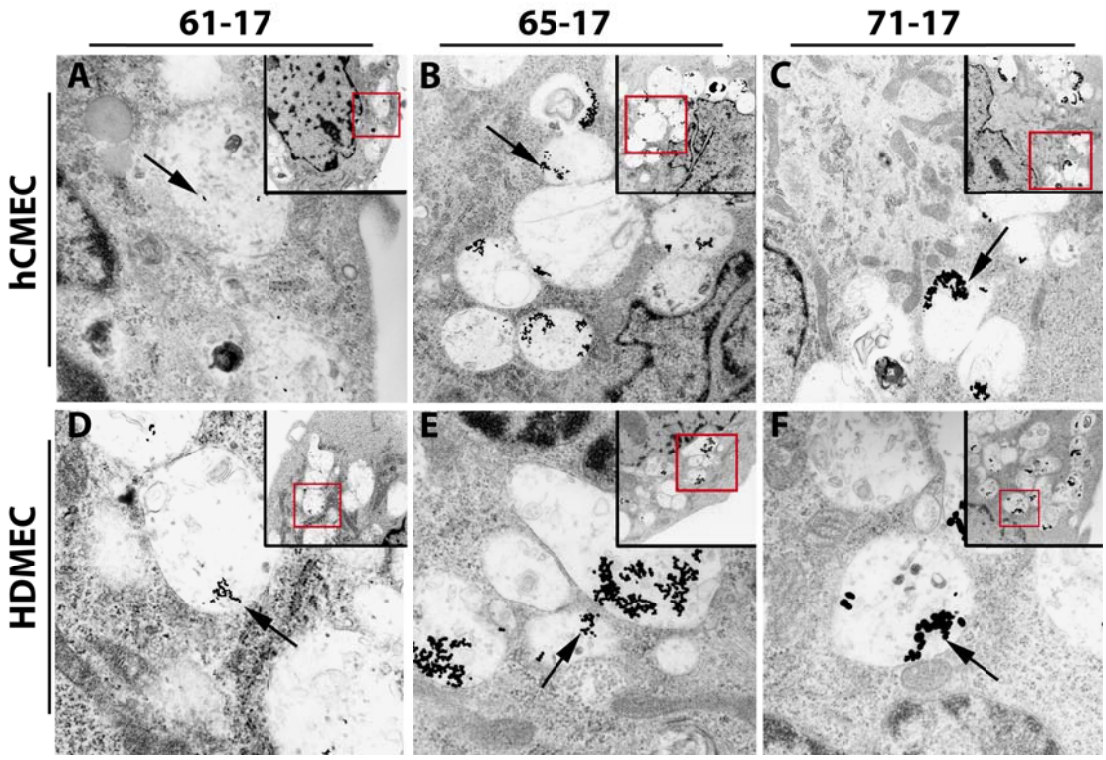

Fig. 37: TEM images of hCMEC and HDMEC after treatment with different sized hydroxypropylamine-coated gold nanoparticles for 24 hours

hCMEC (**A**-**C**) and HDMEC (**D**-**E**) were treated with 10µg/ml gold nanoparticles, fixed with glutaraldehyde and prepared for TEM microscopy. Arrows indicate the gold nanoparticles within the cells. Images in the upper right-hand corners with the red perimeter represent the overview of the magnified main image (Images 3500x; small images 2100x.

The results presented in Fig. 38 were generated by semi-quantitative real-time PCR and illustrate that differences in the expression of various pro-inflammatory mediators after exposure to 150µg/ml of different sized hydroxypropylamine-coated gold nanoparticles could be found at the mRNA level. All mediators examined exhibited a large induction of expression when exposed to TNFα while the control remained low and constant with time. However, the expression patterns, after exposure to different-sized nanoparticles varied at different time points. The mRNA level of MCP-1 after 4 hours exposure to all sizes of nanoparticles significantly increased compared to the untreated control. Over time this level decreased to the basal level of expression, although the expression of MCP-1 after exposure to the medium-sized nanoparticles remained upregulated for 24 and 48 hours and did not decrease to the basal level until after 72 hours of exposure.

The expression of IL-8 was only slightly upregulated following treatment with the 35nm sized gold nanoparticles (65-17). The highest expression level could be found after 24 hours of exposure, while the expression level decreased to the basal level after 72 hours of treatment.

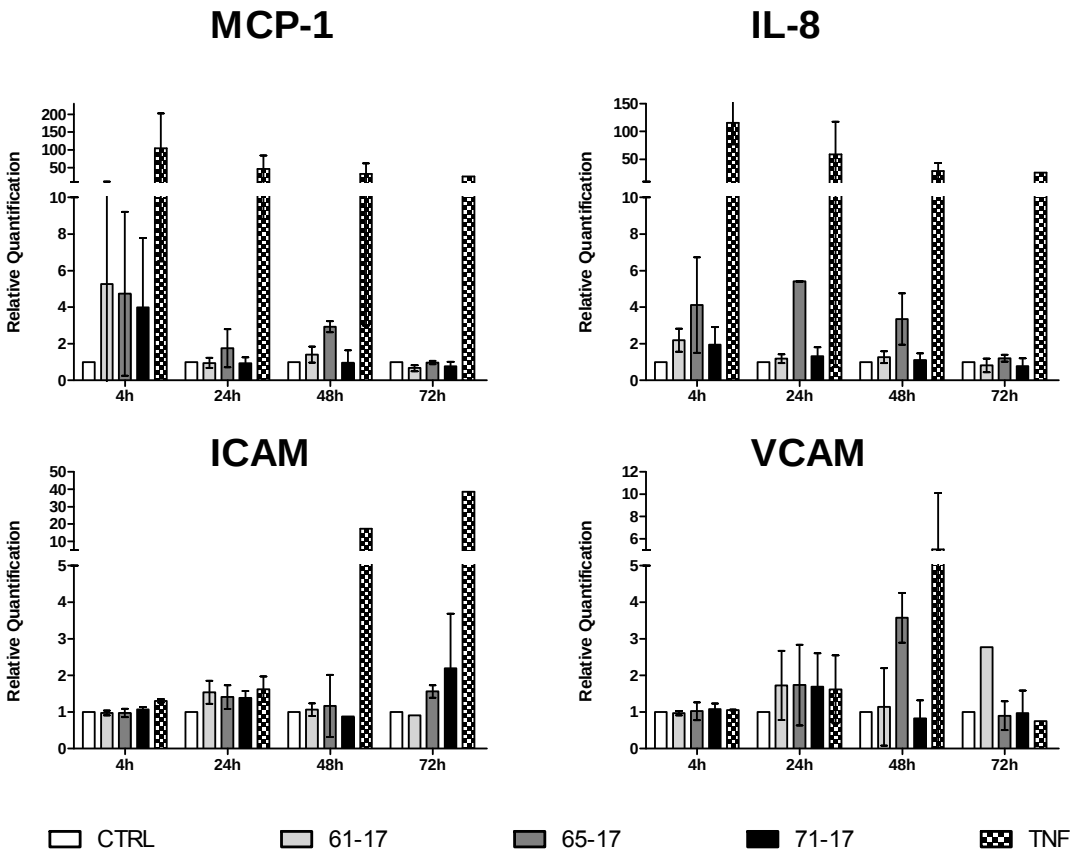

Fig. 38: Expression of pro-inflammatory factors in hCMEC after treatment with 150µg/ml hydroxypropylamine-coated gold nanoparticles at various time points as determined by real-time PCR

hCMEC were stimulated with 150µg/ml hydroxypropylamine-coated gold nanoparticles with different sizes. The concentrations of pro-inflammatory factors were determined using real-time PCR after 4h, 24h, 48h and 72h. As positive control cells were stimulated with TNFα (150U/ml). Details are described in the text (means ± SD, n=3).

The results determined by real-time PCR analysis reflected the results measured by ELISA. The expression of pro-inflammatory factors determined by ELISA after stimulation with 150µg/ml of hydroxypropylamine-coated nanoparticles is depicted in Fig. 39. After 4 hours of exposure with different-sized gold nanoparticles the expression levels of none of the investigated pro-inflammatory mediators were increased after treatment of the cells with the different gold nanoparticles compared to the untreated control cells. However, the concentrations of the pro-inflammatory factors after exposure to TNFα were significantly increased compared to the control cells. The MCP-1 protein was nearly expressed at maximum level even after 4 hours of incubation while the expression of the other pro-inflammatory factors increased over time.

The expression of MCP-1, IL-8, ICAM and VCAM increased after the treatment with 65-17 for 24 hours. However, after the treatment with 61-17 and 71-17 for 24 hours the expression level of these factors did not increase compared to the untreated control cells. The expression of MCP-1 and IL-8 reached their maximum after 24 hours of incubation, while the expression of the cell adhesion molecules increased over time only after exposure to the medium-sized nanoparticles. In summary, the expression patterns of pro-inflammatory mediators of hCMEC were influenced by the incubation with different sizes of gold nanoparticles with the same surface modification and different amounts of the investigated factors were expressed at different time points of the treatment and increased with exposure time.

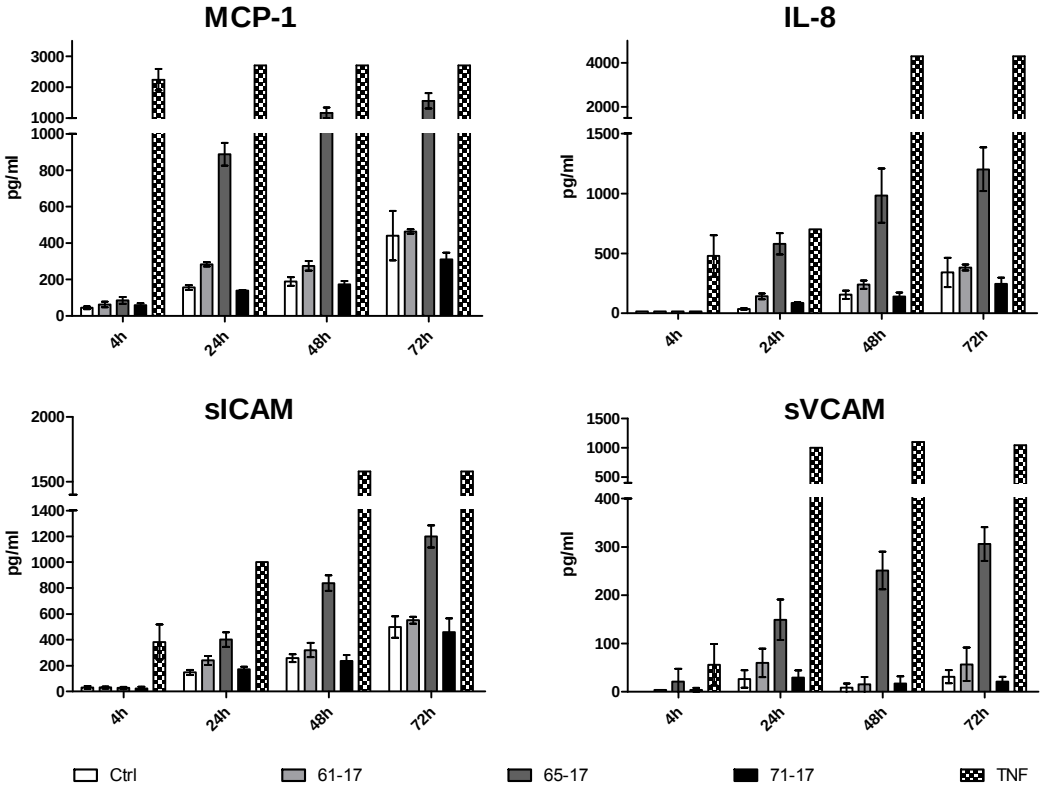

Fig. 39: Expression of pro-inflammatory factors in hCMEC after treatment with 150µg/ml hydroxypropylamine-coated gold nanoparticles at various time points determined by ELISA

hCMEC were stimulated with 150µg/ml hydroxypropylamine-coated gold nanoparticles of different sizes. The concentrations of pro-inflammatory factors were determined using ELISA after 4h, 24h, 48h and 72h. As positive control cells were stimulated with TNFα (150U/ml). Details are described in the text (means ± SD, n=3).

4.4.3 Exposure of PBECs cultured on transwell filters with different sizes of hydroxypropylamine-coated gold nanoparticles

After the isolation of porcine brain microvessels the outgrowing endothelial cells formed a tight barrier on transwell filter membranes and this was confirmed by TEER measurements (~284 Ohm x cm², Fig. 41). The cells were incubated with a

high concentration of hydroxypropylamine-coated gold nanoparticles (100g/ml and 500µg/ml) for 3 hours. After extensively washing with Hepes buffer and fixation with glutaraldehyde TEM analysis was performed to determine the amount of uptake into the endothelial cells. In Fig. 40 the black arrows indicate internalized gold nanoparticles. In Fig. 40 B, D and F, high magnification images revealed that the gold nanoparticles were internalized and located in vesicles. After 3 hours of incubation the gold nanoparticles were not located in the perinuclear region. In addition to the short incubation time a possible transcytosis could also be a reason for the absence of gold nanoparticles in vesicles around the nuclei. Although a high concentration of gold nanoparticles was used the number of internalized gold nanoparticles was very low.

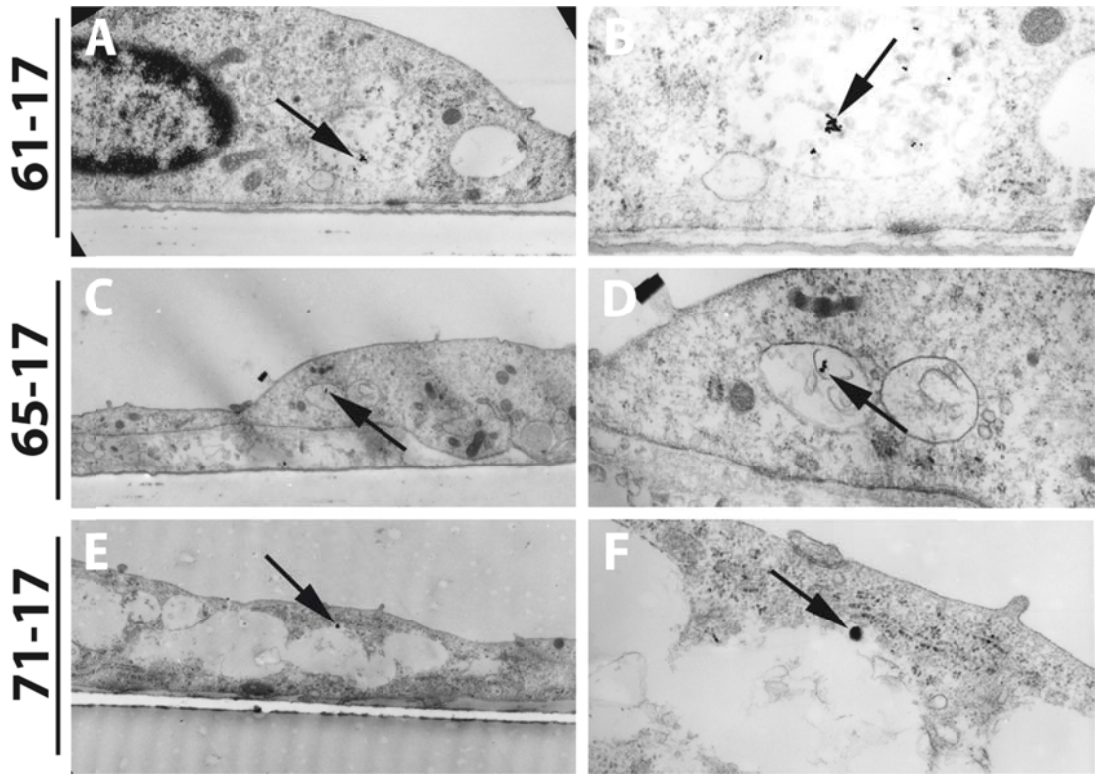

Fig. 40: Uptake of hydroxypropylamine-coated gold nanoparticles in PBECs seeded on transwell filter membranes

After the isolation of PBECs the microvessels were directly seeded on transwell filter membranes. After culturing the cells for 8 days they were treated with 500µg/ml hydroxypropylamine-coated gold nanoparticles for 3 hours. Cells were washed with PBS and fixed with glutaraldehyde followed by transmission electron microscopy. Black arrows indicate gold nanoparticles which are located in vesicles within the cells. (magnifications: (**A**) 22000x, (**B**, **F**) 44500x, (**C**) 10500x, (**D**) 36500x, (**E**) 16500x).

During the exposure of PBEC on transwell filter membranes to 100µg/ml and 500µg/ml of different sized hydroxypropylamine-coated gold nanoparticles the TEER-values were measured every 30 minutes (Fig. 41). In addition, 50µl medium from the basolateral compartment of three different wells for each stimulation were

collected and the gold concentration in parts per billion determined by ICP-AES as a measure of the transport properties of the respective type of gold nanoparticle (Fig. 42).

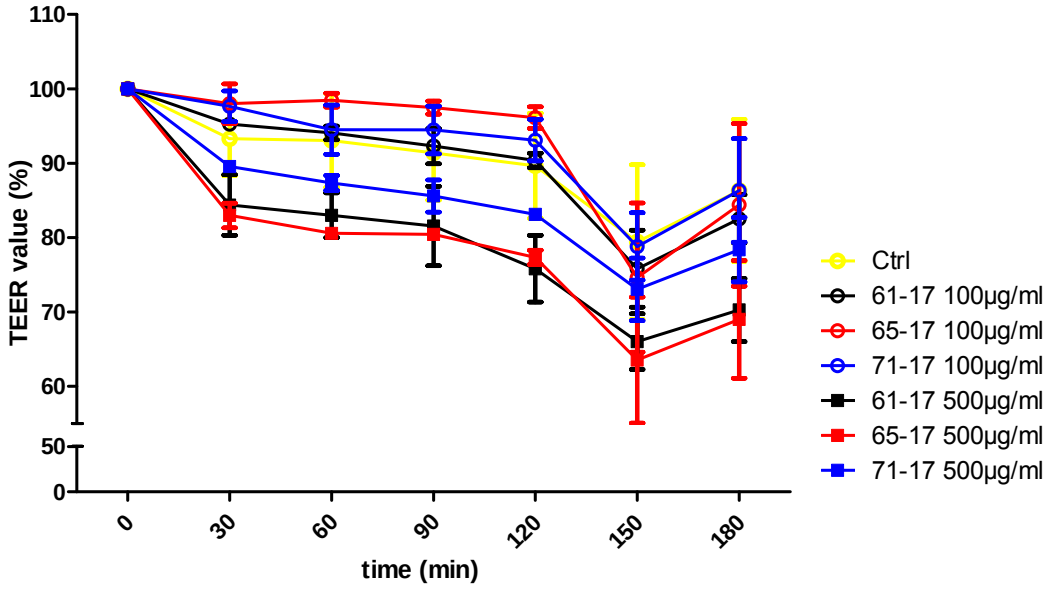

Fig. 41: Mean TEER-values in percent of PBECs cultured on transwell filters during exposure to gold nanoparticles

Mean TEER-values of 3 different wells for each stimulation were measured at time point 0 and set to 100%. Every 30 minutes during the incubation TEER-values were measured. The mean percentage was determined and is demonstrated as a data point for every stimulation. The TEER-values at the beginning of the experiment were ~ 220 Ohm x cm² (one donor, n=3).

In Fig. 41, it is evident that the TEER-values of the cells that were exposed to different concentrations of gold nanoparticles decreased with time. In addition, the TEER-values of the control cells also decreased. Furthermore, the permeability of the cells incubated with the higher amount of gold nanoparticles (500µg/ml) increased more markedly, compared to the permeability of the cells that were exposed to 100µg/ml. After exposure to 500µg/ml of 65-17 and 61-17 the TEER values decreased to 70%. After 150 minutes of incubation all measured TEER values strongly decreased, but recovered after 180 min of exposure.

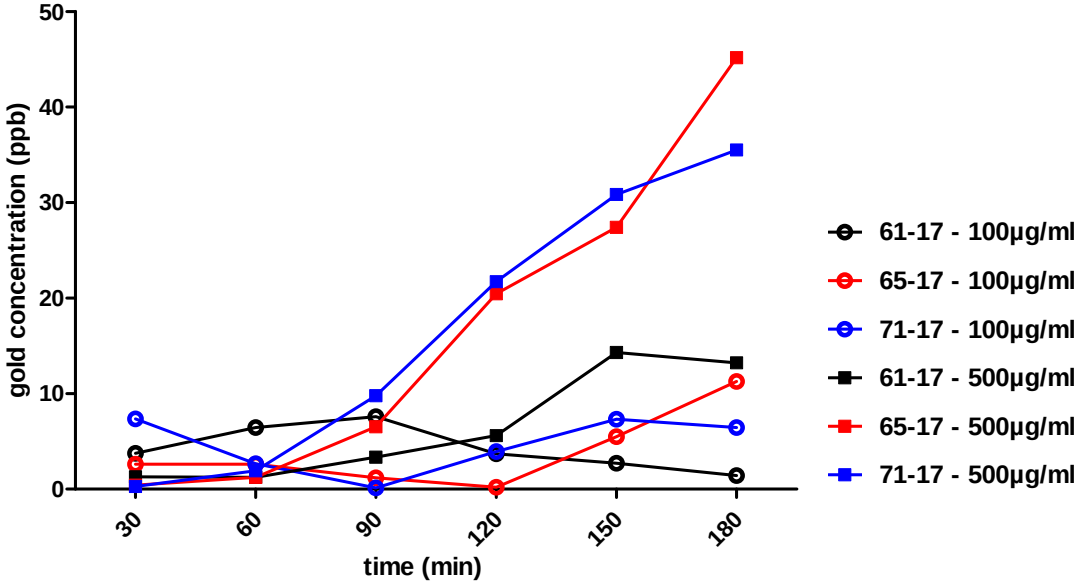

Fig. 42: Gold nanoparticle concentrations in ppb in the basolateral compartment of the transwell plate after incubation of PBECs with different concentrations of hydroxypropylamine-coated gold nanoparticles of different sizes

In Fig. 42 it is demonstrated that only small amounts of gold could be detected in cells incubated with 100µg/ml gold nanoparticles. Thus, a comparison of the amounts of gold transported across the cells was not possible. However a higher gold concentration in the basolateral compartment could be detected by ICP-AES after stimulation with 500µg/ml gold nanoparticles. The medium sized (65-17) as well as the larger particles (71-17) passed the barrier generated by the PBECs to a greater extent than the small nanoparticles (61-17). The measured gold concentration of 65-17 was 4-fold higher compared to the concentration of 61-17 after 3 hours of exposure to 500µg/ml of the corresponding nanoparticles.

5 Discussion

The first goal of this study was the establishment of a reproducible *in vitro* model of the human blood-brain barrier (BBB). Due to the difficulty in obtaining fresh human brain tissue for the isolation of cells, porcine brain tissue was initially used. After the commencement of this project a human brain endothelial cell line was described in the literature and subsequently obtained by our laboratory. During these studies the human brain endothelial cell line (hCMEC/D3) was compared to primary brain endothelial cells isolated from pigs. The characteristics of both brain cell types had to be determined and were compared to other primary human endothelial cells from different locations of the body for specific endothelial cell markers. Furthermore, the ability of brain endothelial cells to form an *in vitro* BBB and exhibit characteristics of the *in vivo* BBB was evaluated using various relevant techniques.

The second goal of this thesis was the investigation of the uptake behaviour of various gold nanoparticles by brain endothelial cell types and to compare this with primary human endothelial cells isolated from other parts of the human body and various human epithelial cell lines.

The overall aim was to determine if cell reactions to gold nanoparticle exposure differ from cell type to cell type and if different physico-chemical characteristics of gold nanoparticles influence their interaction with these cell types. This included studies to determine if exposure to different gold nanoparticles might lead to the induction of cytotoxicity, the expression of pro-inflammatory cytokines or influence the uptake behavior. In addition, if and how the gold nanoparticles entered the cell and if they are able to be exocytosed at the basolateral membrane of the endothelium was to be determined.

In the next sections the results of this study presented in chapter 4 will be discussed in relation to previously published data. New insights for the field of nanoscience will be emphasized.

5.1 Establishment of *in vitro* blood-brain barrier models

To establish an *in vitro* model of the blood-brain barrier it is of great importance to use well characterized endothelial cells. Due to the lack and difficulties in obtaining fresh human brain tissue it is possible to use permanent human brain endothelial cell lines or primary endothelial cells derived from other animal species as a substitute primary human brain endothelial cell type. To characterize endothelial cells different specific cell markers, such as PECAM-1 and von Willebrand factor

(vWF) were identified by Albelda and Jaffe, respectively (Jaffe et al., 1974; Albelda et al., 1990). These markers were also expressed in primary human dermal microvascular endothelial cells (HDMEC) (Unger et al., 2002a) which were used as control cells for the expression of endothelial cell markers in this study.

The expression of the two above mentioned endothelial cell markers, PECAM-1 and vWF, and additionally the expression of VE-cadherin in HDMEC and hCMEC/D3 were compared by immunocytochemical staining. In addition, the immunostaining of typical junctional proteins needed to form a tight blood-brain barrier (ZO-1, occludin, beta catenin, etc.) as well as the expression of ABC efflux transporters (MDR-1, BCRP, MRP-1) present in the BBB as determined by reverse transcriptase polymerase chain reaction identified hCMECs as brain endothelial cells. These findings are in accordance with the results which were previously published by Weksler et al. (Weksler et al., 2005).

Parallel to the human cell line characterization primary microvascular endothelial and HUVEC cells and pericytes derived from porcine brain tissue were characterized. By using the techniques described above the primary isolated porcine brain endothelial cells were shown to be endothelial cells. The characteristic morphology and the outgrowth of the cells from the isolated capillary fragments showed high similarities to the endothelial cells derived from human brain tumor tissue described by Unger et al. (Unger et al., 2002b). In addition, the formation of vesicular structures after seeding endothelial cells in a collagen type I gel was an additional characteristic typical of endothelial cells.

The characterization of pericytes is quite difficult due to a lack of specific markers and the multipotent character of the cells to differentiate into fibroblast-like cells, osteoblasts, chondrocytes or adipocytes (Sims, 2000; Allt and Lawrenson, 2001; Bondjers et al., 2003). It is known that pericytes express markers, such as smooth muscle actin (SMA), desmin, neuronal-glial-2 (NG-2), aminopeptidase A and N and vimentin (Nehls and Drenckhahn, 1993; Armulik et al., 2005) but are negative for the expression of CD31 and vWF (endothelial cell markers) (Shimizu et al., 2008). Due to the pluripotent character of pericytes, Armulik and his group suggested that a characterization of pericytes had to be done with a broad spectrum of markers and with a combination of methods to prevent miss-classification (Armulik et al., 2005; Lai and Kuo, 2005). In addition to the above mentioned markers, a glycolipid expressed in the plasma membrane, 3G5, has been identified as a specific marker for pericytes within the microvasculature (Nayak et al., 1992). Endothelial cells and also smooth muscle cells which share many markers with pericytes are negative for the 3G5 antigen (Nayak et al., 1988; Bergers and Song, 2005). The production of a

mAb against 3G5 has been achieved. By using hydridoma cells, purchased by LGC Promochem, grown in a bioreactor, mAb 3G5 was released into the supernatant. It was possible to identify pericytes in monoculture as well as in triculture with brain endothelial cells and astrocytes. Staining human brain sections exhibited patterns comparable to the results published by Armulik's group and by Nayak and co-workers (Nayak et al., 1988; Armulik et al., 2005).

After characterizing human cerebral microvascular endothelial cells (hCMEC/D3) and demonstrating that most endothelial cell markers as well as BBB markers were present, the cells were cultured to determine whether they also exhibited barrier properties. When Weksler et al seeded the cells on transwell filter membranes little or no transendothelial electrical resistance (TEER) was observed and similar results could also be demonstrated in these present studies. Changing the culture conditions did not enhance the TEER. Images made by electron microscopy of confluent hCMECs on filter membranes demonstrated that the cells did not form a homogenous cell layer and did not exhibit tight junctions. The addition of hydrocortisone, which is known to decrease proliferation and increase differentiation and therefore potentially tighten the barrier (Hoheisel et al., 1998), also failed to prevent the formation of double layers of cells in some regions of the transwell, which additionally exhibited a poor expression of tight junction proteins. This study demonstrated for the first time that the growth of hCMEC was not contact inhibited. This could be the reason why the measured transendothelial electrical resistance (TEER) was low and confirmed in these studies (Weksler et al., 2005).

Due to the importance of a high TEER to characterize and define a tight barrier, primary porcine brain microvascular endothelial cells (PBEC) were used in an attempt to set up a barrier with a low permeability coefficient and high TEER. In the literature several blood-brain barrier models have been described. Zhang and his group also used porcine brain endothelial cells and successfully set up a barrier model with TEER values of 300 to 420 Ohm x cm² (Zhang et al., 2006). *In vivo* the electrical resistance of tightly connected brain endothelial cells was described to be between 1500 to 2000 Ohm x cm² (Crone and Olesen, 1982). It should be noted that the resistance of capillary endothelium in other parts of the body are quite low (3.3 Ohm x cm²) (Crone and Christensen, 1981). Although TEER values *in vivo* have not been achieved *in vitro,* the barrier attained with primary porcine brain endothelial cells in this thesis gave results comparable to those described by Zhang et al. (Zhang et al., 2006). The highest TEER values in the monoculture model of porcine endothelial cells were observed at day 13 and began to decrease afterwards. This decrease in TEER was also described for the rat BBB model system by Garcia-

Garcia and co-workers (Garcia-Garcia et al., 2005). The difference in TEER of hCMEC and the primary culture of porcine brain endothelial cells could also be explained by comparing the electron microscopy images. The cell-cell contacts of PBECs were more distinctive compared to hCMEC. In addition, PBECs generated a monolayer of cells that were completely contact inhibited thus explaining the barrier properties generated.

The complexity of the neurovascular unit and especially the importance of the interaction of the different cell types (endothelial cells, pericytes, astrocytes) involved in barrier functions make it difficult to set up an *in vitro* blood-brain barrier model which exhibits all of the *in vivo* properties (Choi and Kim, 2008). Therefore the initial *in vitro* models were developed as systems which were rapidly established and reproducible and thus available for screening purposes (Dehouck et al., 1990). Further studies revealed that the interaction of the different cell types improved the barrier properties *in vitro*. More complex models were set up with cells from different species (Gaillard et al., 2001; Kido et al., 2002; Jeliazkova-Mecheva and Bobilya, 2003) and a 3D model was developed by the group of Al Ahmad (Al Ahmad et al., 2010).

The interaction of bovine brain endothelial cells and rat astrocytes in coculture increased the transbilayer electrical resistance (TER) and also decreased paracellular transport (Dehouck et al., 1990; Gaillard et al., 2001). In addition, Galla and his group demonstrated that astrocytes or astrocyte-conditioned media increased the tightness of the barrier but that cell-cell interactions also increased cellular factors of the model system (Franke et al., 2000). Lai et al. described a triculture with endothelial cells, astrocytes and pericytes that exhibit many characteristics of the *in vivo* BBB system (Lai and Kuo, 2005). Also the group of Garberg claimed that only a representative and complex model system can provide meaningful information for *in vivo* applications (Garberg et al., 2005). However, the complexity of establishing an *in vitro* BBB model increases with the addition of each cell type. Besides the cell-cell interactions of astrocytes and brain endothelial cells the intercellular cross-talk of brain endothelial cells and pericytes are also of major importance in the neurovascular unit.

Nakagawa and co-workers compared several mono-, co- and tricultures with rat brain capillary endothelial cell, pericytes and astrocytes. The outcome of the comparison was that the presence of pericytes strengthens the tightness of the BBB model (Nakagawa et al., 2007). However, Galla's group published data indicating that the increase in the level of vascular endothelial growth factor (VEGF) released by porcine pericytes decreased the transbilayer electrical resistance (TER) of the

primary porcine BBB model system, while the use of a neutralizing VEGF antibody lead to an increase of the resistance. They also demonstrated that brain endothelial cells in coculture with pericytes showed a decreased expression of the tight junction-associated protein, occludin. In conclusion, they postulated that a decrease in the TER was caused by the cross-talk of pericytes and endothelial cells by various secreted factors, which were also the results shown in the present study (Zozulya et al., 2008; Thanabalasundaram et al., 2010).

The tightness of the *in vitro* barriers can also be determined by transport assays of model drug substances such as [^{14}C]-sucrose or different-sized FITC-dextrans. The unit for measuring the tightness of the barrier is indicated as the permeability coefficient. Although the TEER values of hCMEC and monocultures of PBEC varied significantly the permeability coefficients measured by the transport of different sized FITC-dextrans were almost identical. Nearly the same permeability coefficients for hCMECs were described by Weksler and Förster. Moreover, Weksler et al. demonstrated that these permeability coefficients indicated a tighter barrier compared to the barrier properties of monocultures of primary bovine brain endothelial cells (Weksler et al., 2005; Forster et al., 2008). As previously mentioned electron microscopy revealed that hCMEC grew in double layers and this could be the reason for a low permeability coefficient of the hCMEC culture. After short exposure times the double layer of cells might prevent the paracellular transport of the substances, although the cells show a lack of tight junctions as demonstrated by low TER and electron microscopy. It might also be possible that a prolongation of the exposure could lead to an increased permeability. Thus, in addition to measuring the electrical resistance and determining the permeability coefficient the investigation of the morphology of the cells by different microscopic techniques is necessary.

Nevertheless, the hCMEC cells exhibited brain endothelial cell characteristics and were used for uptake studies of gold nanoparticles in conventional monocultures seeded on culture plates in which the tightness of the barrier was not crucial. A co-culture model exhibiting high TER values could not be established. However, monocultures of PBEC which exhibit high TEER values, a typical brain endothelial morphology with tight junctions and a low permeability coefficient were used on transwell filter membranes to mimic the *in vivo* BBB.

5.2 Effects of the presence of sodium citrate on the surface of gold nanoparticles on cytotoxicity and uptake behavior in different human endothelial cells

In general, the physico-chemical properties of nanoparticles influence how cells react to them. It has been demonstrated by several groups that size, shape and surface modification of gold nanoparticles can affect their cytotoxicity as well as their internalization by different cell types (Chithrani et al., 2006; Eghtedari et al., 2009; Rayavarapu et al., 2010). Uboldi et al. have recently demonstrated that the cytotoxicity caused by gold nanoparticles on human lung epithelial cells correlates with the presence of sodium citrate on the gold nanoparticle surfaces (Uboldi et al., 2009). Whether the same effects occurred in various human endothelial cell types after exposure to the same gold nanoparticles was a goal of the present investigations. These gold nanoparticles with sizes of 10-11nm and 25nm and different amounts of sodium citrate on the surface of the gold nanoparticles (see chapter 4.4.1) were investigated by examining cytotoxicity and uptake behavior in cells. Kunzmann and co-workers demonstrated that the use of primary cells which are closer to the *in vivo* situation are of great importance in studying nanoparticle interactions (Kunzmann et al., 2010). The results generated in the present studies also support these conclusions.

It could be demonstrated in these studies that only high concentrations of gold nanoparticles (500µM and 1mM) influenced cell viability, proliferation rate and cytotoxicity, and that the reactions with primary human dermal microvascular endothelial cells (HDMEC) were more marked compared to the human cerebral microvascular endothelial cell line, hCMEC. These observations could be explained on the basis of the different characteristics of brain endothelial cells and endothelial cells derived from the dermal microvasculature (Dyer and Patterson, 2010). In light of the observations published by Uboldi et al. the unaltered or slightly decreased cell viability of endothelial cells after exposure to gold nanoparticles were comparable to human lung epithelial cells (Uboldi et al., 2009). In addition, the present studies with endothelial cells also agreed with further reports demonstrating that gold nanoparticles with surface modifications such as sodium citrate or biotinylated residues did not have an effect on a human leukemia cell line (Connor et al., 2005).

Interestingly, the comparison of the effect of the proliferation rate of epithelial cells after exposure to high concentrations of particles as shown by Uboldi et al. was higher compared to those of endothelial cells presented in this study (Uboldi et al., 2009). After exposure to high concentrations of gold nanoparticles with a higher

concentration of sodium citrate on the particle surface the proliferation rate of epithelial cells was dramatically decreased compared to the rate detected in endothelial cells. However, the same pattern of effects in the presence of sodium citrate on the surface of the particles was observed in endothelial and epithelial cells and was independent of the size of the particles (11nm, 25nm) as previously reported (Uboldi et al., 2009).

In addition to the increased effect on cells by gold nanoparticles with a higher concentration of sodium citrate, the uptake of the different gold nanoparticles was also investigated. Images made by transmission electron microcopy revealed that the gold nanoparticles were internalized by both epithelial and endothelial cells. According to Uboldi et al. the gold nanoparticles internalized were located in enclosed vesicles near the perinuclear region (Uboldi et al., 2009). No differences in the localization of the different sized gold nanoparticles were observed. In contrast to our findings, Rothen-Rutishauser and co-workers demonstrated that 25nm-sized gold nanoparticles could be detected freely dispersed in the cytoplasm of airway epithelial cells (Rothen-Rutishauser et al., 2007). Observations by other groups demonstrated that the distribution within the cells was indeed size-dependent. Pernodet et al. described that 14nm-sized citrate-coated gold nanoparticles were found in vesicles within human dermal fibroblasts (Pernodet et al., 2006). However, smaller gold nanoparticles (1.4nm) could cross the cell nuclear membrane and interact with the DNA in different human cell lines (Tsoli et al., 2005).

An analysis of the TEM images showed that epithelial cells exhibited a higher uptake rate with all of the gold nanoparticles investigated. These findings were confirmed in these studies by using the sensitive quantification of the gold nanoparticles by spectroscopy (ICP-AES). According to Uboldi et al. the uptake of gold nanoparticles was not influenced by the presence of sodium citrate (Uboldi et al., 2009).

The more dramatic effect on the proliferation rate of epithelial cells compared to endothelial cells might be explained by the higher amounts of internalized gold nanoparticles in combination with the presence of sodium citrate. AuS0302-RIT nanoparticles, in fact, are internalized in a very high amount while the proliferation rate in epithelial cells just slightly decreased compared to AuS0302-RIS02 and –RIS04 after 24 hour exposure. Nevertheless, the influence of internalized particles with contaminants (sodium citrate) on the surface which is not internalized into the cells cannot be excluded in general. Due to the small number of gold nanoparticles within endothelial cells an extrinsic effect of sodium citrate might play a role in the

reduction of the proliferation process or be the cause of the mild increase of cytotoxicity in hCMEC/D3.

The dramatic differences in the quantity of internalized gold nanoparticles between epithelial and endothelial cells are difficult to explain. Xia et al. showed different uptake mechanisms of cationic polystyrene nanospheres by human endothelial cells (HMEC) and epithelial cells (BEAS-2B). However these results were not correlated with a different amount of internalized nanospheres. Nevertheless, the BEAS-2B cells reacted in a more sensitive manner compared to endothelial cells and this resulted in necrotic cell death. They explained the more sensitive character as being due to the first-line-of-defense features in pulmonary cell types and also showed this response in macrophage-like cells (RAW 264.7) (Xia et al., 2008). In our study, the more sensitive character of the epithelial cells after exposure to AuS0302-nanoparticles was reflected by the decreased proliferation rate measured by the proliferation factor Ki-67 and not due to an increased cytotoxicity after exposure to the gold nanoparticles, as reported by the group of Xia et al. The higher sensitivity could also not be explained by Xia and co-workers. A reason for the difference in uptake by epithelial and endothelial cells might also result from a different interaction of nanoparticles with specific domains of the cell surface. Nel et al. described that different forces are present which resist or promote nanoparticle wrapping between the particle and the cell surface. On the one hand, the physico-chemical characteristics of the particles, such as size or surface modification are of great importance. On the other hand, Nel et al. described promotive forces which are correlated with the components of the cell membrane and the cytoskeleton. These factors were termed “energy-dependent membrane and cytoskeleton components” that could be responsible e.g., for the formation of clathrin cages that bind to cytoskeletal proteins. Besides these promotive forces, the resistive forces are also of significance for nanoparticle wrapping, e.g. the elasticity of the cell membrane (Nel et al., 2009). These factors could be different from cell-type to cell-type and might influence and be responsible for the differences observed in the uptake of the same nanoparticles by various cell types. This hypothesis needs to be investigated in further experiments and was not possible within the scope of this thesis.

In conclusion, it was demonstrated that interaction of gold nanoparticles with different cell types is concentration-dependent. Moreover, epithelial and endothelial cells exhibit different uptake behaviours of gold nanoparticles with sizes between 10nm and 25nm in diameter. Nanoparticle-cell-surface interactions might be responsible for the uptake behaviour. The presence of sodium citrate, a manufacturing contaminant, on the surface of gold nanoparticles reduced cell

proliferation in all of the cell types and played a greater role in the effects on proliferation than did the size of the nanoparticles. These effects are enhanced by the amount of internalized gold nanoparticles.

How different surface modifications as well as various sizes of gold nanoparticle influence different endothelial cell types will be discussed in the following chapters and will demonstrate that surface modifications of nanoparticles must be chosen carefully on account of their varying impact in cellular reactions.

5.3 Screening of gold nanoparticles with different sizes and various surface modifications synthesized by the same procedure

In the recent literature many functionalized gold nanoparticles with different surface modifications and targeting molecules have been described. Due to the absence of standard nanoparticles and standard operating procedures for screening nanoparticles cell reactions to gold nanoparticles synthesized by different groups, by various methods and which exhibit different physico-chemical properties results generated by different groups are not easily comparable.

In the studies described here, 15 different gold nanoparticles were synthesized by the same chemical procedure. The gold nanoparticles consisted of 3 different sizes and 5 different surface modifications. In addition, two different human endothelial cell types from different circulatory regions of the body were compared, and it was shown that within endothelial cell types unique patterns of behaviour after exposure to gold nanoparticles could be demonstrated.

After showing that the gold nanoparticles induced no cytotoxicity it was demonstrated that all types of gold nanoparticles were internalized by both endothelial cell types (HDMEC and hCMEC). Using optical microscopy it was shown that the amounts of the different gold nanoparticles within the cells varied. According to the results of Nativo and Arnida the uptake of PEGylated gold nanoparticles by human carcinoma cells (HeLa cells) and a prostate cancer cell line (PC-3) was less compared to gold nanoparticles with other modifications (Nativo et al., 2008; Arnida et al., 2009). However, positively charged nanoparticles with an ethanediamine surface modification were internalized to a very high extent while the negatively charged taurine-coated gold nanoparticles were taken up to much lesser degree by both endothelial cell types. Nanoparticles with positive net charges are known to interact with the negative charges of the extracellular matrix and promote endocytosis. Various studies have demonstrated that these charge effects are not limited to gold nanoparticles (Thorek and Tsourkas, 2008; Liang et al., 2009; Chen

et al., 2011). The optical images also revealed that the endothelial cells internalized various numbers of different-sized gold nanoparticles, depending on cell type and nanoparticle size and coating. Due to the limitation of the resolution of optical microscopy single gold nanoparticles could not be observed. To quantify the internalized gold nanoparticles with different surface modifications and sizes in an exposed group of cells inductively coupled plasma atomic emission spectroscopy (ICP-AES) was used. This precise and highly sensitive method was suitable for detecting very small differences in the quantity of gold nanoparticles. This method was used to quantify internalized gold nanoparticles in HeLa cells by Chithrani and co-workers (Chithrani et al., 2006). However, the ICP-AES results in this study are presented in two different ways. In addition to methods described by others, in which the number of the nanoparticles taken up per cell was determined, this study also determined the percentage of the initial concentration of gold nanoparticles that were subsequently internalized by the cells. Therefore, it was not only possible to determine which nanoparticles were internalized in a high number but also possible which particles were taken up at a higher percentage related to the initial concentration. Both data are important for characterizing the uptake behaviour of nanoparticles designed to be used for *in vivo* applications such as drug delivery. On the one hand high numbers of internalized nanoparticles ensure high drug delivery, but on the other hand the higher the number of particles taken up by the targeted cells the smaller the possible side effects to untargeted organs. Hirn and co-workers have recently shown in rats that after intravenous injection the biodistribution of different-sized gold nanoparticles differs (Hirn et al., 2010). In other publications it has been shown that nanoparticles often accumulate in the liver, kidneys and spleen (Peters et al., 2006; Balasubramanian et al., 2010). Therefore a major goal is to produce nanoparticles that are taken up in high quantity into specifically targeted cells, and in addition, are internalized in a high percentage related to the initial concentration to prevent side effects to other organs.

The ICP-AES analysis revealed that the positively charged particles were taken up most readily. These data confirmed the results from optical microscopy and the data of the above-mentioned groups. In addition, it could be shown by ICP-AES that the smallest cationic particles (61-2) were internalized in a significantly higher amount in HDMEC than in hCMEC even after 4 hours. Nevertheless, the uptake of cationic particles was dramatically higher and the percentage of internalized nanoparticles related to the initial concentrations was over 100%. This demonstrates that due to the high quantity of gold nanoparticles which was internalized by the cells brings the ICP-AES method to its limit. Thus, the results need to be interpreted with care. In

addition, such high numbers of internalized nanoparticles were associated with numerous vacuoles. Mironava claimed that a high number of vacuoles disrupted the cytoskeleton, prevented the motility of cells and could end in apoptosis (Mironava et al., 2010). However, in this study no cytotoxicity of endothelial cells was detected after 48 hour. Prolonged exposure times were not investigated but might lead to effects that could be correlated with the disruption of the cytoskeleton. In addition to the possible effects on the cell motility it was shown that after longer storage times the stability of the positively charged gold nanoparticles was not as high as for the other particles. Therefore, the investigation was focused on the gold nanoparticles with neutral and negative charges which exhibited a good stability.

In addition to the charge effect and the low uptake of PEGylated gold nanoparticles detected by image analysis it was shown in the present study by ICP-AES quantification that the uptake was time-dependent. Furthermore, the smallest nanoparticles (18nm) were internalized in the highest number. Compared to the initial concentration, these nanoparticles were taken up at a very low percentage compared to their larger-sized counterparts. In general, the biggest gold nanoparticles with a diameter of 65nm were internalized in high percentages compared to initial concentrations. These size-effects were also described by Chithrani et al. who postulated that 50nm sized gold nanoparticles were taken up in higher numbers by HeLa cells compared to 14nm gold nanoparticles (Chithrani et al., 2006).

A comparison of the uptake behaviour of uncharged particles by ICP-AES revealed that the hydroxypropylamine-coated gold nanoparticles (-17) showed a completely different uptake pattern than the glucosamine- and PEG-coated gold nanoparticles. As known from the literature, PEG coating prevents the uptake and leads to a prolongation in the circulation with time (Niidome et al., 2006). This in accordance with my studies and may be the reason for the low amount of internalization in both human endothelial cell types. In addition, it was demonstrated that in comparison to the other coatings, hydroxypropylamine-coated nanoparticles showed a difference in uptake dependent on size. Relatively high numbers of the medium-sized nanoparticles could be found in both hCMEC and HDMEC with a relatively high percentage of the nanoparticles taken up related to the initial concentration. Moreover, a significant difference in the uptake of the medium-sized gold nanoparticles (65-17) in HDMEC and hCMEC was detected by ICP-AES after an exposure time of 24 hours (Fig. 31). This effect is unique compared to all investigated particles and will be further discussed in the following section (see chapter 5.4).

Although Zhang et al. presented in their publication that gold nanoparticles of 60nm did not cause cytotoxicity or induction of pro-inflammatory mediators (IL-6, TNF-α) in macrophages (Zhang et al., 2010), the ELISA studies presented here demonstrated an induction of pro-inflammatory mediators in endothelial cells. Different coated gold nanoparticles activated human brain endothelial cells (hCMEC) in a different manner. Cells exposed to glucosamine-coated nanoparticles were especially affected, as seen by induction of the expression of interleukin (IL) -6, IL-8, MCP-1, and the cell adhesion molecules, ICAM and VCAM. These factors are known to be induced in endothelial cells in the presence of endotoxins, derived from bacterial lipopolysaccharide (LPS) (Makó et al., 2010; Buttenschoen et al., 2010). However, none of the gold nanoparticles in this study induced the expression E-selectin after cells were exposed to nanoparticles for 4 hours. Therefore, a contamination of the particles with endotoxins or LPS could be excluded (data not shown). Therefore, induction of pro-inflammatory mediators is a characteristic factor of the coated gold nanoparticles themselves. Moreover, while the induction of IL-8 by the largest PEGylated gold nanoparticles (71-28) has been shown by ELISA and the medium sized hydroxypropylamine-coated gold nanoparticles (65-17) also induced the expression of the pro-inflammatory mediators investigated, the effects induced by the glucosamine-coated gold nanoparticles was not related to a particular size of the nanoparticles. Considering the fact that various amounts of glucosamine-coated gold nanoparticles of different sizes were internalized in hCMEC (see ICP-AES results), the induction of pro-inflammatory factors could also not be attributed to the amount of nanoparticles taken up. Thus, the presence of glucosamine-coated gold nanoparticles might affect the endothelial cells from the exterior. Kennedy and co-workers showed that an increase in reactive oxygen species (ROS) and in the expression of pro-inflammatory factors occurred in human aortic endothelial cells after exposure to zinc oxide nanoparticles (Kennedy et al., 2009). Oxidative stress is known to induce several cellular reactions, such as apoptosis and the increased expression of pro-inflammatory cytokines (Marano et al., 2010). These factors also increased when cells were exposed to fetal bovine serum-coated gold nanoparticles (Li et al., 2010a). In addition, others demonstrated that glucosamine can induce oxidative stress in primary human chondrocytes (Valvason et al., 2008), which therefore might lead to the induction of inflammatory processes. In contrast, others have shown that the direct influences of glucosamine on cells acted in an anti-inflammatory manner (Shea, 2001). Nevertheless in combination with gold nanoparticles the induction of pro-inflammatory factors was quite high compared to the untreated control. However, a correlation of oxidative stress and the induction of

inflammatory processes in the investigated endothelial cells has not been demonstrated but could possibly be an explanation for the induction of pro-inflammatory responses of the cells after exposure to all sizes of glucosamine-coated gold nanoparticles.

In conclusion, due to the lack of stability after longer storage of the positively charged ethanediamine-coated gold nanoparticles, the lower amount of negatively charged particles that were internalized by endothelial cells, the induction of pro-inflammatory mediators by glucosamine-coated gold nanoparticles and the diverse uptake behaviour of hydroxypropylamine-coated gold nanoparticles in comparison to the other gold nanoparticles, the latter nanoparticles were investigated in more detail. Interestingly, it could be shown that the characteristics of the medium size and the hydroxypropylamine coating may enhance the uptake of nanoparticles in specific cell types. Further results of the hydroxypropylamine-coated nanoparticles will be discussed in the following section.

5.4 Detailed investigation of different sized hydroxylpropylamine-coated gold nanoparticles

As stated above, the hydroxypropylamine-coated gold nanoparticles are the most promising gold nanoparticles for specific targeting of brain endothelial cells. Based on the fact that these gold nanoparticles were stable when stored, well characterized and show a different uptake behaviour in the two types of endothelial cells compared to the other gold nanoparticles they were investigated in more detail.

After demonstrating that a concentration of 100µg/ml gold nanoparticles exhibited no cytotoxic effect this concentration was used in the uptake studies. With optical microscopy it was shown that gold nanoparticles of various sizes were internalized in different amounts. The particles were located near the cell membrane after 4 hours of incubation. A prolongation of the incubation time to 24 hours led to an accumulation of the gold nanoparticles in the perinuclear region within both endothelial cell types (hCMEC/HDMEC). Localization within the cells and the accumulation in the perinuclear region was confirmed by transmission electron microscopy (TEM). However, differences in the numbers of internalized gold nanoparticles in the different cell types could not be detected by the ultrastructural images. Furthermore, TEM analysis revealed that all of the nanoparticles were located within vesicles. This finding gave a first indication that the gold nanoparticles were internalized by endocytotic pathways. Zhang and co-workers also suggested an endocytosis uptake mechanism for 60nm gold nanoparticles in murine macrophage cells (Zhang et al., 2010). Many studies have been published

describing the uptake mechanisms of nanoparticles. The most important characteristics that influence the uptake of nanoparticles in cells are thought to be size and surface properties (Dobrovolskaia and McNeil, 2007) as well as the type of cells. Anionic dendrimers are known to be internalized via caveolin-mediated endocytosis, while mesoporous silica nanoparticles are internalized via a clathrin-mediated pathway (Kunzmann et al., 2010). The interaction of nanoparticles with the plasma membrane and thus the amount of internalization can be tuned by a positive net charge on the nanoparticle surface and by targeting molecules such as ligands for receptors or cell-penetrating peptides (Torchilin, 2008; Liang et al., 2009). Depending on the type of ligand, the nanoparticles are internalized by different endocytotic pathways such as caveolin- or clathrin-mediated pathways and are entrapped in endosomes. In addition to the internalization by classic endocytotic pathways, it has been demonstrated using model lipid membranes that high positively charged gold nanoparticles overcome the lipid cell membrane by penetration followed by diffusion into the cell (Lin et al., 2010). In addition, Taylor et al. demonstrated that certain gold nanoparticles are internalized by passive diffusion instead of active endocytotic pathways (Taylor et al., 2010). However, in this study it was shown that all sizes of hydroxypropylamine-coated gold nanoparticles were located in vesicles within the cells. Thus passive diffusion was not involved. The immunostaining of typical endocytotic markers and the co-localization with fluorescently labeled transferrin indicated internalization by a specific uptake route. Although no co-localization with specific endocytotic markers for caveolin- or clathrin-dependent uptake routes could be demonstrated with hydroxypropylamine-coated gold nanoparticles, it was shown that after an exposure time of 24 hours the gold nanoparticles are surrounded by flotillin-1 and flotillin-2. According to Kunzmann et al. other, unknown endocytotic pathways for nanoparticle uptake exist (Kunzmann et al., 2010). The co-localization with flotillin might be an indicator for such an alternative pathway and also excluded a passive transport of the gold nanoparticles across the membrane. Glebov et al. have clearly identified flotillin-1 as a protein which is located in specific microdomains of cell membranes which are separated from clathrin- or caveolin regions and also demonstrated that flotillin as cargo protein is taken up by a different route (Glebov et al., 2006). The clathrin- and caveolin-independent uptake route by flotillin has also been described by others (Doherty and McMahon, 2009). Investigations to determine a specific uptake pathway for hydroxypropylamine-coated gold nanoparticles was not performed. Several groups used specific inhibitors of uptake routes and quantified the differences in the amount of uptake to try and determine the main pathway for

nanoparticle internalization. Damke et al. demonstrated that the inhibition of specific uptake routes led to an upregulation of other uptake pathways (Damke et al., 1995). In addition, an inter-connection of different pathway routes may be possible, is thus complex and cannot easily be excluded (Glebov et al., 2006). Therefore, investigations with inhibitors were not carried out with the gold nanoparticles in this project, as this would be a major study in itself. In conclusion, hydroxypropylamine-coated gold nanoparticles seem to be internalized by a clathrin- and caveolin-independent endcytotic pathway.

As mentioned above the size and shape of the nanoparticles can influence uptake behaviour in cells. As summarized by Nel et al. an optimal diameter and shape favour the uptake of nanoparticles by cell membrane absorption (Nel et al., 2009). In the present study a size effect was also shown by different methods. The optical images, the TEM analysis and the ICP-AES quantification revealed significant differences in the uptake of different sized gold nanoparticles in the two endothelial cell types. The medium-sized nanoparticles were internalized in a relatively high amount and also in a high percentage compared to the initial concentration (discussed in chapter 5.3). In addition, a significantly higher number of the medium-sized gold nanoparticles were found in hCMEC than in HDMEC. Although the particles do not possess a specific brain cell targeting moiety it was demonstrated that the uptake of these particles into brain endothelial cells was enhanced by a hydroxypropylamine surface modification. The differences in the amount of internalized 35nm hydroxypropylamine gold nanoparticles may be due to the heterogeneity of the endothelial cells or their membranes in the primary culture of HDMEC in contrast to hCMEC, which are clones (see discussion chapter 5.2). The size as well as the coating appeared to be favoured by endothelial cells from the brain. In general, differences in the uptake mechanisms are present in endothelial cells from different parts of the body but it has also been demonstrated that even endothelium of the same organ is heterogeneous (Pries and Kuebler, 2006). These findings might also help explain the different uptake patterns of the two endothelial cell types regarding the medium-sized hydroxypropylamine-coated gold nanoparticles.

Although cytotoxicity as tested by the MTS and LDH assays after gold nanoparticle exposure was not observed and the quantification of the uptake showed high uptake rates further *in vitro* investigations were required to guarantee nanoparticle safety and biocompatibility. For this reason the induction of pro-inflammatory mediators after the exposure of hCMEC to the three sizes of hydroxypropylamine-coated gold nanoparticles was investigated at the mRNA and at protein levels. Low

concentrations of the nanoparticles (10µg/ml) did not induce the expression of pro-inflammatory factors, such as IL-6, sICAM and sVCAM. The results indicated no change in IL-6 expression after gold nanoparticle exposure and agree with previous findings by Zhang et al. in which murine macrophages did not show an increased expression of pro-inflammatory mediators, such as IL-6 and TNFα, after treatment with 60nm gold nanoparticles (Zhang et al., 2010). The low levels of sICAM and sVCAM expression is an additional factor that demonstrated that none of the gold nanoparticles induce inflammatory activation. CAMs are known to be induced in endothelial cells after treatment with TNFα and IL-1β and are an indicator for activated endothelial cells (Beekhuizen and van Furth, 1993). The results of Brandenberger et al. (2011) also demonstrate that 15nm gold nanoparticle do not affect IL-8 expression after the exposure of A549 epithelial cells for 24 hours and are consistent with our findings with the smallest Au-NPs (12nm). However, the level of IL-8 increased after 24 hours. Although the basal level of the control cells was also higher the levels of IL-8 were below 100pg/ml which is regarded as a physiological level in endothelial cells (Pigott et al., 1992). The highest level of IL-8 was detected after exposure to 10µg/ml 65-17 for 24hours, which was still 200-fold lower compared to the IL-8 expression after exposure to TNFα. These results led to further investigation of the induction of pro-inflammatory mediators in hCMEC by using higher concentrations of the three sizes of hydroxypropylamine-coated gold nanoparticles.

An increase in nanoparticle concentration resulted in an increased expression of all pro-inflammatory mediators studied. The results were determined by real-time PCR and ELISA and correlation between the transcriptional and translational level was observed. Interestingly, only the medium-sized gold nanoparticles (65-17) induced the expression of all pro-inflammatory mediators to an extent comparable to the expression profiles of the positive control (TNF-α) (Pigott et al., 1992). The expression of these factors was not related to the number of internalized particles. It has been shown by Marano et al. that oxidative stress is caused by extracellular reactive oxygen species (ROS) production. From theoretical considerations smaller particles with a higher surface to volume ratio should induce more ROS. However, as a lower level of pro-inflammatory mediators was induced by the smaller nanoparticles compared to the medium-sized particles, the production of ROS does not appear to be responsible for increased induction of cytokine expression. Nevertheless,, Marano et al. revised the paradigm of oxidative stress to explain the effects caused by nanoparticles. They concluded that the interaction of nanoparticles with a cell can cause a special activation of signaling pathways,

triggered via the protein corona of the nanoparticles and binding to specific receptors (Marano et al., 2010). Depending on the size and the chemical composition, specific nanoparticles activated different signaling cascades. Since the three NPs in the study had the same chemical composition, only the size of the nanoparticles could be the reason for the different expression patterns of the pro-inflammatory cytokines. Mailänder and Landfester also reported that nanoparticles interact with surface proteins of cells and induce downstream processes within the cells (Mailänder and Landfester, 2009). Nanoparticles are known to bind to EGF receptors and induce apoptosis, proliferation and also inflammation (Unfried et al., 2007). Due to the size effect it is possible that these receptors are activated by the 35nm gold nanoparticles with a specific protein corona and not by the smaller or larger nanoparticles, and that this is strongly influenced by the chemical composition of the surface modification. In addition, another hypothesis is that nanoparticles can modulate cells without direct contact with the cell membrane by influencing secreted factors (Marano et al., 2010). It is evident from these considerations that a detailed investigation of downstream processes within the cells must be investigated in further studies to clarify the increased production of pro-inflammatory mediators after exposure to the medium sized hydroxypropylamine-coated gold nanoparticles compared to the smaller and larger counterparts.

Nevertheless, it has been clearly demonstrated in this thesis that the hydroxypropylamine coating of gold nanoparticles resulted in an increased uptake by brain endothelial cells compared to the dermal microvascular endothelial cells and compared to nanoparticles with other neutral coatings, such as PEG or glucosamine. Due to their positive uptake characteristics in brain endothelial cells, hydroxypropylamine-coated gold nanoparticles were also examined for the ability to exhibit transcytosis over the BBB model formed by primary porcine brain endothelial cells. TEM images confirmed the uptake of the various particles but failed to demonstrate a transcytosis process at the apical or basolateral membrane. Although the sections of the cells were quite thin, a higher number of gold particles than expected were found within the cells, especially after considering the results presented in Fig. 35 in which the uptake after the treatment with 100µg/ml gold nanoparticles in hCMEC was shown. Due to the thin sections and the limited number of TEM images a quantification and comparison of the amount of internalized gold nanoparticles with different sizes by image evaluation was not possible. However, it was shown by ICP-AES quantification that the number of gold nanoparticles in the basolateral medium increased with the exposure time, and that the larger nanoparticles traversed the barrier in higher amounts compared to the

smaller nanoparticles, especially after exposure of the cells to high concentrations of nanoparticles (500µg/ml). In addition, it was demonstrated that the higher initial concentration of particles resulted in a higher number of particles in the basolateral compartment. The decreasing TEER, especially after exposure to high concentrations of gold nanoparticles (500µg/ml), which is correlated with a decrease of tight junctions, suggests that the higher transport could be a result of disruption of the barrier and a possible paracellular transport of the particles. However, the TEER after the cells were exposed to 61-17 and 65-17 decreased at the same rate and level, but lower levels of the smallest nanoparticles (61-17) were detected in the basolateral compartment compared to the larger nanoparticles. Considering the smaller size of 61-17, it is likely that paracellular transport is responsible for the enhanced transport through the barrier, compared to larger gold nanoparticles. However, the amount of small particles was lower compared to the larger counterparts as stated above. Thus a paracellular transport as a result of disruption of the barrier could not be completely ruled out but may not be the only explanation for a higher quantity of gold nanoparticles in the basolateral compartment. In addition, similar results were observed after exposure to 100µg/ml of the different sized gold nanoparticles. However in these studies, the TEER remained stable. In conclusion, the smaller gold nanoparticles (61-17) passed through the barrier to a lower extent compared to the two larger nanoparticles (65-17 and 71-17).

Trickler et al. (2010) also investigated the influence of different-sized gold nanoparticles on the disruption of the BBB and demonstrated a size effect in the uptake into rat brain endothelial cells. No differences in the permeability of the barrier were detected. However, Trickler examined very low concentrations of gold nanoparticles (0.24-15.63 µg/cm²) which could explain the stability of the barrier observed in their studies (Trickler et al., 2010). Most likely, the disruption of the porcine blood-brain barrier model was caused by the high concentration of gold nanoparticles (500µg/ml) used in my studies.

A possible explanation for the decreased TEER values could be the induction of pro-inflammatory cytokines or cell reactions such as a mild decrease in cell viability or increase in cytotoxicity after the exposure to 500µg/ml gold nanoparticles even though this was not significantly detected in the various assays. For lower concentrations of gold nanoparticles (100µg/ml) an induction of the expression of pro-inflammatory mediators after exposure to 65-17 was demonstrated in hCMEC. Pro-inflammatory factors are known to influence barrier tightness (Tsao et al., 2001; de Boer and Gaillard, 2006). However, after 3 hours of incubation no decrease in TEER values after exposure to 100µg/ml 65-17 was detected compared to the

untreated control. It is of course possible that this lack of effect was related to the short incubation time. Thus, the influence of the high concentration of particles could not be ruled out completely and might involve disruption at a few single cells in the barrier, but below the level of detection. This could help explain the higher amount of medium-sized gold nanoparticles compared to the smaller counterparts, but the same reduction in barrier function also means that endocytotic and transcytotic processes in the endothelial cells should be considered as further relevant mechanisms. In summary, the transport of 35nm and 65nm hydroxypropylamine-coated gold nanoparticles to brain endothelial cells was preferential compared to the transport of smaller nanoparticles with a size of 18nm in diameter. However, further studies need to be carried out to confirm these findings and unravel the underlying mechanisms.

In conclusion, it was demonstrated that after screening a library of 15 different nanoparticles only hydroxypropylamine-coated gold nanoparticles showed a different uptake behaviour in dermal and brain microvascular endothelial cells. The gold nanoparticles were not toxic, but 100µg/ml medium-sized particles induced the expression of pro-inflammatory factors at the mRNA and protein levels. To study the possibility of transcytosis a BBB model generated by primary porcine brain endothelial cells was exposed to different sized hydroxypropylamine-coated gold nanoparticles for 3 hours. 100µg/ml gold nanoparticles did not affect the barrier permeability. Only a low concentration of the particles could be detected in the basolateral compartment, but this might simply reflect the short incubation time. In contrast, a higher concentration of the same gold nanoparticles (500µg/ml) led to an increase of barrier permeability and to a higher accumulation of gold nanoparticles in the basolateral compartment. A paracellular transport mechanisms via the disruption of the BBB model layer could not be excluded, although the higher accumulation of the larger gold nanoparticles in the basolateral compartment compared to the smaller particles suggests possibletranscytosis of gold nanoparticles through the endothelial cell barrier and might be the preferred route for the larger hydroxypropylamine-coated gold nanoparticles.

Nevertheless, it was successfully demonstrated in this study that specific physico-chemical characteristics such as size and hydroxypropylamine surface modification resulted in a higher uptake in brain endothelial cells. Moreover, there are indications that the coating might be responsible for overcoming the barrier in a non-disruptive manner.

In future experiments the investigation should concentrate on the effects of gold nanoparticles after exposure to the differentiated endothelial cells in the *in vitro* porcine model system of the BBB. In combination with *in vivo* examination of selected gold nanoparticles the refinement of potential brain-targeting by gold nanoparticles could be achieved. However, due to the complexity of the body, the clearance properties of the blood cells and the accumulation of nanoparticles in the liver, kidneys and spleen the targeted transport of nanoparticles to the brain remains a major hurdle *in vivo*. Nevertheless, the experiments in this study reveal that the combination of size and surface modification can be used to increase nanoparticle uptake by brain endothelial cells. The addition of a specific targeting molecule for endothelial cells in combination with the size and surface modification might further improve the targeting of the brain and minimize the clearance by blood cells and other organs.

6 Appendix

Polydispersity index (PDI):

$$PDI = \frac{\text{weight average molecular weight}}{\text{number average molecular weight}} ;$$

Weight average molecular weight = $\sum (N_i M_i^2) / \sum (N_i M_i)$

Number average molecular weight = $\sum (N_i M_i) / \sum (N_i)$

7 References

Abbott, N.J.; Rönnbäck, L.; Hansson, E. (2006). Astrocyte-endothelial interactions at the blood-brain barrier. Nat. Rev. Neurosci. *7*, 41-53.

Al Ahmad, A.; Taboada, C. B.; Gassmann, M; Ogunshola, O. O. (2010). Astrocytes and pericytes differentially modulate blood-brain barrier characteristics during development and hypoxic insult. J. Cereb. Blood Flow Metab.

Alam, M.I.; Beg, S.; Samad, A.; Baboota, S.; Kohli, K.; Ali, J.; Ahuja, A; Akbar, M. (2010). Strategy for effective brain drug delivery. European journal of pharmaceutical sciences : official journal of the European Federation for Pharmaceutical Sciences.

Albelda, S.M.; Oliver, P. D.; Romer, L. H.; Buck, C. A. (1990). EndoCAM: a novel endothelial cell-cell adhesion molecule. J. Cell Biol. *110*, 1227-1237.

Alexander, J.S.; Jackson, S. A.; Chaney, E.; Kevil, C. G.; Haselton, F. R. (1998). The role of cadherin endocytosis in endothelial barrier regulation: involvement of protein kinase C and actin-cadherin interactions. Inflammation *22*, 419-433.

Allt, G.; Lawrenson, J. G. (2001). Pericytes: cell biology and pathology. Cells Tissues Organs (Print) *169*, 1-11.

Alyautdin, R.N.; Petrov, V. E.; Langer, K.; Berthold, A.; Kharkevich, D. A.; Kreuter, J. (1997). Delivery of loperamide across the blood-brain barrier with polysorbate 80-coated polybutylcyanoacrylate nanoparticles. Pharm. Res. *14*, 325-328.

Armulik, A.; Abramsson, A.; Betsholtz, C. (2005). Endothelial/pericyte interactions. Circ. Res. *97*, 512-523.

Arnida; Malugin, A.; Ghandehari, H. (2009). Cellular uptake and toxicity of gold nanoparticles in prostate cancer cells: a comparative study of rods and spheres. Journal of Applied Toxicology.

Balasubramanian, S.K.; Jittiwat, J.; Manikandan, J.; Ong, C.-N.; Yu, L. E.; Ong, W.-Y. (2010). Biodistribution of gold nanoparticles and gene expression changes in the liver and spleen after intravenous administration in rats. Biomaterials, 2034-2042.

Beekhuizen, H.; van Furth, R. (1993). Monocyte adherence to human vascular endothelium. Behring Inst. Mitt., 63-86.

Bergers, G.; Song, S. (2005). The role of pericytes in blood-vessel formation and maintenance. Neuro-oncology *7*, 452-464.

Bhaskar, S.; Tian, F.; Stoeger, T.; Kreyling, W.; La Fuente, J. M. de; Grazú, V,; Borm, P,; Estrada, G.; Ntziachristos, V.; Razansky, D. (2010). Multifunctional Nanocarriers for diagnostics, drug delivery and targeted treatment across blood-brain barrier: perspectives on tracking and neuroimaging. Part Fibre Toxicol *7*, 3.

Bhattacharya, R.; Mukherjee, P. (2008). Biological properties of "naked" metal nanoparticles. Adv. Drug Deliv. Rev. *60*, 1289-1306.

Boer, A.G. de; Gaillard, P. J. (2006). Blood–brain barrier dysfunction and recovery. Journal of Neural Transmission *113*, 455-462.

Boisselier, E.; Astruc, D. (2009). Gold nanoparticles in nanomedicine: preparation, imaging, diagnostics, therapies and toxicity. Chem. Soc. Rev, 1759-1782.

Bondjers, C.; Kalén, M.; Hellström, M.; Scheidl, S. J.; Abramsson, A.; Renner, O.; Lindahl, P.; Cho, H.; Kehrl, J.; Betsholtz, C. (2003). Transcription profiling of platelet-

derived growth factor-B-deficient mouse embryos identifies RGS5 as a novel marker for pericytes and vascular smooth muscle cells. Am. J. Pathol. *162*, 721-729.

Brandenberger, C.; Rothen-Rutishauser, B.; Mühlfeld, C.; Schmid, O.; Ferron, G. A.; Maier, K. L.; Gehr, P.; Lenz, A. -G. (2011). Effects and uptake of gold nanoparticles deposited at the air-liquid interface of a human epithelial airway model. Toxicology and Applied Pharmacology *In Press, Uncorrected Proof*.

Butt, A.M.; Jones, H. C.; Abbott, N. J. (1990). Electrical resistance across the blood-brain barrier in anaesthetized rats: a developmental study. J. Physiol. (Lond.) *429*, 47-62.

Buttenschoen, K.; Radermacher, P.; Bracht, H. (2010). Endotoxin elimination in sepsis: physiology and therapeutic application. Langenbeck's Archives of Surgery *395*, 597-605.

Cai, D.; Mataraza, J. M.; Qin, Z.-H.; Huang, Z.; Huang, J.; Chiles, T. C.; Carnahan, D.; Kempa, K.; Ren, Z. (2005). Highly efficient molecular delivery into mammalian cells using carbon nanotube spearing. Nat. Methods *2*, 449-454.

Chauveau, F.; Cho, T. H.; Berthezène, Y.; Nighoghossian, N.; Wiart, M. (2010). Imaging inflammation in stroke using magnetic resonance imaging. Int J Clin Pharmacol Ther *48*, 718-728.

Chen, L.; Mccrate, J. M.; Li, H. (2011). The role of surface charge on the uptake and biocompatibility of hydroxyapatite nanoparticles with osteoblast cells. Nanotechnology *22*, 105708.

Chithrani, B.D.; Ghazani, A. A.; Chan, W. C. W. (2006). Determining the Size and Shape Dependence of Gold Nanoparticle Uptake into Mammalian Cells. Nano Letters *6*, 662-668.

Cho, W.-S.; Cho, M.; Jeong, J.; Choi, M.; Cho, H.-Y.; Han, B. S.; Kim, S. H.; Kim, H. O.; Lim, Y. T.; Chung, B. H.. (2009). Acute toxicity and pharmacokinetics of 13nm-sized PEG-coated gold nanoparticles. Toxicology and Applied Pharmacology, 16-24.

Choi, J.-S.; Choi, H. J.; Jung, D. C.; Lee, J.-H.; Cheon, J. (2008). Nanoparticle assisted magnetic resonance imaging of the early reversible stages of amyloid beta self-assembly. Chem. Commun. (Camb.), 2197-2199.

Choi, Y.K.; Kim, K.-W. (2008). Blood-neural barrier: its diversity and coordinated cell-to-cell communication. BMB Rep *41*, 345-352.

Christian, P.; Kammer, F. von der; Baalousha, M.; Hofmann, T. (2008). Nanoparticles: structure, properties, preparation and behaviour in environmental media. Ecotoxicology *17*, 326-343.

Connor, E.E.; Mwamuka, J.; Gole, A.; Murphy, C. J.; Wyatt, M., D. (2005). Gold Nanoparticles Are Taken Up by Human Cells but Do Not Cause Acute Cytotoxicity13. Small *1*, 325-327.

Correale, J.; Villa, Andrés. Cellular Elements of the Blood-Brain Barrier. Neurochemical Research.

Costantino, H.R.; Illum, L.; Brandt, G.; Johnson, P. H.; Quay, S. C. (2007). Intranasal delivery: physicochemical and therapeutic aspects. Int J Pharm *337*, 1-24.

Crone, C.; Christensen, O. (1981). Electrical resistance of a capillary endothelium. J. Gen. Physiol. *77*, 349-371.

Crone, C.; Olesen, S. P. (1982). Electrical resistance of brain microvascular endothelium. Brain Res. *241*, 49-55.

Damke, H.; Baba, T.; van der Bliek, A. M.; Schmid, S. L. (1995). Clathrin-independent pinocytosis is induced in cells overexpressing a temperature-sensitive mutant of dynamin. J. Cell Biol. *131*, 69-80.

Dauchy, S.; Miller, F.; Couraud, P.-O.; Weaver, R. J.; Weksler, B. B.; Romero, I.-A.; Scherrmann, J.-M.; Waziers, I. de; Declèves, X. (77). Expression and transcriptional regulation of ABC transporters and cytochromes P450 in hCMEC/D3 human cerebral microvascular endothelial cells. Biochemical Pharmacology *2009*, 897-909.

Dehouck, M.P.; Méresse, S.; Delorme, P.; Fruchart, J. C.; Cecchelli, R. (1990). An easier, reproducible, and mass-production method to study the blood-brain barrier in vitro. J. Neurochem. *54*, 1798-1801.

Dixit, V.; van den Bossche, Jeroen; Sherman, Debra M.; Thompson, David H.; Andres, Ronald P. (2006). Synthesis and grafting of thioctic acid-PEG-folate conjugates onto Au nanoparticles for selective targeting of folate receptor-positive tumor cells. Bioconjug. Chem. *17*, 603-609.

Dobrovolskaia, M.A.; McNeil, Scott E. (2007). Immunological properties of engineered nanomaterials. Nat Nanotechnol *2*, 469-478.

Doherty, G.J.; McMahon, Harvey T. (2009). Mechanisms of endocytosis. Annu. Rev. Biochem. *78*, 857-902.

Drion, N.; Lemaire, M.; Lefauconnier, J. -M; Scherrmann, J. -M (1996). Role of P-Glycoprotein in the Blood-Brain Transport of Colchicine and Vinblastine. Journal of Neurochemistry *67*, 1688-1693.

Dyer, L.A.; Patterson, Cam (2010). Development of the endothelium: an emphasis on heterogeneity. Semin. Thromb. Hemost. *36*, 227-235.

Eghtedari, M.; Liopo, A. V.; Copland, J. A.; Oraevsky, A. A.; Motamedi, M. (2009). Engineering of Hetero-Functional Gold Nanorods for the in vivo Molecular Targeting of Breast Cancer Cells. Nano Letters *9*, 287-291.

Faraji, A.H.; Wipf, P. (2009). Nanoparticles in cellular drug delivery. Bioorganic & Medicinal Chemistry *17*, 2950-2962.

Fernández-Carneado, J.; Kogan, M. J.; Pujals, S.; Giralt, E. (2004). Amphipathic peptides and drug delivery. Biopolymers *76*, 196-203.

Forster, C.; Burek, M.; Romero, I. A.; W., B. B.; Couraud, P.-O.; Drenckhahn, D. (2008). Differential effects of hydrocortisone and TNF{alpha} on tight junction proteins in an in vitro model of the human blood-brain barrier. J Physiol *586*, 1937-1949.

Franke, H.; Galla, H.; Beuckmann, C. T. (2000). Primary cultures of brain microvessel endothelial cells: a valid and flexible model to study drug transport through the blood-brain barrier in vitro. Brain Res. Brain Res. Protoc. *5*, 248-256.

Frens, G. (1973). Controlled Nucleation for the Regulation of the Particle Size in Monodisperse Gold Suspensions. Nat. Phys. Sci., 20.

Futaki, S. (2002). Arginine-rich peptides: potential for intracellular delivery of macromolecules and the mystery of the translocation mechanisms. Int J Pharm *245*, 1-7.

Gabathuler, R. (2010). Approaches to transport therapeutic drugs across the blood-brain barrier to treat brain diseases. Neurobiol. Dis. *37*, 48-57.

Gaillard, P.J.; Voorwinden, L H; Nielsen, J L; Ivanov, A; Atsumi, R; Engman, H; Ringbom, C; de Boer, A G; Breimer, D D (2001). Establishment and functional characterization of an in vitro model of the blood-brain barrier, comprising a co-

culture of brain capillary endothelial cells and astrocytes. Eur J Pharm Sci *12*, 215-222.

Garberg, P.; Ball, M.; Borg, N.; Cecchelli, R.; Fenart, L.; Hurst, R. D.; Lindmark, T.; Mabondzo, A.; Nilsson, J. E.; Raub, T. J., et al. (2005). In vitro models for the blood-brain barrier. Toxicol In Vitro *19*, 299-334.

Garcia, C.M.; Darland, D. C.; Massingham, L. J.; D'Amore, Patricia A. (2004). Endothelial cell-astrocyte interactions and TGF beta are required for induction of blood-neural barrier properties. Brain Res. Dev. Brain Res. *152*, 25-38.

Garcia-Garcia, E.; Gil, S.; Andrieux, K.; Desmaële, D.; Nicolas, V.; Taran, F.; Georgin, D.; Andreux, J. P.; Roux, F.; Couvreur, P. (2005). A relevant in vitro rat model for the evaluation of blood-brain barrier translocation of nanoparticles. Cell. Mol. Life Sci. *62*, 1400-1408.

Gerdes, J.; Lemke, H.; Baisch, H.; Wacker, H. H.; Schwab, U.; Stein, H. (1984). Cell cycle analysis of a cell proliferation-associated human nuclear antigen defined by the monoclonal antibody Ki-67. J. Immunol. *133*, 1710-1715.

Gibson, J.D.; Khanal, Bishnu P.; Zubarev, Eugene R. (2007). Paclitaxel-functionalized gold nanoparticles. J. Am. Chem. Soc. *129*, 11653-11661.

Gibson, M.I.; Danial, M.; Klok, H.-A. (2011). Sequentially Modified, Polymer-Stabilized Gold Nanoparticle Libraries: Convergent Synthesis and Aggregation Behavior. ACS Combinatorial Science, null-null.

Glebov, O.O.; Bright, N. A.; Nichols, B. J. (2006). Flotillin-1 defines a clathrin-independent endocytic pathway in mammalian cells. Nat. Cell Biol. *8*, 46-54.

Greßler, S.; Fiedeler, U.; Simkó, M.; Gazsò, A.; Nentwich, M. (2010a). Self-cleaning, dirt and water repellent coatings on the basis of nanotechnology. Nano, 1-6.

Greßler, S.; Gazsò, A.; Simkó, Myrtill; Fiedeler, U.; Nentwich, M. Nanotechnology in Cosmetics. Nano *2010*, 1-6.

Greßler, S.; Gazsò, A.; Simkó, Myrtill; Nentwich, M.; Fiedeler, U. (2010b). Nanoparticles and nanostructured materials in the food industry. nano trust dossiers, 1-6.

Greßler, S.; Simkó, M.; Gazsò, A.; Fiedeler, U.; Nentwich, M. (2010c). Nano-Textiles. Nano, 1-5.

Hainfeld, J.F.; Slatkin, D. N.; Focella, T. M.; Smilowitz, H. M. (2006). Gold nanoparticles: a new X-ray contrast agent. Br J Radiol *79*, 248-253.

Hauck, T.S.; Ghazani, A. A.; Chan, W C. W. (2008). Assessing the effect of surface chemistry on gold nanorod uptake, toxicity, and gene expression in mammalian cells. Small *4*, 153-159.

Hawkins, B.T.; Davis, Thomas P. (2005). The blood-brain barrier/neurovascular unit in health and disease. Pharmacol. Rev. *57*, 173-185.

Hirase, T.; Staddon, J. M.; Saitou, M.; Ando-Akatsuka, Y.; Itoh, M.; Furuse, M.; Fujimoto, K.; Tsukita, S.; Rubin, L. L. (1997). Occludin as a possible determinant of tight junction permeability in endothelial cells. J. Cell. Sci. *110 (Pt 14)*, 1603-1613.

Hirn, S.; Semmler-Behnke, M.; Schleh, C.; Wenk, A.; Lipka, J.; Schäffler, M.; Takenaka, S.; Möller, W.; Schmid, G.; Simon, U. (2010). Particle size-dependent and surface charge-dependent biodistribution of gold nanoparticles after intravenous administration. European journal of pharmaceutics and biopharmaceutics : official journal of Arbeitsgemeinschaft fur Pharmazeutische Verfahrenstechnik e.V.

Hirsch, L.R.; Stafford, R. J.; Bankson, J. A.; Sershen, S. R.; Rivera, B.; Price, R. E.; Hazle, J. D.; Halas, N. J.; West, J. L. (2003). Nanoshell-mediated near-infrared thermal therapy of tumors under magnetic resonance guidance. Proc. Natl. Acad. Sci. U.S.A. *100*, 13549-13554.

Hoheisel, D.; Nitz, T.; Franke, H.; Wegener, J.; Hakvoort, A.; Tilling, T.; Galla, H. J. (1998). Hydrocortisone reinforces the blood-brain barrier properties in a serum free cell culture system. Biochem Biophys Res Commun *244*, 312-316.

Hong, R.; Han, G.; Fernández, J. M.; Kim, B.; Forbes, N. S.; Rotello, V. M. (2006). Glutathione-mediated delivery and release using monolayer protected nanoparticle carriers. J. Am. Chem. Soc. *128*, 1078-1079.

Hu, C.; Peng, Q.; Chen, F.; Zhong, Z.; Zhuo, R. (2010). Low Molecular Weight Polyethylenimine Conjugated Gold Nanoparticles as Efficient Gene Vectors. Bioconjugate Chemistry *21*, 836-843.

Ingber, D.E. (1990). Fibronectin controls capillary endothelial cell growth by modulating cell shape. Proc. Natl. Acad. Sci. U.S.A. *87*, 3579-3583.

Jaffe, E.A.; Hoyer, L. W.; Nachman, R. L. (1974). Synthesis of von Willebrand factor by cultured human endothelial cells. Proc. Natl. Acad. Sci. U.S.A. *71*, 1906-1909.

Jain, P.K.; Eustis, S.; El-Sayed, M. A. (2006). Plasmon coupling in nanorod assemblies: optical absorption, discrete dipole approximation simulation, and exciton-coupling model. J Phys Chem B *110*, 18243-18253.

Jeliazkova-Mecheva, V.V.; Bobilya, D. J. (2003). A porcine astrocyte/endothelial cell co-culture model of the blood-brain barrier. Brain Res. Brain Res. Protoc. *12*, 91-98.

Jordan, A.; Scholz, R.; Maier-Hauff, K.; van Landeghem, F. K. H.; Waldoefner, N.; Teichgraeber, U.; Pinkernelle, J.; Bruhn, H.; Neumann, F.; Thiesen, B. (2006). The effect of thermotherapy using magnetic nanoparticles on rat malignant glioma. J. Neurooncol. *78*, 7-14.

Ke, W.; Shao, K.; Huang, R.; Han, L.; Liu, Y.; Li, J.; Kuang, Y.; Ye, L.; Lou, J.; Jiang, C. (2009). Gene delivery targeted to the brain using an Angiopep-conjugated polyethyleneglycol-modified polyamidoamine dendrimer. Biomaterials.

Kennedy, I.M.; Wilson, D.; Barakat A., I. HEI Health Review Committee (2009). Uptake and inflammatory effects of nanoparticles in a human vascular endothelial cell line. Res Rep Health Eff Inst, 3-32.

Kido, Y.; Tamai, I.; Nakanishi, T.; Kagami, T.; Hirosawa, I.; Sai, Y.; Tsuji, A. (2002). Evaluation of blood-brain barrier transporters by co-culture of brain capillary endothelial cells with astrocytes. Drug Metab Pharmacokinet *17*, 34-41.

Kim, C.-k.; Ghosh, P.; Rotello, V. M. (2009a). Multimodal drug delivery using gold nanoparticles. Nanoscale *1*, 61-67.

Kim, D.; Park, S.; Lee, J. H.; Jeong, Y. Y.; Jon, S. (2007). Antibiofouling polymer-coated gold nanoparticles as a contrast agent for in vivo X-ray computed tomography imaging. J. Am. Chem. Soc. *129*, 7661-7665.

Kim, E.; Yang, J.; Jihye, C.; Haam, S. (2009b). Synthesis of gold nanorod-embedded polymeric nanoparticles by a nanoprecipitation method for use as photothermal agents. Nanotechnology *20*, 365602.

Kreuter, J. (2001). Nanoparticulate systems for brain delivery of drugs. Adv. Drug Deliv. Rev. *47*, 65-81.

Kreuter, J.; Shamenkov, D.; Petrov, V.; Ramge, P.; Cychutek, K.; Koch-Brandt, C.; Alyautdin, R. (2002). Apolipoprotein-mediated transport of nanoparticle-bound drugs across the blood-brain barrier. J Drug Target *10*, 317-325.

Kunzmann, A.; Andersson, B.; Thurnherr, T.; Krug, H.; Scheynius, A.; Fadeel, B. (2010). Toxicology of engineered nanomaterials: Focus on biocompatibility, biodistribution and biodegradation. Biochimica et biophysica acta.

Lai, C.-H.; Kuo, K.-H. (2005). The critical component to establish in vitro BBB model: Pericyte. Brain Res. Brain Res. Rev. *50*, 258-265.

Li, J.J.; Hartono, D.; Ong, C.-N.; Bay, B.-H.; Yung, L.-Y. L. (2010a). Autophagy and oxidative stress associated with gold nanoparticles. Biomaterials *31*, 5996-6003.

Li, T.; Albee, B.; Alemayehu, M.; Diaz, R.; Ingham, L.; Kamal, S.; Rodriguez, M.; Whaley Bishnoi, S. (2010b). Comparative toxicity study of Ag, Au, and Ag–Au bimetallic nanoparticles on Daphnia magna. Analytical and Bioanalytical Chemistry *398*, 689-700.

Liang, G.; Pu, Yuepu; Yin, Lihong; Liu, Ran; Ye, Bing; Su, Yaoyao; Li, Yanfen (2009). Influence of Different Sizes of Titanium Dioxide Nanoparticles on Hepatic and Renal Functions in Rats with Correlation to Oxidative Stress. Journal of Toxicology and Environmental Health, Part A: Current Issues *72*, 740-745.

Lin, J.; Zhang, Hongwu; Chen, Zhen; Zheng, Yonggang (2010). Penetration of Lipid Membranes by Gold Nanoparticles: Insights into Cellular Uptake, Cytotoxicity, and Their Relationship. ACS Nano.

Löscher, W.; Potschka, Heidrun (2005). Role of drug efflux transporters in the brain for drug disposition and treatment of brain diseases. Prog. Neurobiol. *76*, 22-76.

Love, J.C.; Estroff, L. A.; Kriebel, Jennah K.; Nuzzo, Ralph G.; Whitesides, George M. (2005). Self-assembled monolayers of thiolates on metals as a form of nanotechnology. Chem. Rev. *105*, 1103-1169.

Lück, M. (1997). Plasmaproteinadsorption als möglicher Schlüsselfaktor für eine kontrollierte Arzneistoffapplikation mit partikulären Trägern. Ph.D. thesis, Free University of Berlin.

Lundqvist, M.; Stigler, Johannes; Elia, Giuliano; Lynch, Iseult; Cedervall, Tommy; Dawson, Kenneth A. (2008). Nanoparticle size and surface properties determine the protein corona with possible implications for biological impacts. Proc. Natl. Acad. Sci. U.S.A. *105*, 14265-14270.

Luo, D.; Saltzman, W. M. (2000). Enhancement of transfection by physical concentration of DNA at the cell surface. Nat. Biotechnol. *18*, 893-895.

Luo, X.; Pan, Shirong; Feng, M.; Wen, Yuting; Z., Wei (2010). Stability of poly(ethylene glycol)-graft-polyethylenimine copolymer/DNA complexes: influences of PEG molecular weight and PEGylation degree. Journal of Materials Science: Materials in Medicine *21*, 597-607.

Lynch I.; Dawson, K. (2008). Protein-nanoparticle interactions. nanotoday *3*, 40-47.

Mailänder, V.; Landfester, K. (2009). Interaction of nanoparticles with cells. Biomacromolecules *10*, 2379-2400.

Makó, V.; Czúcz, Judit; Weiszhár, Zsóka; Herczenik, Eszter; Matkó, János; Prohászka, Zoltán; Cervenak, László (2010). Proinflammatory activation pattern of human umbilical vein endothelial cells induced by IL-1β, TNF-α, and LPS. Cytometry *77A*, 962-970.

Marano, F.; Hussain, Salik; Rodrigues-Lima, Fernando; Baeza-Squiban, Armelle; Boland, Sonja (2010). Nanoparticles: molecular targets and cell signalling. Arch. Toxicol.

Markert, S.; Lassmann, S.; Gabriel, B.; Klar, M.; Werner, M.; Gitsch, G.; Kratz, F.; Hasenburg, A. Alpha-folate receptor expression in epithelial ovarian carcinoma and non-neoplastic ovarian tissue. Anticancer Res. *28*, 3567-3572.

McIntosh, C.M.; Esposito, E. A.; Boal, A. K.; Simard, J. M.; Martin, C. T.; Rotello, V. M. (2001). Inhibition of DNA transcription using cationic mixed monolayer protected gold clusters. J. Am. Chem. Soc. *123*, 7626-7629.

Michel Demeule, J.-C.C.Y.B.C.C.T.N.A.R.R.G.J.-P.C.R.B. (2008). Involvement of the low-density lipoprotein receptor-related protein in the transcytosis of the brain delivery vector Angiopep-2. Journal of Neurochemistry *106*, 1534-1544.

Mirkin, C.A.; Letsinger, R. L.; Mucic, R. C.; Storhoff, J. J. (1996). A DNA-based method for rationally assembling nanoparticles into macroscopic materials. Nature *382*, 607-609.

Mironava, T.; Hadjiargyrou, Michael; Simon, Marcia; Jurukovski, Vladimir; Rafailovich, Miriam H. (2010). Gold nanoparticles cellular toxicity and recovery: Effect of size, concentration and exposure time. Nanotoxicology. Nanotoxicology *4*, 120-137.

Morita, K.; Sasaki, H.; Furuse, M.; Tsukita, S. (1999). Endothelial claudin: claudin-5/TMVCF constitutes tight junction strands in endothelial cells. J. Cell Biol. *147*, 185-194.

Mpourmpakis, G.; Vlachos, D. G. (2009). Growth Mechanisms of Metal Nanoparticles via First Principles. Phys. Rev. Lett. *102*, 155505.

Nakagawa, S.; Deli, M. A.; Nakao, S.; Honda, M.; Hayashi, Kentaro; Nakaoke, Ryota; Kataoka, Yasufumi; Niwa, Masami (2007). Pericytes from brain microvessels strengthen the barrier integrity in primary cultures of rat brain endothelial cells. Cell. Mol. Neurobiol. *27*, 687-694.

Nam, J.; Won, N.; Jin, Ho; Chung, Hyokyun; Kim, Sungjee (2009). pH-Induced Aggregation of Gold Nanoparticles for Photothermal Cancer Therapy. Journal of the American Chemical Society *131*, 13639-13645.

NanoCare Consortium (2009). Gesundheitsrelevante Aspekte synthetischer Nanomaterialien, 1-19.

Nativo, P.; Prior, Ian A.; Brust, Mathias (2008). Uptake and Intracellular Fate of Surface-Modified Gold Nanoparticles. ACS Nano *2*, 1639-1644.

Nayak, R.; Berman, A.; George, K.; Eisenbarth, G.; King, G. (1988). A monoclonal antibody (3G5)-defined ganglioside antigen is expressed on the cell surface of microvascular pericytes. J Exp Med, 1003-1015.

Nayak, R.C.; Attawia, Mohamed A.; Cahill, Christopher J.; King, George L.; Ohashi, Hiromi; Moromisato, Rocio (1992). Expression of a monoclonal antibody (3G5) defined ganglioside antigen in the renal cortex. Kidney Int *41*, 1638-1645.

Nehls, V.; Drenckhahn, D. (1993). The versatility of microvascular pericytes: from mesenchyme to smooth muscle? Histochemistry *99*, 1-12.

Nel, A.E.; Madler, Lutz; Velegol, Darrell; Xia, Tian; Hoek, Eric M. V.; Somasundaran, Ponisseril; Klaessig, Fred; Castranova, Vince; Thompson, Mike (2009). Understanding biophysicochemical interactions at the nano-bio interface. Nat Mater *8*, 543-557.

Niidome, T.; Yamagata, M.; Okamoto, Y.; Akiyama, Y.; Takahashi, H.; Kawano, T.; Katayama, Yoshiki; Niidome, Yasuro (2006). PEG-modified gold nanorods with a stealth character for in vivo applications. Journal of Controlled Release *114*, 343-347.

Nitta, T.; Hata, M.i; Gotoh, S.; Seo, Y.; Sasaki, H.; Hashimoto, N.; Furuse, M.; Tsukita, S. (2003). Size-selective loosening of the blood-brain barrier in claudin-5-deficient mice. J. Cell Biol. *161*, 653-660.

NSTC (2002). The Initiative and Its Implementation Plan. Detailed Technical Report Associated with the Supplemental Report to the President's FY 2003 Budget., 19.

Olivier, J.-C. (2005). Drug transport to brain with targeted nanoparticles. NeuroRx *2*, 108-119.

Pan, Y.; Sabine Neuss; Annika Leifert; Monika Fischler; Fei Wen; Ulrich Simon; Günter Schmid; Wolfgang Brandau; Willi Jahnen-Dechent (2007). Size-Dependent Cytotoxicity of Gold Nanoparticles. Small *3*, 1941-1949.

Pan, Y.; Leifert, A.; Ruau, D.; Neuss, S.; Bornemann, J.; Schmid, G.; Brandau, W.; Simon, U.; Jahnen-Dechent, W. (2009). Gold nanoparticles of diameter 1.4 nm trigger necrosis by oxidative stress and mitochondrial damage. Small *5*, 2067-2076.

Pardridge, W.M. (2001). Brain drug targeting and gene technologies. Jpn. J. Pharmacol. *87*, 97-103.

Park, E.K.; Lee, Sang Bong; Lee, Young Moo (2005). Preparation and characterization of methoxy poly(ethylene glycol)/poly(epsilon-caprolactone) amphiphilic block copolymeric nanospheres for tumor-specific folate-mediated targeting of anticancer drugs. Biomaterials *26*, 1053-1061.

Patel, L.N.; Zaro, Jennica L.; Shen, Wei-Chiang (2007). Cell penetrating peptides: intracellular pathways and pharmaceutical perspectives. Pharm. Res. *24*, 1977-1992.

Pernodet N; Fang X; Sun Y; Bakhtina A; Ramakrishnan A; Sokolov, J; Ulman, A.; Rafailovich, R (2006). Adverse Effects of Citrate/Gold Nanoparticles on Human Dermal Fibroblasts. Small *2*, 766-773.

Peters, A.; Veronesi, B.; Calderón-Garcidueñas, L.; Gehr, P.; Chen, L. C.; Geiser, M.; Reed, W.; Rothen-Rutishauser, B.; Schürch, S.; Schulz, H. (2006). Translocation and potential neurological effects of fine and ultrafine particles a critical update. Part Fibre Toxicol *3*, 13.

Pigott, R.; Dillon, L. P.; Hemingway, I. H.; Gearing, A. J. (1992). Soluble forms of E-selectin, ICAM-1 and VCAM-1 are present in the supernatants of cytokine activated cultured endothelial cells. Biochem. Biophys. Res. Commun. *187*, 584-589.

Poller, B.; Drewe, J.; Krähenbühl, S.; Huwyler, J.; Gutmann, H. (2010). Regulation of BCRP (ABCG2) and P-glycoprotein (ABCB1) by cytokines in a model of the human blood-brain barrier. Cell. Mol. Neurobiol. *30*, 63-70.

Pries, A.R.; Kuebler, W. M. (2006). Normal endothelium. Handb Exp Pharmacol, 1-40.

Rayavarapu, R., G.; Petersen, W.; Hartsuiker, L.; Chin, P.; Janssen, H.; Leeuwen, F. W. G. von; Cees Otto; Srirang Manohar; Ton G van Leeuwen (2010). In vitro toxicity studies of polymer-coated gold nanorods. Nanotechnology *21*, 145101.

Rapoport, S.I. (2000). Osmotic opening of the blood-brain barrier: principles, mechanism, and therapeutic applications. Cell. Mol. Neurobiol. *20*, 217-230.

Reese, T.S.; Karnovsky, M. J. (1967). Fine structural localization of a blood-brain barrier to exogenous peroxidase. J. Cell Biol. *34*, 207-217.

Régina, A.; Demeule, M.; Ché, C.; Lavallée, I.; Poirier, J.; Gabathuler, R.; Béliveau, R.; Castaigne, J-P (2008). Antitumour activity of ANG1005, a conjugate between paclitaxel and the new brain delivery vector Angiopep-2. Br. J. Pharmacol. *155*, 185-197.

Rothen-Rutishauser, B.; Mühlfeld, C.; Blank, F.; Musso, C.; Gehr, P. (2007). Translocation of particles and inflammatory responses after exposure to fine particles and nanoparticles in an epithelial airway model. Part Fibre Toxicol *4*, 9.

Sasaki, K.; Murakami, T.; Kawasaki, M.; Takahashi, M. (1987). The cell cycle associated change of the Ki-67 reactive nuclear antigen expression. J. Cell. Physiol. *133*, 579-584.

Sau, T.K.; Murphy, Catherine J. (2004). Seeded high yield synthesis of short Au nanorods in aqueous solution. Langmuir *20*, 6414-6420.

Saxl, O. What is Nanotechnology? A Guide. Nanomagazine.

Schinkel (1999). P-Glycoprotein, a gatekeeper in the blood-brain barrier. Adv. Drug Deliv. Rev. *36*, 179-194.

Schmid, G. (1992). Large Clusters and Colloids. Metals in the Embryonic State. Chem. Rev., 1709-1727.

Schmid, G.; Klein, N.; Korste, L.; Kreibig, U.; Schönauer, D. (1988). Large transition metal clusters--VI. Ligand exchange reactions on Au55(PPh3)12Cl6--the formation of a water soluble Au55 cluster. Polyhedron *7*, 605-608.

Schnyder, A.; Huwyler, J. (2005). Drug transport to brain with targeted liposomes. NeuroRx *2*, 99-107.

Scholzen, T.; Gerdes, J. (2000). The Ki-67 protein: from the known and the unknown. J. Cell. Physiol. *182*, 311-322.

Schroeder, U.; Sommerfeld, P.; Ulrich, S.; Sabel, B. A. (1998). Nanoparticle technology for delivery of drugs across the blood-brain barrier. J Pharm Sci *87*, 1305-1307.

Selvi, B.R.; Jagadeesan, D.; Suma, B. S.; Nagashankar, G.; Arif, M.; Balasubramanyam, K.; Eswaramoorthy, M.; Kundu, Tapas K. (2008). Intrinsically fluorescent carbon nanospheres as a nuclear targeting vector: delivery of membrane-impermeable molecule to modulate gene expression in vivo. Nano Lett. *8*, 3182-3188.

Sereemaspun, A.; Rojanathanes, R.; Wiwanitkit, V. (2008). Effect of gold nanoparticle on renal cell: an implication for exposure risk. Ren Fail *30*, 323-325.

Shea, B. (2001). Review: glucosamine is more effective than selected non-steroidal anti-inflammatory drugs and placebo for reducing pain and more effective than placebo for improving function in patients with osteoarthritis. Evidence Based Nursing *4*, 121.

Shimizu, F.; Sano, Y.; Maeda, T.; Abe, M.; Nakayama, H.; Takahashi, R.; Ueda, M.; Ohtsuki, S.; Terasaki, T.; Obinata, M. (2008). Peripheral Nerve pericytes originating from the blood–nerve barrier expresses tight junctional molecules and transporters as barrier-forming cells. J. Cell. Physiol. *217*, 388-399.

Sims, D.E. (2000). Diversity within pericytes. Clin. Exp. Pharmacol. Physiol. *27*, 842-846.

Sokolov, K.; Follen, M.; Aaron, J.; Pavlova, I.; Malpica, A.; Lotan, R.; Richards-Kortum, R. (2003). Real-time vital optical imaging of precancer using anti-epidermal growth factor receptor antibodies conjugated to gold nanoparticles. Cancer Res. *63*, 1999-2004.

Sopjani, M.; Föller, M.; Lang, F. (2008). Gold stimulates Ca2+ entry into and subsequent suicidal death of erythrocytes. Toxicology *244*, 271-279.

Sperling, R.A.; Gil, P.; Zhang, F.; Zanella, M.; Parak, W. J. (2008). Biological applications of gold nanoparticles. Chem. Soc. Rev, 1896-1908.

Stewart, P.A. (2000). Endothelial vesicles in the blood-brain barrier: are they related to permeability? Cell. Mol. Neurobiol. *20*, 149-163.

Tao-Cheng, J.H.; Brightman, M. W. (1988). Development of membrane interactions between brain endothelial cells and astrocytes in vitro. Int. J. Dev. Neurosci. *6*, 25-37.

Taylor, U.; Klein, S.; Petersen, S.; Kues, W.; Barcikowski, S.; Rath, D. (2010). Nonendosomal cellular uptake of ligand-free, positively charged gold nanoparticles. Cytometry *77A*, 439-446.

Thanabalasundaram, G.; Pieper, C.; Lischper, M.; Galla, H.-J. (2010). Regulation of the blood-brain barrier integrity by pericytes via matrix metalloproteinases mediated activation of vascular endothelial growth factor in vitro. Brain Res. *1347*, 1-10.

Thorek, D.L.J.; Tsourkas, A. (2008). Size, charge and concentration dependent uptake of iron oxide particles by non-phagocytic cells. Biomaterials *29*, 3583-3590.

Tilling, T.; Korte, D.; Hoheisel, D. (1998). Basement Membrane Proteins Influence Brain Capillary Endothelial Barrier Function In Vitro. Journal of Neurochemistry *71*, 1151-1157.

Timpl, R. (1989). Structure and biological activity of basement membrane proteins. Eur. J. Biochem. *180*, 487-502.

Torchilin, V.P. (2008). Tat peptide-mediated intracellular delivery of pharmaceutical nanocarriers. Adv. Drug Deliv. Rev. *60*, 548-558.

Trickler, W.J.; Lantz, S. M.; Murdock, R. C.; Schrand, A. M.; Robinson, B. L.; Newport, G. D.; Schlager, John J.; Oldenburg, Steven J.; Paule, Merle G.; Slikker Jr, William, et al. (2010). Brain microvessel endothelial cells responses to gold nanoparticles: In vitro pro-inflammatory mediators and permeability. Nanotoxicology. Nanotoxicology, 1-14.

Tsao, N.; HsuU, H. P.; WU, C. M.; LIU, C. C.; LEI, H. Y. (2001). Tumour necrosis factor-{alpha} causes an increase in blood-brain barrier permeability during sepsis. J Med Microbiol *50*, 812-821.

Tsoli M; Kuhn, H.; Brandau, W.; Esche, H.; Schmid, G. (2005). Cellular Uptake and Toxicity of Au-Clusters. Small *1*, 841-844.

Turkevich, J.; Stevenson, P. C.; Hillier, J. (1951). A Study of the Nucleation and growth processes in the synthesis of colloidal gold. Discuss. Faraday Soc., 55-75.

Ubbink, J.; Krüger, J. (2006). Physical approaches for the delivery of active ingredients in foods. Trends in Food Science & Technology, 244-254.

Uboldi, C.; Bonacchi, D.; Lorenzi, G.; Hermanns, M I.; Pohl, C.; Baldi, G.; Unger, R. E; Kirkpatrick, C J. (2009). Gold nanoparticles induce cytotoxicity in the alveolar type-II cell lines A549 and NCIH441. Particle and fibre toxicology *6*, 18.

Ulbrich, K.; Hekmatara, T.; Herbert, E.; Kreuter, J. (2009). Transferrin- and transferrin-receptor-antibody-modified nanoparticles enable drug delivery across the blood-brain barrier (BBB). Eur J Pharm Biopharm *71*, 251-256.

Ulbrich, K.; Knobloch, T.; Kreuter, J. (2011). Targeting the insulin receptor: nanoparticles for drug delivery across the blood-brain barrier (BBB). J Drug Target *19*, 125-132.

Ulbrich, K.; Michaelis, M.; Rothweiler, F.; Knobloch, T.; Sithisarn, P.; Cinatl, J.; Kreuter, J. (2010). Interaction of folate-conjugated human serum albumin (HSA) nanoparticles with tumour cells. International Journal of Pharmaceutics.

Unfried, K.; Albrecht, C.; Klotz, L.-O.; Mikecz, A. von; Grether-Beck, S.; Schins, R. P. F. (2007). Cellular responses to nanoparticles: Target structures and mechanisms. Nanotoxicology. Nanotoxicology *1*, 52-71.

Unger, R.E.; Krump-Konvalinkova, V.; Peters, K.; Kirkpatrick, C. J. (2002a). In Vitro Expression of the Endothelial Phenotype: Comparative Study of Primary Isolated Cells and Cell Lines, Including the Novel Cell Line HPMEC-ST1.6R. Microvascular Research *64*, 384-397.

Unger, R.E.; Oltrogge, J. B.; Briesen, H. von; Engelhardt, B.; Woelke, U.; Schlote, W.; Lorenz, R.; Bratzke, H.-J.; Kirkpatrick, C. J. (2002b). ISOLATION AND MOLECULAR CHARACTERIZATION OF BRAIN MICROVASCULAR ENDOTHELIAL CELLS FROM HUMAN BRAIN TUMORS. In Vitro Cellular & Developmental Biology - Animal *38*, 273-281.

Vallhov, H.; Qin, Jian; Johansson, Sara M.; Ahlborg, Niklas; Muhammed, Mamoun A.; Scheynius, Annika; Gabrielsson, Susanne (2006). The importance of an endotoxin-free environment during the production of nanoparticles used in medical applications. Nano Lett. *6*, 1682-1686.

Valvason, C.; Musacchio, E.; Pozzuoli, A.; Ramonda, R.; Aldegheri, R.; Punzi, L. (2008). Influence of glucosamine sulphate on oxidative stress in human osteoarthritic chondrocytes: effects on HO-1, p22Phox and iNOS expression. Rheumatology *47*, 31-35.

Vinogradov, S.V. (2010). Nanogels in the race for drug delivery. Nanomedicine (Lond) *5*, 165-168.

Vinogradov, S.V.; Kohli, E.; Zeman, A. D. (2005a). Cross-linked polymeric nanogel formulations of 5'-triphosphates of nucleoside analogues: role of the cellular membrane in drug release. Mol. Pharm. *2*, 449-461.

Vinogradov, S.V.; Zeman, Arin D.; Batrakova, E. V.; Kabanov, A. V (2005b). Polyplex Nanogel formulations for drug delivery of cytotoxic nucleoside analogs. J Control Release *107*, 143-157.

Vroman, L. (1962). Effect of Adsorbed Proteins on the Wettability of Hydrophilic and Hydrophobic Solids. Nature *196*, 476-477.

Weksler, B.B.; Subileau, E. A.; Perrière, N.; Charneau, P.; Holloway, K.; Leveque, M.; Tricoire-Leignel, H.; Nicotra, A.; Bourdoulous, S.; Turowski, P., et al. (2005). Blood-brain barrier-specific properties of a human adult brain endothelial cell line. FASEB J. *19*, 1872-1874.

Zhang, Q.; Hitchins, Victoria M.; Schrand, Amanda M.; Hussain, Saber M.; Goering, Peter L. (2010). Uptake of gold nanoparticles in murine macrophage cells without cytotoxicity or production of pro-inflammatory mediators. Nanotoxicology.

Zhang, Y.; Li, C. S W; Ye, Yuyang; Johnson, Kjell; Poe, Julie; Johnson, Shannon; Bobrowski, Walter; Garrido, Rosario; Madhu, Cherukury (2006). Porcine brain microvessel endothelial cells as an in vitro model to predict in vivo blood-brain barrier permeability. Drug Metab. Dispos. *34*, 1935-1943.

Zozulya, A.; Weidenfeller, C.; Galla, H.-J. (2008). Pericyte-endothelial cell interaction increases MMP-9 secretion at the blood-brain barrier in vitro. Brain Res. *1189*, 1-11.

8 List of figures

FIG. 1: NANOPARTICLE COMPOSITION AND CHARACTERISTICS INFLUENCE THE ADSORPTION OF PROTEINS 7

FIG. 2: STRATEGIES FOR BRAIN TARGETING 8

FIG. 3: FORMATION OF POLYMER MONOLAYER ONTO PRE-FORMED CITRATE-COATED GOLD NANOPARTICLES 12

FIG. 4: NEUROVASCULAR UNIT OF THE BLOOD-BRAIN BARRIER 16

FIG. 5: TIGHT AND ADHERENT JUNCTIONS OF BRAIN ENDOTHELIAL CELLS 17

FIG. 6: TRANSPORT PATHWAYS ACROSS THE BRAIN ENDOTHELIAL CELLS 19

FIG. 7: POLARIZED LOCATION OF ABC- EFFLUX TRANSPORTERS IN BRAIN ENDOTHELIAL CELLS 20

FIG. 8: DIFFERENT BBB MODELS ON TRANSWELL FILTER MEMBRANES 21

FIG. 9: MORPHOLOGY AND FORMATION OF VASCULAR-LIKE STRUCTURES OF HCMEC IN PASSAGE 27 50

FIG. 10: EXPRESSION OF ENDOTHELIAL CELL MARKERS IN HCMEC AND HDMEC 51

FIG. 11: EXPRESSION OF AJ- AND TJ-PROTEINS IN HCMEC 52

FIG. 12:ANALYSIS OF ABC-TRANSPORTER GENE EXPRESSION IN HCMEC, HDMEC AND HUVEC BY PCR 52

FIG. 13: OUTGROWTH OF PRIMARY PORCINE BRAIN ENDOTHELIAL CELLS AFTER ISOLATION 53

FIG. 14: MORPHOLOGY OF PBECS AND PRIMARY PORCINE BRAIN PERICYTES (PPBPS) AND VASCULARIZATION OF PBECS IN COLLAGEN TYPE I GEL. 54

FIG. 15: EXPRESSION OF TIGHT JUNCTION AND ADHERENS JUNCTION PROTEINS IN PBEC AND SMOOTH MUSCLE ACTIN EXPRESSION IN PERICYTES 55

FIG. 16: STAINING OF PORCINE PERICYTES WITH MAB 3G5 56

FIG. 17: INCREASING TRANSENDOTHELIAL ELECTRICAL RESISTANCE (TEER) OF PBECS CULTURED ON TRANSWELL FILTER MEMBRANES 57

FIG. 18: DETERMINATION OF THE PERMEABILITY COEFFICIENT (P_{APP}) OF PBECS CULTURED ON FILTER MEMBRANES 58

FIG. 19: ELECTRON MICROSCOPY IMAGES OF A PBEC LAYER ON TRANSWELL FILTER MEMBRANES 59

FIG. 20: ELECTRON MICROSCOPY IMAGES OF A HCMEC LAYER ON TRANSWELL FILTER MEMBRANES 60

FIG. 21: DETERMINATION OF THE PERMEABILITY COEFFICIENT (P_{APP}) OF HCMEC CULTURED ON FILTER MEMBRANES 62

FIG. 22: CELL VIABILITY AND PROLIFERATION RATE OF ENDOTHELIAL CELLS MEASURED AFTER EXPOSURE TO GOLD NANOPARTICLES 64

FIG. 23: CYTOTOXICITY OF ENDOTHELIAL CELLS MEASURED AFTER EXPOSURE TO GOLD NANOPARTICLES 65

FIG. 24: INTERNALIZATION OF GOLD NANOPARTICLES INTO ENDOTHELIAL AND EPITHELIAL CELLS AFTER AN EXPOSURE TIME OF 24 HOURS. 67

FIG. 25: QUANTIFICATION OF INTERNALIZED GOLD NANOPARTICLES IN DIFFERENT CELL TYPES BY ICP-AES 69

FIG. 26: CELL VIABILITY OF HCMEC AND HDMEC AFTER EXPOSURE TO VARIOUS GOLD NANOPARTICLES FOR 48 HOURS71

FIG. 27: UPTAKE OF VARIOUS GOLD NANOPARTICLES BY HCMEC AFTER 24 HOURS OF EXPOSURE 73

FIG. 28: UPTAKE OF VARIOUS GOLD NANOPARTICLES IN HDMEC AFTER 24 HOURS OF EXPOSURE 74

FIG. 29: TEM ANALYSIS OF THE INTERNALIZATION OF 35NM-SIZED GOLD NANOPARTICLES WITH DIFFERENT SURFACE MODIFICATIONS IN HDMEC AFTER 24 HOURS. 75

FIG. 30: QUANTIFICATION OF INTERNALIZED GOLD NANOPARTICLES IN HDMEC AND HCMEC BY ICP-AES 77

FIG. 31: QUANTIFICATION OF INTERNALIZED GOLD NANOPARTICLES IN HDMEC AND HCMEC BY ICP-AES 79

FIG. 32: CYTOKINE EXPRESSION OF HCMEC AFTER STIMULATION WITH DIFFERENT GOLD NANOPARTICLES 81

FIG. 33: CELL VIABILITY AND CYTOTOXICITY OF ENDOTHELIAL CELLS AFTER EXPOSURE TO HYDROXYPROPYLAMINE-COATED GOLD NANOPARTICLES OF DIFFERENT SIZES 83

FIG. 34: OPTICAL MICROSCOPY OF INTERNALIZED HYDROXYPROPYLAMINE-COATED GOLD NANOPARTICLES IN HCMEC AND HDMEC AFTER 4H OF INCUBATION 84

FIG. 35: DETECTION OF HYDROXYPROPYLAMINE-COATED GOLD NANOPARTICLES IN HDMEC AND HCMEC BY OPTICAL MICROSCOPY AFTER 24 HOURS EXPOSURE 85

FIG. 36: TEM IMAGES OF HCMEC AND HDMEC AFTER TREATMENT WITH DIFFERENT SIZED HYDROXYPROPYLAMINE-COATED GOLD NANOPARTICLES FOR 4 HOURS 86

FIG. 37: TEM IMAGES OF HCMEC AND HDMEC AFTER TREATMENT WITH DIFFERENT SIZED HYDROXYPROPYLAMINE-COATED GOLD NANOPARTICLES FOR 24 HOURS 87

FIG. 38: EXPRESSION OF PRO-INFLAMMATORY FACTORS IN HCMEC AFTER TREATMENT WITH 150µG/ML HYDROXYPROPYLAMINE-COATED GOLD NANOPARTICLES AT VARIOUS TIME POINTS AS DETERMINED BY REAL-TIME PCR 88

FIG. 39: EXPRESSION OF PRO-INFLAMMATORY FACTORS IN HCMEC AFTER TREATMENT WITH 150µG/ML HYDROXYPROPYLAMINE-COATED GOLD NANOPARTICLES AT VARIOUS TIME POINTS DETERMINED BY ELISA 89

FIG. 40: UPTAKE OF HYDROXYPROPYLAMINE-COATED GOLD NANOPARTICLES IN PBECS SEEDED ON TRANSWELL FILTER MEMBRANES 90

FIG. 41: MEAN TEER-VALUES IN PERCENT OF PBECS CULTURED ON TRANSWELL FILTERS DURING EXPOSURE TO GOLD NANOPARTICLES 91

FIG. 42: GOLD NANOPARTICLE CONCENTRATIONS IN PPB IN THE BASOLATERAL COMPARTMENT OF THE TRANSWELL PLATE AFTER INCUBATION OF PBECS WITH DIFFERENT CONCENTRATIONS OF HYDROXYPROPYLAMINE-COATED GOLD NANOPARTICLES OF DIFFERENT SIZES 92

9 List of tables

TABLE 1: INSTRUMENTS 24

TABLE 2: MICROSCOPES 24

TABLE 3: CONSUMABLES 25

TABLE 4: CHEMICALS 26

TABLE 5: BUFFERS 27

TABLE 6: SOLUTIONS AND CELL CULTURE MEDIA 28

TABLE 7: ENZYMES 29

TABLE 8: FITC-DEXTRANS, ALL PURCHASED FROM SIGMA-ALDRICH, ST. LUIS, USA 30

TABLE 9: NANOPARTICLES (PDI: POLY DISPERSITY INDEX; - : UNKNOWN) 30

TABLE 10: PRIMARY ANTIBODIES 31

TABLE 11: SECONDARY ANTIBODIES 32

TABLE 12: STANDARDS 33

TABLE 13: OLIGONUCLEOTIDES (ALL OLIGONUCLEOTIDES WERE PURCHASED FROM MICROSYNTH (WWW.MICROSYNTH.CH) WITH AN ANNEALING TEMPERATURE OF ~60°C) 33

TABLE 14: KIT-SYSTEMS 34

TABLE 15: PRIMARY CELLS AND CELL LINES 34

TABLE 16: CELL MEDIA FOR DIFFERENT CELL TYPES 39

TABLE 17: PIPETTING SCHEME AND PCR PROGRAM 46

TABLE 18: PCR PIPETTING SCHEME AND PCR PROGRAMM 47

TABLE 19: CYTOKINE STANDARD DILUTIONS 48

TABLE 20: PROPERTIES OF RIT/RIS GOLD NANOPARTICLES (FOR DETAILS SEE 2.9) 63

TABLE 21: CODINGS OF GOLD NANOPARTICLES (`YY': STANDS FOR THE DIFFERENT SIZES) 70